

รายงานวิจัยฉบับสมบูรณ์

โครงการโพรบสำหรับตรวจวัดโลหะหนักโดยใช้โรดามีนประยุกต์ บนอนุภาคนาโน, ฟลูออโรจินิค เวสิเคิล, พอลิเมอร์นำไฟฟ้า

โดย รศ.ดร. ชาติไทย แก้วทองและคณะ

มิถุนายน 2562

รายงานวิจัยฉบับสมบูรณ์

โครงการโพรบสำหรับตรวจวัดโลหะหนักโดยใช้โรดามีนประยุกต์ บนอนุภาคนาโน, ฟลูออโรจินิค เวสิเคิล, พอลิเมอร์นำไฟฟ้า

รศ.ดร. ชาติไทย แก้วทอง ภาควิชาเคมี คณะวิทยาศาสตร์ มหาวิทยาลัยมหาสารคาม

> สนับสนุนโดยสำนักงานกองทุนสนับสนุนการวิจัย และมหาวิทยาลัยมหาสารคาม

(ความเห็นในรายงานนี้เป็นของผู้วิจัย สกว. และต้นสังกัด ไม่จำเป็นต้องเห็นด้วยเสมอไป)

Acknowledgement

The authors gratefully acknowledge funding from the Thailand Research Fund (RSA5980072)

Research Group July 2019

บทคัดย่อ

รหัสโครงการ : RSA5980072

ชื่อโครงการ : โพรบสำหรับตรวจวัดโลหะหนักโดยใช้โรดามีนประยุกต์บนอนุภาคนาโน, ฟลูออ โรจินิค เวสิเคิล, พอลิเมอร์นำไฟฟ้า

ชื่อนักวิจัย: นายชาติไทย แก้วทอง ภาควิชาเคมี คณะวิทยาศาสตร์ มหาวิทยาลัย มหาสารคาม

นายมังกร ศรีสะอาด ภาควิชาเคมี คณะวิทยาศาสตร์ มหาวิทยาลัย มหาสารคาม

E-mail Address: kchatthai@gmail.com

ระยะเวลาโครงการ : 16 มิถุนายน 2559 - 16 มิถุนายน 2562

นำอนุพันธ์โรดามีนต่อกับพอลิอะคริลิค แอซิด หรือ PAA จะทำให้ได้สาร PAA ดัดแปรกับโรดามีน (PAA-Rho1-4) ซึ่งคุณสมบัติไม่ชอบน้ำ ตัวตรวจวัดทางพอลิเมอร์มีการเตรียมที่เรียบง่ายโดยใช้ ปฏิกิริยาเอไมด์ระหว่าง PAA และ อัตราส่วนโมลต่างๆของโรดามีนจะได้สาร PAA-Rho1, PAA-Rho2, PAA-Rho3 และ PAA-Rho4 นอกจากนี้การรวมกันของโรดามีนเข้ากับโครงสร้างหลักพอลิโซเดียม-4-สไตรีนซัลโฟเนต (PSS) จะทำให้ได้ตัวตรวจวัดทางพอลิเมอร์ชนิดใหม่ (PSS-Rho1-4) องค์ประกอบ ทางเคมีของตัวตรวจวัดทั้งหมดได้ทำการศึกษาโดยใช้ IR และ ¹H NMR สเปกโตรสโกปี โครงสร้างทาง เคมีและความบริสุทธิ์ของตัวตรวจวัดทางพอลิเมอร์ได้ทำการอธิบายลักษณะโดยใช้ TGA, NMR, TEM และ IR

ส่วน A: เราได้ทำการออกแบบและสังเคราะห์ตัวตรวจวัดทางพอลิเมอร์โดยการต่ออนุพันธ์ของโรดามีน ซึ่งเป็นโพรบการเรื่องแสงและเปลี่ยนแปลงทางสีเข้ากับโครงร้างหลักของ PAA และ PSS สำหรับ ตรวจวัดไอออน Au³⁺ อย่างจำเพาะเจาะจง โดยใช้เป็นตัวตรวจวัดสีย้อมเรื่องแสงทางเคมี และตัว ตรวจวัดฟิล์มเรื่องแสง

ส่วน B: เราได้ทำการพัฒนาตัวตรวจวัดจากผลของตัวทำละลายที่มีต่อการเปลี่ยนแปลงสีของโรดามีน สำหรับ Cr³+ โดยใช้โรดามีนที่มีใช้ทั่วไปทางการค้าละลายกับ THF จะได้โรดามีนแลคแทม (**RhoL**) ผ่านความสมดุลของสวิทเตอร์ไอออนโรดามีนแลคโทน ส่วน C: เราได้ทำการนำเสนอตัวตรวจวัดเชิงแสงที่มีวิธีการเตรียมที่เรียบง่ายและมีการตอบสนองที่ ว่องไวโดยการตรึงอนุพันธ์ของโรดามีนลงบนอะกาโรสไฮโดรเจลเพื่อใช้เป็นโพรบของทอง ส่วน D: เราได้รายงานตัวตรวจวัด pH เชิงแสงและเรื่องแสงโดยใช้โรดามีนดัดแปรบนกระดาษเซลลูโรส ที่มีความว่องไว

คำหลัก : โรดามีน, คีโมเซ็นเซอร์, โลหะหนัก, พีเอช, ทอง(III), โครเมียม(III)

Abstract

Project Code: RSA5980072

Project Title: Heavy Metal Probes Using Rhodamine-Based Modified Nanoparticles, fluorogenic vesicles and Conducting Polymers

Investigator: Mr. Chatthai Kaewtong, Department of Chemistry, Faculty of Science, Mahasarakham University

Mr. Mongkorn Srisa-ad, Department of Chemistry, Faculty of Science, Mahasarakham University

E-mail Address : kchatthai@gmail.com

Project Period: 16 June 2016 - 16 June 2019

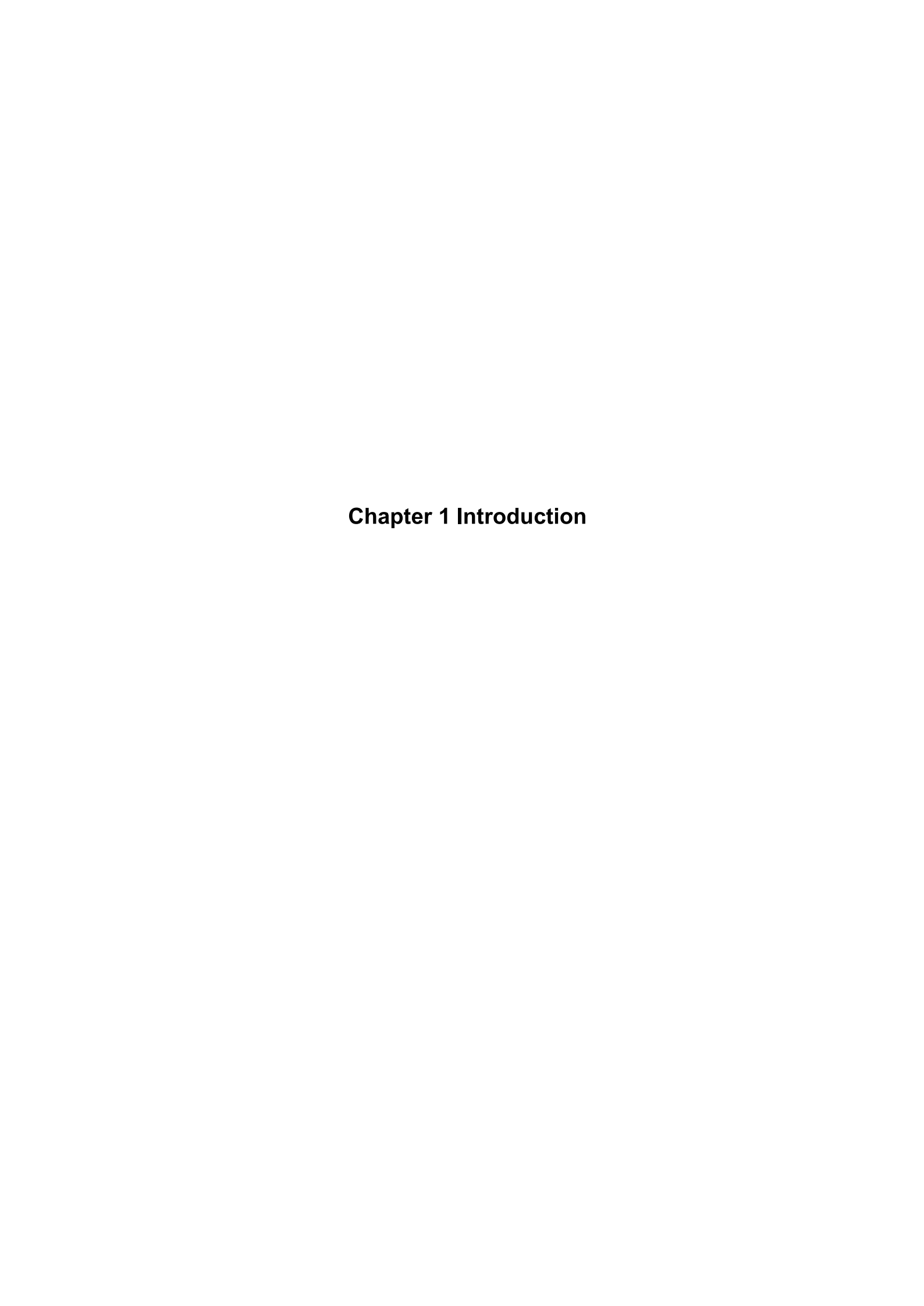
Rhodamine derivatives are grafted on poly(acrylic acid) or PAA to obtain hydrophobically modified PAA (**PAA-Rho1-4**) bearing rhodamine moieties. Polymeric sensors are simply prepared by amidation reactions between PAA and various mole ratios of rhodamine to obtain **PAA-Rho1**, **PAA-Rho2**, **PAA-Rho3** and **PAA-Rho4**. In addition, the incorporation of rhodamine moiety into the poly(sodium-4-styrenesulfonate) (PSS) backbones produced novel polymeric chemosensors (**PSS-Rho1-4**). Chemical compositions of all chemosensors are studied by IR and ¹H NMR spectroscopy. Chemical structures and purity of polymeric sensors are characterized by TGA, NMR, TEM and IR.

Part A: We have designed and synthesized the polymeric sensors by grafting rhodamine derivatives as colorimetric, fluorescent probes into PAA and PSS skeleton for selective detection of Au³⁺ ions used as fluorescence chemosensor dye and fluorescent film sensors. Part B: we developed a solvatochromic rhodaminebased sensor for Cr³⁺ using commercially available rhodamine simply dissolved in THF to produce rhodamine lactone (**RhoL**) via the rhodamine lactone—zwitterion equilibrium.

Part C: we exposed the simple way for preparation and response features of a new highly sensitive optical sensor by immobilization of rhodamine derivative on agarose hydrogel as a gold probe

Part D: we report a pH optical and fluorescent sensor based on rhodamine modified on activated cellulose paper

Keywords : Rhodamine, chemoseneor, heavy metal, Au^{3+} , pH, Cr^{3+}



Heavy metal has been widely used in many fields of modern society such as medicine [1], catalysis [2] and electronics [3]. They are the most dangerous and ubiquitous of pollutants, causes serious environmental and health problems because it can easily pass through skin, respiratory, and gastrointestinal tissues into the human body, where it damages the central nervous and endocrine systems. Therefore, it is important to explore new methods for analyzing heavy metals in vitro and in vivo.

Conventional methods for the recovery of heavy metals from aqueous solutions include precipitation [7], ions exchange [8], and solvent extraction [9]. Nevertheless, these methods are not effective (incomplete metal removal) or economical (high cost, high reagent and/or energy requirement) because gold-containing wastewater is often characterized by low concentration (<100 mg/L). Compared with conventional methods, adsorption offers distinct advantages for metal ions recovery, including high efficiency, low operating costs, and minimal volume of sludge, etc. [10]. In the past few years, molecular sensor has become a powerful tool for sensing and imaging trace amount of sample because if its simplicity and sensitivity. The molecular sensors contain two basic functional units: a receptor unit and a signaling unit.

Many recent developments have shown that rhodamine spirolactam is a promising structural scaffold for the design of selective chemosensors. Its structure can undergo a change from the spirolactam to an open ring amide, resulting in a magenta-colored, highly fluorescent compound [11].

Figure 1. Spirolactam ring-opening process of rhodamine derivative.

In general, a rhodamine derivative displays a red color change and strong fluorescence in acidic solution by activating a carbonyl group in a spirolactone or spirolactam moiety as shown in Figure 1. In a similar way, an appropriate ligand on spirolactam ring can induce color changes as well as fluorescent changes upon the addition of metal ions even though this process is somewhat dependent on the solvent system.

Rhodamine dyes are widely used as fluorescent probes owing to their high absorption coefficient and broad fluorescence in the visible region of electromagnetic spectrum, high fluorescence quantum yield and photostability after complexes with metal.

Figure 1. Proposed Mechanism for the Fluorescent Changes of 1 upon the Addition of Pb²⁺

Czarnik et al. [12] reported pioneering work utilizing this unique process. In their study, rhodamine-B hydrazide was used as a fluorescent chemodosimeter for Cu²⁺. In 2005 Yoon et al. [13] reported another rhodamine-B derivative as a fluorescent chemosensor for Pb²⁺. Among the various metal ions, compound **1** showed significant fluorescent enhancement only with Pb²⁺ in acetonitrile, even though there was relatively small fluorescent enhancement with Cu²⁺ and Zn²⁺. Yoon et al. used three different methods to verify the complexation and its mechanism, ESI mass spectroscopy, IR and ¹³C NMR spectroscopy. As shown in Figure 1.

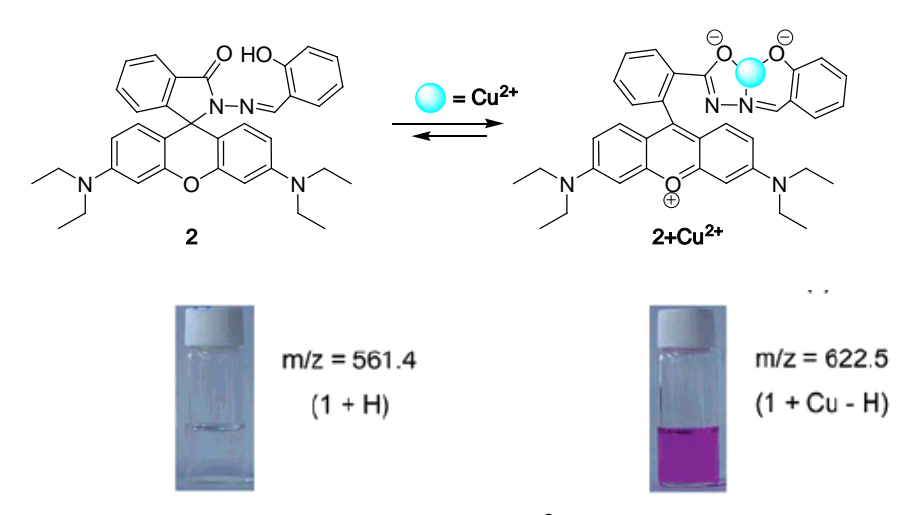


Figure 2. Chemical structures of compound 2, 2-Cu²⁺

In 2006, salicylaldehyde rhodamine B hydrazine [14] (2) was synthesized and displayed selective Cu²⁺-amplified absorbance and fluorescence emission above 500 nm in neutral buffered media by Tong et al. Upon the addition of Cu²⁺, the spirolactam ring of 2 was

opened and a 1:1 metal-ligand complex was formed (Figure 2). The detection of Cu²⁺ by **2** at a lower micromolar level was successful even in buffered water.

Bishwajit Ganguly et al. [15] have developed sensitive and selective receptors (3 and 4) for Cr³⁺ and Hg²⁺, where binding to these two ions induces a turn on response in electronic and fluorescence spectra in the visible region. Thus, these receptors could be used as a dual probe for visual detection through change in color and fluorescence. Studies reveal that these two reagents could be used for recognition and sensing of Hg²⁺/Cr³⁺. Further, confocal laser microscopic studies confirmed that the reagents could also be used as an imaging probe for detection of uptake of these ions in A431 cells (Figure 3).

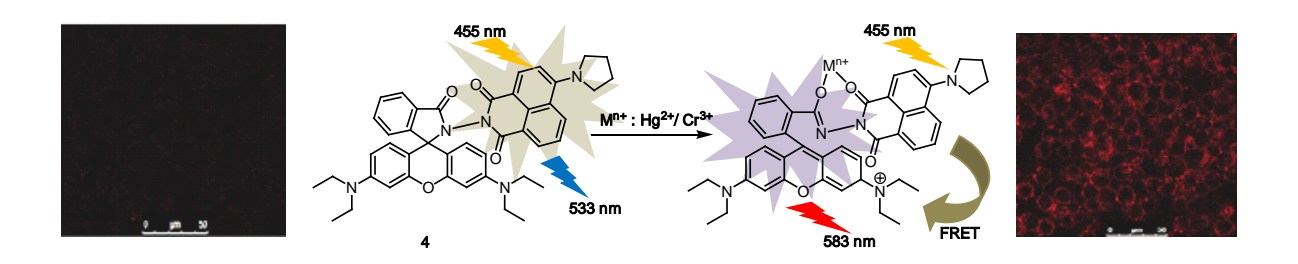


Figure 3. Presentation showing the possible metal ion binding mode of **4** and confocal microscopic images of A431 cells (A) before and after loaded with Hg^{2+}/Cr^{3+}

Recently, Puhui Xie et al. [16] have reported a novel turn-on FRET fluorescent sensor based on a rhodamine and dansyl conjugate which mechanism is shown in Figure 4. The sensor exhibits a clear Fe³⁺ induced change in the intensity ratio of the two well-separated emission band of dansyl unit and rhodamine 101. The dansyl moiety serves as the energy donor, and a very efficient ring-opening reaction induced by Fe(III) generates the long-wavelength rhodamine 101 fluorophore that can act as the energy acceptor. This strategy provides a ratiometric fluorescent sensor for Fe³⁺, allowing for a large shift (225 nm) between donor excitation and acceptor emission, which rules out any influence of excitation backscattering effects on fluorescence detection. It selectively responds to Fe³⁺ by dual color and fluorescence changes in the red spectral region.

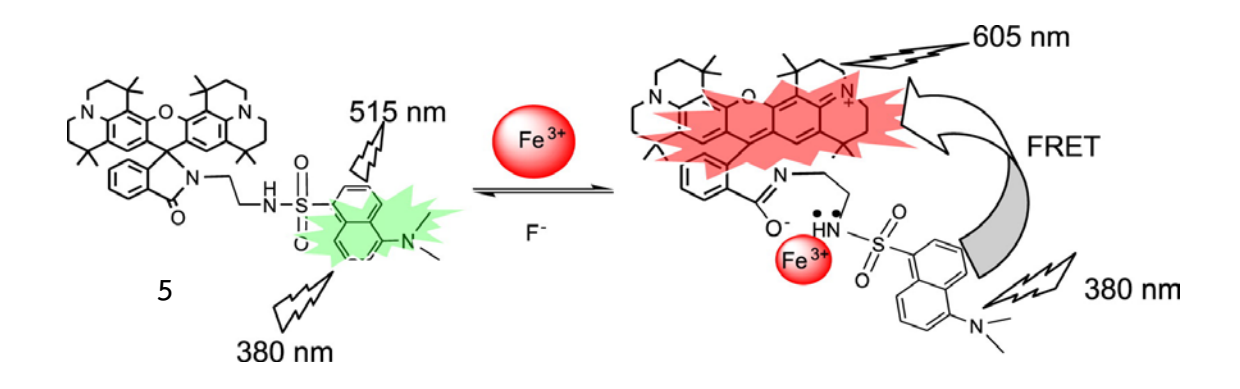


Figure 4. Proposed mechanism for FRET of 5 upon addition of Fe³⁺.

Our previous work showed a reversible-ditopic fluorescent and colorimetric chemosensor based on RhBs used as an Em-FRET ditopic receptor, which combined energy donor from excimer emission (naphthalene excimer) and energy acceptor from dye absorption (rhodamine dve). As shown in Figure 5a, addition of Cu²⁺ ions to a solution of 6 induced a ring-open conformation of spirolactam (Em-FRET ON), whilst ring closure was induced upon addition of CH₃COO⁻ (Em-FRET OFF) [17]. In addition, It is known that the sensitivity and specificity can be enhanced by increasing the number of binding sites of chemosensor. In order to improve the selectivity of chemosensor, nitrogen donor atoms and thiourea group has been introduced into the structure of chemosensor. 6b and 6c were designed and synthesized based on excimer-fluorescent resonance energy transfer (E_m-FRET), combined with energy donor from excimer emission (naphthalene excimer) and energy acceptor from dye absorption (rhodamine dye) (6b) and fluorescent chemosensor (6c) (Figure 5b). The sensitivity and specificity enhancement were observed with increased the number of binding sites of chemosensor 6b and 6c comparing with 6. The complexes of 6b and 6c with anions in the presence and absence of Cu²⁺ exhibited positive cooperativity, which indicates that the complex formation with the Cu²⁺ cation results in increase of ligand affinity for the anion [18].

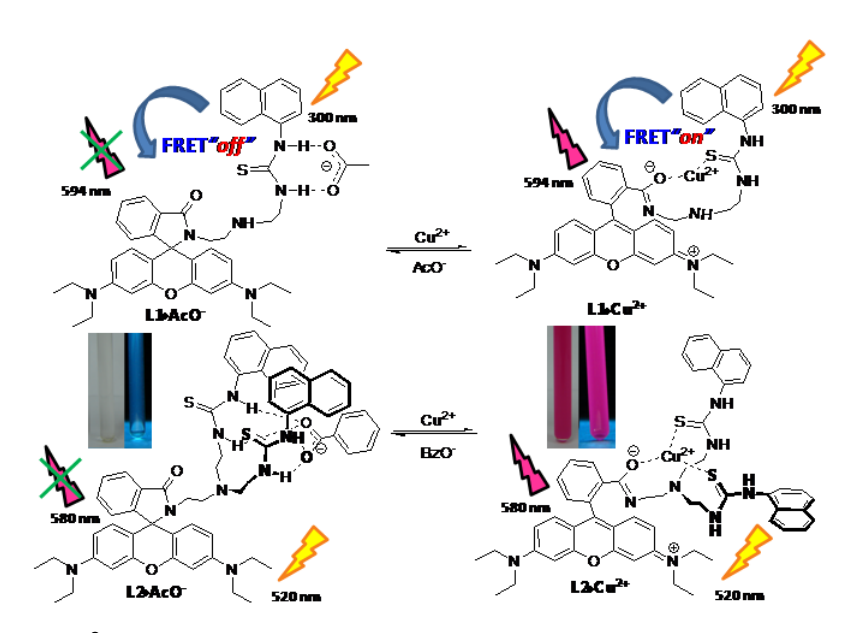


Figure 5. Proposed Cu²⁺-promoted ring opening and CH₃COO⁻-promoted ring closing of spirolactam on RhBs.

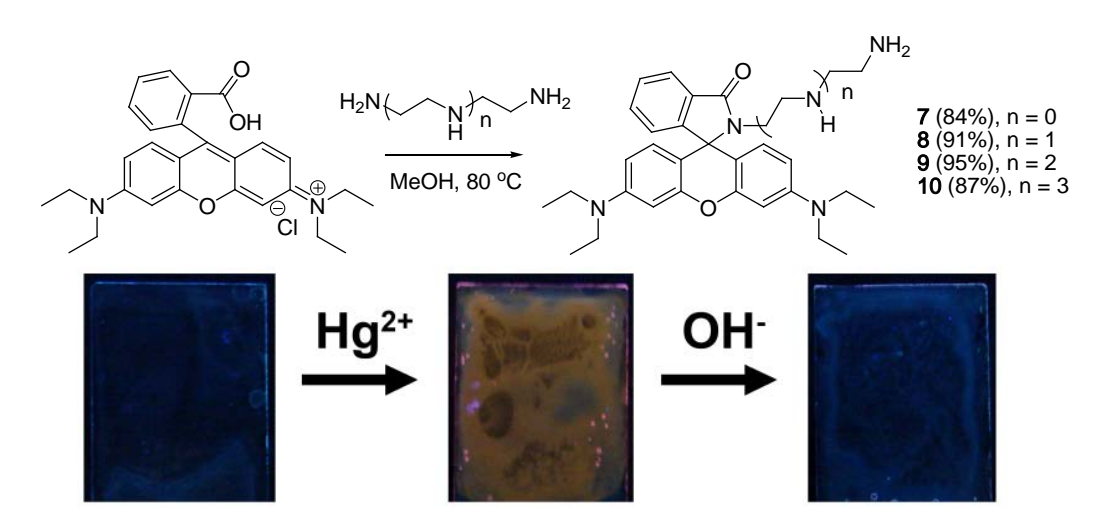


Figure 6. Chemical structures of compound **7-10** and Fluorescence image of poly(methyl methacrylate) polymer sheets doped with ligand **8**. The polymer film on the glass slide was irradiated with a hand-held UV lamp at 360 nm

In 2010 [19], we reported the rhodamine-based reversible chemosensor (**7-10**) which could bind Hg²⁺ with detectable change in color. Upon the addition of Hg²⁺, an overall emission change of 350-fold was observed, and the selectivity was calculated to be 300 times higher than Cu²⁺ for receptors **8–10**. A polymeric thin film can be obtained by doping poly(methyl methacrylate) or PMMA with chemosensor **8**. Such a thin film sensor can be used to detect Hg²⁺ with high sensitivity and can be recovered using diluted NaOH (Figure 6).

Figure 7. Perspective binding interactions of 12 with Fe³⁺ ions

A new rhodamine based probes **11** for the detection of Fe³⁺ were synthesized and their selectivity towards Fe³⁺ ions in the presence of other competitive metal ions were tested. The probe **11** formed a coloured complex with Fe³⁺ as well as Cu²⁺ ions and revealed the lack of adequate number of coordination sites for selective complexation with Fe³⁺. However, probe **11** displayed Fe³⁺ selective complex formation even in the presence of other competitive metal ions, Figure 7 [20].

In 2014, a new rhodamine-based FRET platform (FRET-1) is used to develop a ratiometric fluorescent Cu²⁺ probe (Figure 8). The novel Cu²⁺ probe exhibits several favorable features including a large variation in the emission ratio, well-resolved emission peaks, high sensitivity, and high selectivity. Importantly, it is suitable for fluorescence imaging in living cells [21].

Figure 8. Cu²⁺-promoted hydrolysis of FRET-1 to FRET-dyad.

Liu and co-worker designed and synthesized a water-soluble "turn-on" fluorescent probe (13) for Fe³⁺ based on rhodamine B. The fluorescent probe showed "turn-on" fluorescent and colorimetric responses to Fe³⁺ with a high selectivity in water containing less than 1% organic co-solvent (Figure 9). Furthermore, bioimaging investigations indicated that the new

probe was cell permeable and suitable for monitoring intracellular Fe³⁺ in living cells by a confocal microscopy [22].

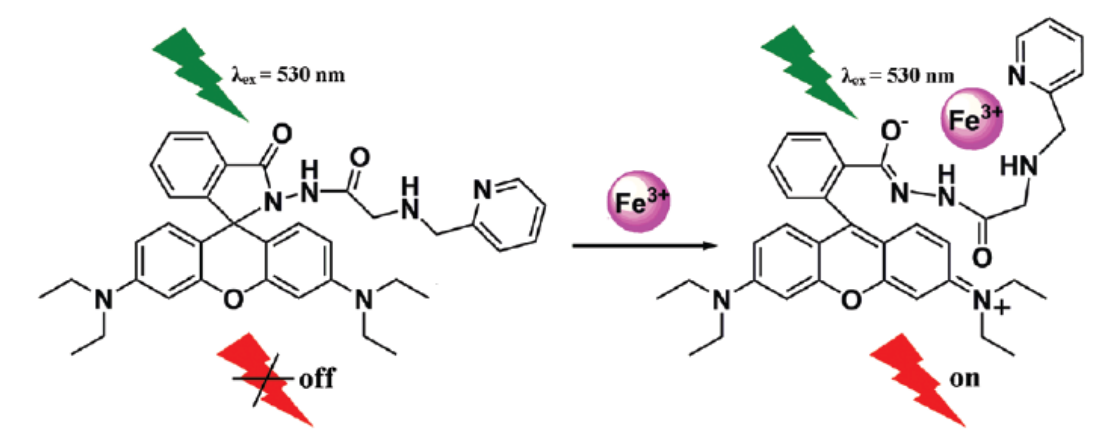


Figure 9. The design of 13 for Fe³⁺ detection.

Surface modification by grafting polymer chains to a suitable substrate is a useful method to manufacture materials which possess specific surface and structural properties. These products can be used in numerous applications such as chromatographic resins or biocompatible materials. Recently, *p-t*-butyl calix[4]arene diol (distal cone) was grafted on poly(acrylic acid) (PAA) to obtain hydrophobically modified PAA (PAA-C) bearing calixarene moieties (Figure 10). The extraction ability measurements of modified PAA toward alkali metal cations (Na⁺, K⁺, Cs⁺) and Ag⁺ showed a remarkable efficiency and selectivity of PAA-C toward Na⁺ [23].

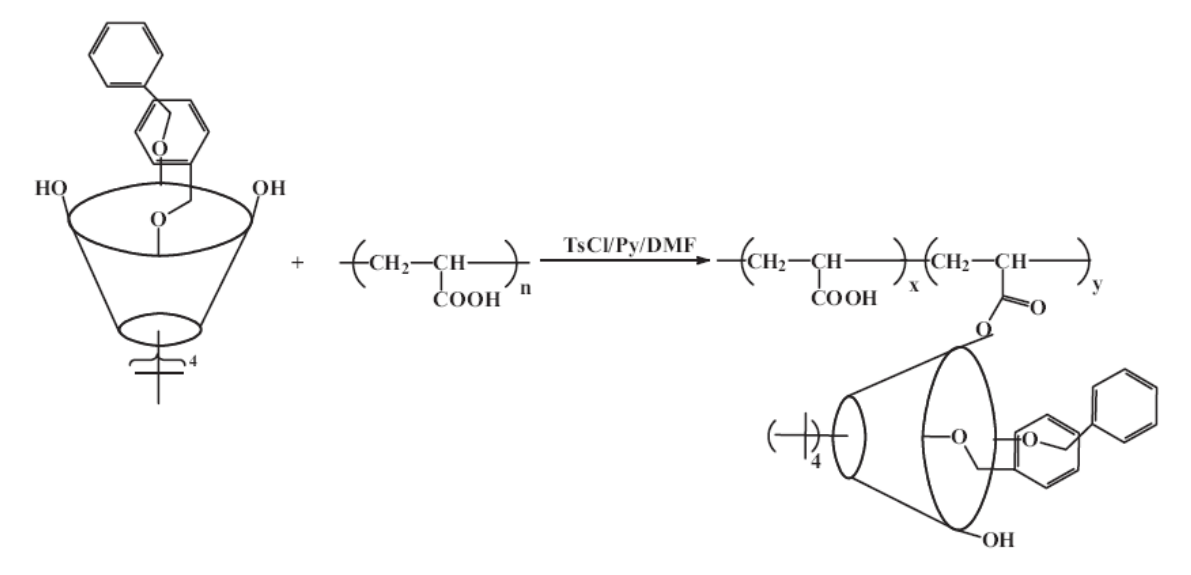


Figure 10. Chemical structures of p-t-Butyl calix[4]arene diol (distal cone) was grafted with poly (acrylic acid) (PAA)

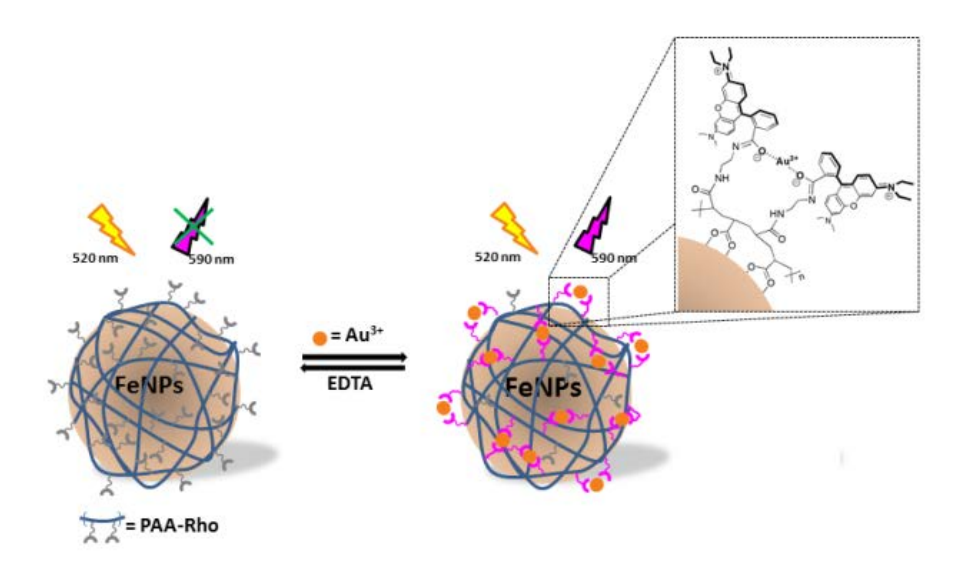


Figure 11. Proposed selective detection mechanism of Au³⁺ by using rhodamine-based modified polyacrylicacid (**PAA-Rho**)-coated FeNPs

Recently, we have investigated a selective detection of Au³⁺ by using rhodamine-based modified polyacrylic acid (PAA) sensors. Polymeric sensors were simply prepared by amidation reactions between PAA and various mole ratios of rhodamine. Chemical structures and purity of polymeric sensors were proven by TGA, NMR, TEM and IR. It was found that polymeric sensor **PAA-Rho2** exhibited the highest selectivity and sensitivity responsive colorimetric and fluorescence Au³⁺-specific sensor over other metal ions. The polymeric sensors were non-fluorescence in the spirolactam form and were selectively converted to the fluorescence-active ring-opened amide form in the presence of Au³⁺ ions lead to fluorescence enhancement and colorimetric change (Figure 11). Moreover, the FeNPs-based polymeric sensor **PAA-Rho2-FeNPs** were designed and synthesized. The Au³⁺ chelation-induced aggregation of FeNPs resulted in TEM, color and fluorescence changed and the sensor properties could be restored using the EDTA solution [24].

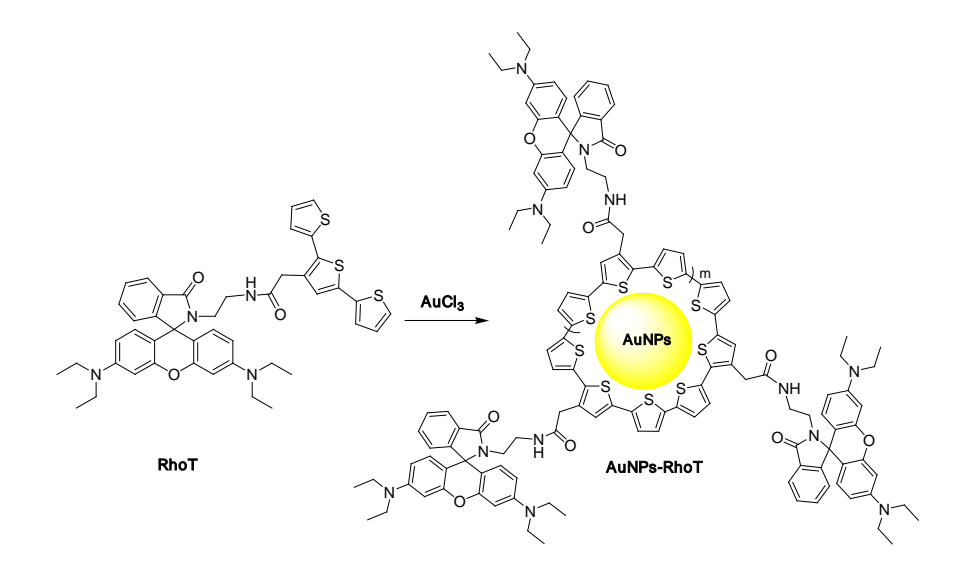


Figure 13. In situ hybrid gold nanoparticles sensors (AuNPs-RhoT) for Hg²⁺

In 2014, the in situ formation of gold nanoparticle/conducting polymer nanocomposite based-chemosensors (**AuNPs-RhoT**) was achieved to explore the sensitive and selective detection of Hg²⁺ in aqueous solution over 12 other metal ions using a colorimetric technique. The hybrid sensor became aggregated in solution in the presence of Hg²⁺ by an ion-templated chelation process as demonstrated in Figure 13 [25].

Although many fluorescence chemosensors for heavy metals have been reported, some systems exhibited limited features in their practical use such as poor aqueous solubility, low sensitivity and selectivity, short emission wavelengths, and/or weak fluorescence intensities. Thus, the development of novel practical assays for heavy metals remains a challenge, and polymeric sensors are one choice to increase a sensitivity and selectivity to detect heavy metals. Receptor-based conducting polymers (CPs) are one class of materials that have been successfully utilized in the development of molecular-based sensoring materials. Carbazole are widely investigated as a monomer to produce conducting polymeric sensors because carbazole units can be modified as a π -conjugated polycarbazole by electropolymerization to produce a conjugated polymeric sensor for cation sensing. For example, demonstrated new conjugated polymer network hexahomotriazacalix[3]arene-carbazole, that has been synthesized and electrochemically cross-linked to form ultrathin films using cyclic voltammetry. The incorporation of hexahomotriazacalix[3]arene moiety as a neutral cation-binding receptor into a conjugated polycarbazole network facilitates high selectivity and sensitivity for Zn²⁺ as shown in Figure 14 [26].

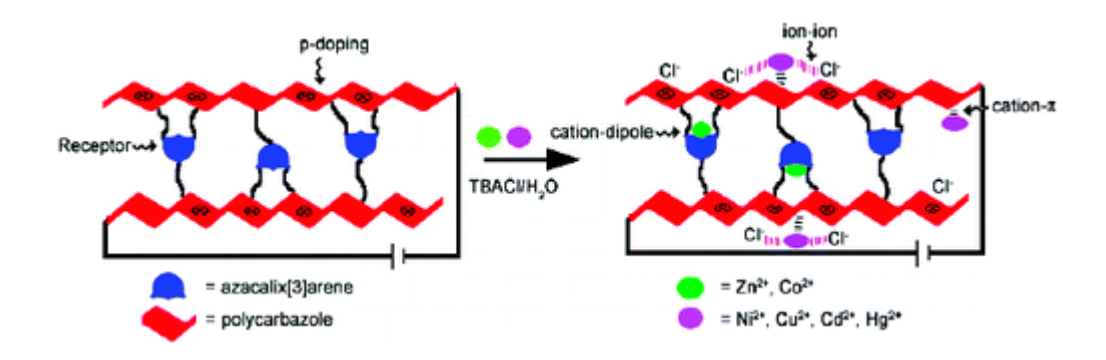


Figure 14. Conjugated polyhexahomotriazacalix[3]arene-carbazole for cation sensing

Recently, we have designed and synthezised an ion-responsive sensory material based on a rhodamine-appended polyterthiophene by electrochemical crosslinking of monomer **RhoT**. The incorporation of rhodamine moiety as a neutral cation-binding receptor into a conjugated polyterthiophene network facilitates high selectivity and sensitivity for Hg^{2+} (Figure 15). The conducting polymeric sensors, **PRhoT**, showed a highest selectivity ($\Delta E = -0.05 \text{ V}$) toward Hg^{2+} over other cations. After placing the sensor into the EDTA solution, the free sensor could be restored. The limit of detection of PRhoT for Hg^{2+} was 0.10 μ M which was lower than that observed using **AuNPs-RhoT** (0.32 μ M) and **RhoT** (1.34 μ M) and the detection time was less than 30 seconds [27].

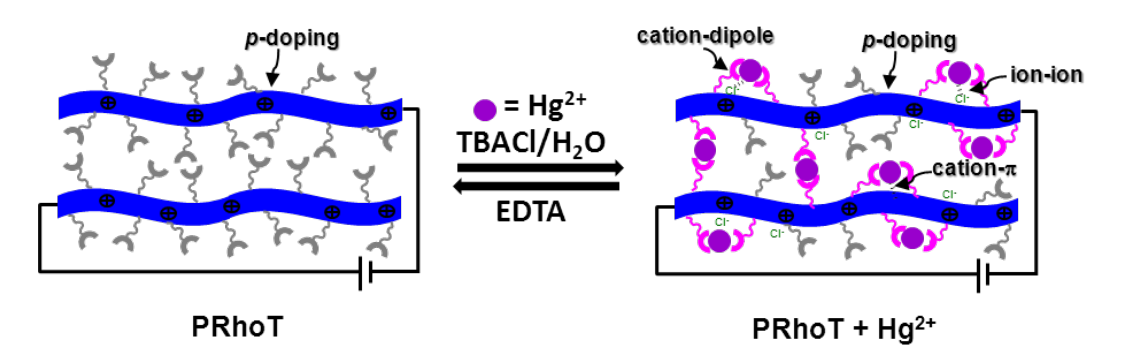


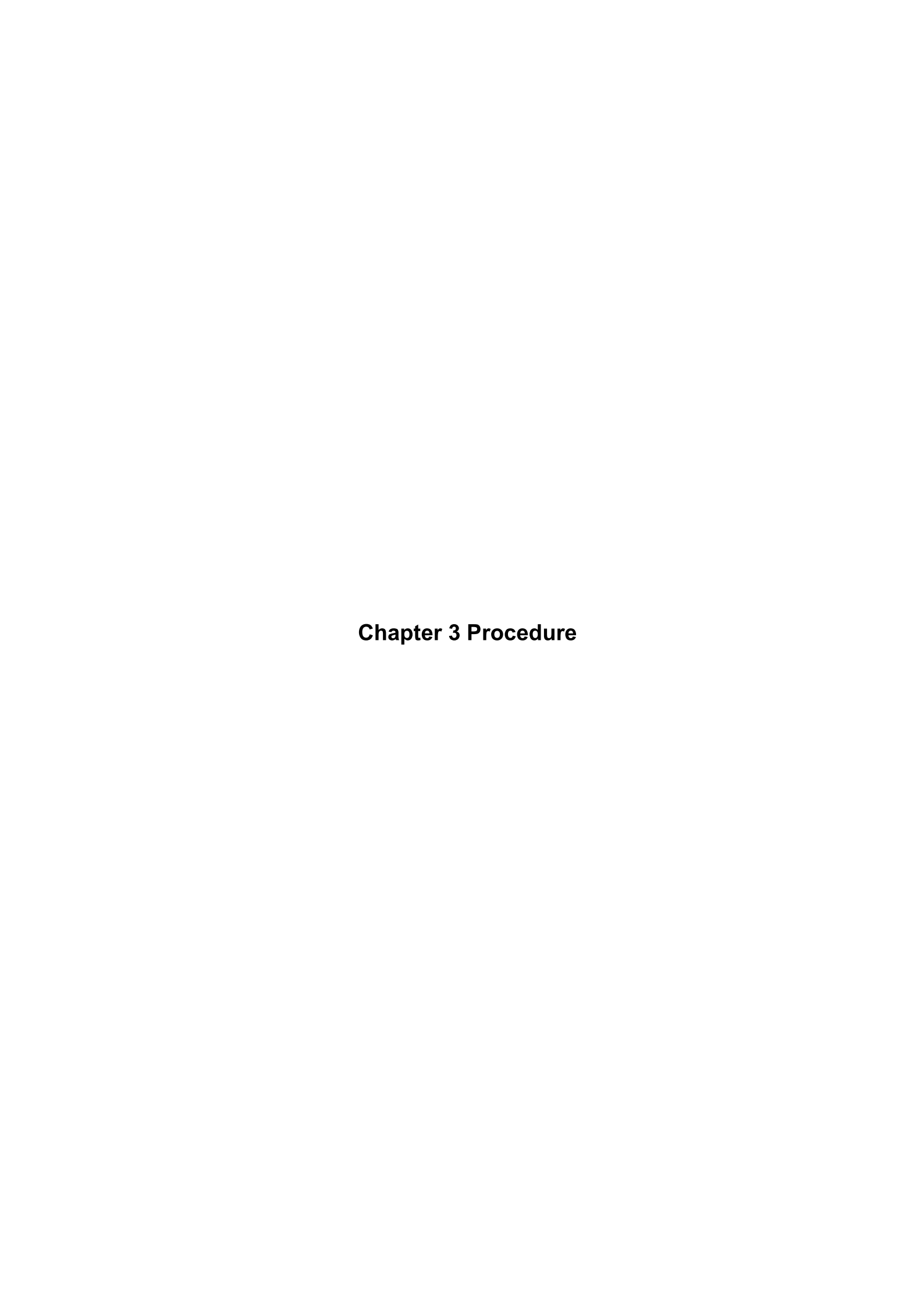
Figure 15. The conjugated polymer-based (PRhoT) chemosensors for Hg²⁺

Since the commercial availability and industrial importance of PAA and PSS as well as the ease of preparation of rhodamines in large scale, we selected rhodamine derivatives as a good ionophore and distributed this compound in the PAA and PSS chains to make both fluorescent and chemo-nanosensors. In this proposal, we would like to address 4 topics of the research.

1. From the literature mentioned above, different functional groups appended on rhodamine backbones allow different binding preference to various metal ions. Our target

sensors are designed to contain rhodamine moieties as cation biding sites and PAA and PSS as backbones to make multiple cation binding sites sensors.

- 2. To further apply compounds **PAA-Rho1-4** and **PSS-Rho1-4** as the polymeric thin film sensors for heavy metal.
- 3. To develop a solvatochromic rhodaminebased sensor using commercially available rhodamine simply dissolved in THF to produce rhodamine lactone (**RhoL**) via the rhodamine lactone–zwitterion equilibrium for heavy metal sensor.
- 4. To expose the simple way for preparation and response features of a new highly sensitive optical sensor by immobilization of rhodamine derivative on agarose hydrogel as a gold probe
- 5. To develop a pH optical and fluorescent sensor based on rhodamine modified on activated cellulose paper



3.1 Equipments and Chemicals

Equipments

- 1. Nuclear Magnetic Resonance Spectrometer (NMR), Varian Mucury 400 MHz
- 2. Rotary vacuum evaporator (Rotavapor R-210)
- 3. Fourier Transform IR Spectrometer, Nicolet Impact 410, USA
- 4. UV-Visible Spectrophotometer (Perkin Elmer Lambda 25)
- 5. Perkin Elmer LS 50 B Luminescence Spectrometer
- 6. Magnetic Stirrer

Chemicals

- 1. acetone
- 2. acetonitrile
- 3. buthylamine
- 4. chloroform
- 5. d -CDCl₃
- 6. d_3 -CD₃CN
- 7. d_6 -DMSO
- 8. dichloromethane
- 9. dimethylsulfoxide (DMSO)
- 10. ethanol
- 11. ethylacetate
- 12. ethylenediamine
- 13. hexane
- 14. hydrochloric acid
- 15. methanol
- 16. naphthalene isothiocyanate
- 17. pyridine
- 18. rhodamine B
- 19. sea sand, Riedel deHaen
- 20. silica gel, particle size: (70-230 mesh ASTM), Merck, Germany
- 21. sodium hydroxide
- 22. sodium sulfate, anhydrous
- 23. TLC Alumnium sheets Silica gel F254 pre-coated, Merck, Germany
- 24. tetrahydrofuran (THF)
- 25. metals

All reagents were standard analytical grade and used without further purification. Commercial grade solvents, such as acetone, hexane, dichloromethane, methanol and ethyl acetate, were distilled before use. MeCN was dried over CaH2 and freshly distilled under a nitrogen atmosphere prior to use.

3.2 Synthesis of N-(rhodamine B)lactam-derivatives (L1-L4)

They were synthesized by adapting the synthesis procedure of similar compounds reported in the literatures. Hodamine B (0.20 g, 0.42 mmol) was dissolved in 30 mL of ethanol and ethylenediamine, diethylenetriamine, triethylenetetraamine and tetraethylenepentaamine (0.22 mL, excess) were added dropwise to the solution and refluxed overnight (24 hours) until the solution lost its red color. The solvent was removed by evaporation. Water (20 mL) was added to the residue and the solution was extracted with CH₂Cl₂ (20 mL × 2). The combined organic phase was washed twice with water and dried over anhydrous Na₂SO₄. The solvent was removed by evaporation, and the product was dried in vacuo, affording a pale-yellow solid of **L1-L4**.

L1: (0.17 g, yield 84%). ¹H NMR (400 MHz, CDCl₃) δ 7.86 - 7.81 (m, 1H, Ar*H*), 7.45 - 7.32 (m, 2H, Ar*H*), 7.08 - 7.03 (m, 1H, Ar*H*), 6.42 (s, 1H, Ar*H*), 6.39 (s, 1H, Ar*H*) 6.37 (s, 2H, Ar*H*), 6.38 - 6.21 (m, 2H, Ar*H*), 3.32 (q, J = 6.8 Hz, 8H, NC H_2 CH₃), 3.12 (t, J = 6.8 Hz, 2H, NC H_2 CH₂), 2.23 (t, J = 6.8 Hz, 2H, NC H_2 CH₂NH₂), 2.05 (s, 2H, CH₂CH₂NH₂) and 1.16 (t, J = 7.2 Hz, 12H, NCH₂CH₃). MS (MALDI-TOF); Calcd for [C₃₀H₃₆N₄O₂][†]: m/z 484.28. Found: m/z 485.91 [M + H][†].

L2: (0.20 g, yield 91%). ¹H NMR (400 MHz, CDCl₃) δ 7.90 - 7.88 (m, 1H, Ar*H*), 7.44 - 7.42 (m, 2H, Ar*H*), 7.09 - 7.07 (m, 1H, Ar*H*), 6.43 (s, 1H, Ar*H*), 6.41 (s, 1H, Ar*H*) 6.37 (s, 2H, Ar*H*), 6.28 - 6.25 (m, 2H, Ar*H*), 3.32 (q, J = 6.8 Hz, 8H, NC H_2 CH₃), 3.26 (t, J = 6.8 Hz, 2H, NC H_2 CH₂), 2.59 (t, J = 6.0 Hz, 2H, NC H_2 CH₂NH), 2.44 -2.38 (m, 4H, NCH₂C H_2 NH), 1.70 (s, 3H, NCH₂CH₂N*H* and CH₂CH₂N H_2) and 1.16 (t, J = 7.2 Hz, 12H, NCH₂C H_3). MS (MALDITOF); Calcd for [C₃₂H₄₁N₅O₂][†]: m/z 527.33. Found: m/z 528.95 [M + H][†].

L3: (0.23 g, yield 95%). ¹H NMR (400 MHz, CDCl₃) δ 7.89 - 7.88 (m, 1H, Ar*H*), 7.48 - 7.43 (m, 2H, Ar*H*), 7.08 (s, 1H, Ar*H*), 6.43 - 6.39 (m, 3H, Ar*H*), 6.37 (s, 1H, Ar*H*), 6.28 - 6.26 (m, 2H, Ar*H*), 3.32 (q, J = 6.8 Hz, 8H, NC H_2 CH₃), 3.28 - 2.3 (m, 12H, NC H_2 CH₂, NC H_2 CH₂NH and NCH₂CH₂NH), 2.04 (s, 4H, NCH₂CH₂NH and CH₂CH₂NH₂) and 1.16 (t, J = 7.2 Hz, 12H,

NCH₂CH₃). MS (MALDI-TOF); Calcd for $[C_{34}H_{46}N_6O_2]^+$: m/z 570.37 Found: m/z 572.02 [M + H] $^+$.

L4: (0.22 g, yield 87%). ¹H NMR (400 MHz, CDCl₃) δ 7.82 - 7.81 (m, 1H, Ar*H*), 7.38 - 7.36 (m, 2H, Ar*H*), 7.15 (s, 1H, Ar*H*), 6.37 - 6.34 (m, 2H, Ar*H*), 6.30 (s, 2H, Ar*H*), 6.21 - 6.19 (m, 2H, Ar*H*), 3.25 (q, J = 6.8 Hz, 8H, NC H_2 CH₃), 3.20 - 2.1 (m, 21H, NC H_2 CH₂, NC H_2 CH₂NH, NCH₂CH₂NH and CH₂CH₂NH₂) and 1.09 (t, J = 7.2 Hz, 12H, NCH₂CH₃). MS (MALDI-TOF); Calcd for [C₃₆H₅₁N₇O₂][†]: m/z 613.41 Found: m/z 615.86 [M + H][†].

Scheme 3.1 The synthesis of receptor L1-L4

3.3 Synthesis of polymeric sensors (PAA-Rho1 – PAA-Rho4)

Typically, a mixture of *N*-(rhodamine B)lactam-derivative (**Rho**) and PAA in 20 mL of dried DMF was allowed to react in the presence of DCC and DMAP. The resulting mixture was heated to 50 °C for 1 hour and then heated at reflux overnight. The mixture was cooled down to the room temperature, and the product was precipitated by adding an excess of water. The above dissolution-precipitation cycle was repeated for three times. After drying in vacuo over overnight at 45°C, **PAA-Rho1** –**PAA-Rho4** were obtained as pale-yellow solids.

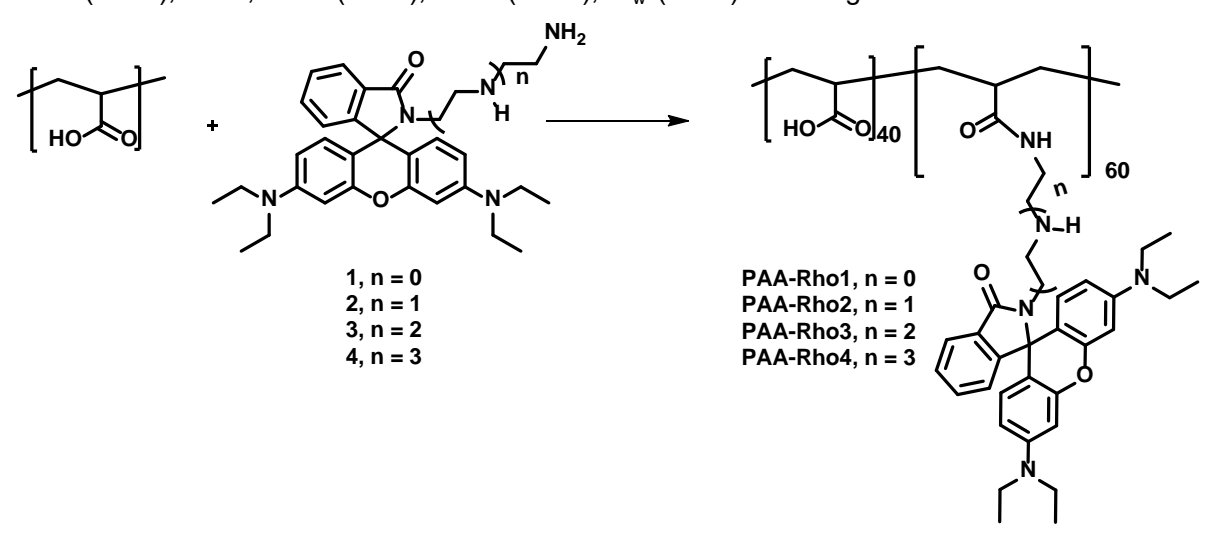
PAA-Rho1 (0.121 g): **Rho1** 0.389 g, 0.802 mmol; PAA 0.040 g; DCC 0.165 g, 0.801 mmol; DMAP 0.049 g, 0.400 mmol.. 1 H NMR (400 MHz, DMSO- d_{6}): 7.93 (bs, NHCO), 7.81 (m, ArH), 7.48 (bs, ArH), 7.02-6.94 (bs,ArH), 6.41-6.20 (bs, ArH), 5.57 (d, J=8Hz, ArH), 3.23-2.15 (m, NHCH₂CH₂), 1.72-1.44 (m, CHCH₂), 1.27-1.16 (m, NCH₂CH₃), and 1.11-0.87 (m, NCH₂CH₃);

IR spectrum (KBr, (cm⁻¹)): 3632-3415 (OH), 3320 (NH), 2968 (=C=H), 2934, 2850 (=C=H), 1684 (C=O), 1625, 1571 (C=C), 1217 (C=O); M_w (NMR) = 5154 g.mol⁻¹.

PAA-Rho2 (0.123 g): **Rho2** 0.422 g, 0.800 mmol; PAA 0.040 g; DCC 0.165 g, 0.800 mmol; DMAP 0.049 g, 0.400 mmol. 1 H NMR (400 MHz, DMSO- d_{6}):7.93 (bs, NHCO), 7.74-7.60 (m, ArH), 7.46 (bs, ArH), 7.06-6.79 (bs, ArH), 6.40-6.02 (bs, ArH) 5.55 (d, J = 8Hz, ArH),3.20-2.95 (m, NHC H_{2} CH₂), 1.79-1.41 (m, CHC H_{2}), 1.29-1.14 (m, NC H_{2} CH₃),and 1.11-0.61 (m, NC H_{2} CH₃); IR spectrum (KBr, (cm⁻¹)): 3593-3435 (OH), 3327 (NH), 2953 (=C—H), 2934, 2850 (—C—H), 1630 (C=O), 1576, 1443 (C=C), 1250 (C—O); M_w (NMR) = 3792 g.mol⁻¹.

PAA-Rho3 (0.086 g): **Rho3** 0.212 g, 0.370 mmol; PAA 0.023 g; DCC 0.078 g, 0.37 mmol; DMAP 0.023 g, 0.190 mmol. 1 H NMR (400 MHz, DMSO- d_{6}): 7.92 (bs, NHCO), 7.75 (bs, ArH), 7.49 (bs, ArH), 7.05-6.89 (bs, ArH), 6.38-6.11 (bs, ArH) 5.58 (d, J = 8Hz, ArH), 3.32-1.96 (m, NHC H_{2} CH $_{2}$), 1.76-1.38 (m, CHC H_{2}), 1.27-1.11 (m, NC H_{2} CH $_{3}$), and 1.10-0.85 (m, NCH $_{2}$ CH $_{3}$); IR spectrum (KBr, (cm $^{-1}$)): 3641-3401 (OH), 3327 (NH), 2978 (=C-H), 2929, 2855 (-C-H), 1679 (C=O), 1624, 1522 (C=C), 1221 (C-O); M_w (NMR) = 4923 g.mol $^{-1}$.

PAA-Rho4 (0.110 g): **Rho4** 0.363 g, 0.592 mmol; PAA 0.030 g; DCC 0.122 g, 0.592 mmol; DMAP 0.036 g, 0.296 mmol. ¹H NMR (400 MHz, DMSO- d_6): 8.19 (bs, NHCO), 7.74 (bs, ArH), 7.49 (bs, ArH), 7.01 (bs, , ArH), 6.43-6.21 (bs, ArH) 5.55 (d, J = 8Hz, ArH), 3.20-2.04 (m, NHC H_2 C H_2), 1.76-1.39 (m, CHC H_2), 1.30-1.12 (m, NC H_2 C H_3) and 1.12-0.57 (m, NCH $_2$ C H_3); IR spectrum (KBr, (cm⁻¹)): 3637-3415 (OH), 3332 (NH), 2978 (=C-H), 2929, 2850 (-C-H), 1630 (C=O), 1570, 1516 (C=C), 1246 (C-O); M_w (NMR) = 4720 g.mol⁻¹.



Scheme 3.2 The synthesis of receptor PAA-Rho1 – PAA-Rho4

3.4 Synthesis of polymeric sensors (PSS-Rho1 – PSS-Rho4)

Typically, a mixture of **Rho** and PSS in 30 mL of dried DMF was allowed to react in the presence of EDC and DMAP. The resulting mixture was heated to 60°C for 1 h and heated at reflux for 5 days. Then, the product was cooled to room temperature and the product was precipitated by adding an excess of water. The above dissolution–precipitation cycle was repeated three times. After drying *in vacuo* overnight at 45°C, **PSS-Rho1** – **PSS-Rho4** were obtained as pale-yellow solids.

PSS-Rho1; **Rho** 0.18 g, 0.3 mmol; PSS 0.20 g; EDC 0.15 g, 0.7 mmol; DMAP 0.04 g, 0.3 mmol.

PSS-Rho2; **Rho** 0.19 g, 0.4 mmol; PSS 0.20 g; EDC 0.11 g, 0.6 mmol; DMAP 0.03 g, 0.3 mmol

PSS-Rho3; **Rho** 0.20 g, 0.6 mmol; PSS 0.20 g; EDC 0.17 g, 0.9 mmol; DMAP 0.05 g, 0.4 mmol.

PSS-Rho4; (0.07 g). **Rho** 0.20 g, 0.4 mmol; PSS 0.10 g; EDC 0.12 g, 0.6 mmol; DMAP 0.03 g, 0.3 mmol. 1 H NMR (400 MHz, DMSO) $\overline{\mathbf{O}}$ 7.96 (s, 1H), 7.52 (s, 1H), 7.02 (s, 22H), 2.27 (d, J = 32.8 Hz, 59H), 2.86 (m, 2H), 2.72 (s, 1H), 2.50 (s, 1H), 2.45 (s, 41H), 1.06 (s, 8H). IR: v = 3250 cm⁻¹(OH), 2971 cm⁻¹ (NH), 1612 cm⁻¹ (C=O), 1320 cm⁻¹ and 1109 cm⁻¹ (S=O). UV-Vis spectra; absorption peak at 280 nm $\overline{\mathbf{\Pi}}$ - $\overline{\mathbf{\Pi}}$ * of rhodamine. Mw (NMR) =103,054.7 g mol⁻¹.

Scheme 3.3 Synthesis of polymeric sensors PSS-Rho1 – PSS-Rho4

3.5 Preparation of the rhodamine lactone (colorless L-form, RhoL)

Rhodamine lactone **(RhoL)** was prepared by our modified method [11]. Briefly, 1.82 mL of 1.1 x 10⁻³ M rhodamine B, 1 mL of 3 N NaOH, 3.18 mL of distilled water and 4 mL of tetrahydrofuran were mixed and then agitated for 2 days.

3.6 Immobilization of RhoL to agarose hydrogel (Arg-RhoL)

Rhodamine B hydrogel was prepared using modified optimal conditions from previous work [1]. Briefly, 0.4 g agarose powder were dissolved in 10 mL of Rhodamine lactone (RhoL) solution followed by boiling in microwave for 30 s. Film casting was done by pouring the above solution into a petri dish and cooling to room temperature for about 1 day. The pH of Arg-RhoL was adjusted by water until the pH of washing becomes 7 and then dried at room temperature for 1 day.

3.7 Sensor response studies of Arg-RhoL

A 1 cm \times 3 cm piece of the **Arg-RhoL** was immersed in 3 mL of 10⁻⁵ M each metal ion solution, then dried overnight at room temperature and placed vertically inside a quartz cell. The absorbance readings were carried out against a blank cell containing a non-immobilized agarose membrane.

3.8 Fabrication of RhoL coated paper

4 μL RhoL (5 mM) in THF solution was dropped on a piece of filter paper (Whattman No.1). The paper was allowed to dry in the air at room temperature until dry before using as paper based cation sensor.

3.9 Complexation studies of ligands by using UV-vis and fluorescence titrations

The complexation abilities of ligands with cations were investigated by spectrophotometric titration in DMSO at 25 °C. 2 mL of the 10 μ M ligand solution was placed in a spectrophotometric cell (1 cm path length). The solutions of cations were added successively into the cell from a microburette. The mixture was stirred for 40 seconds after each addition and its spectral variation was recorded. For UV-vis titration, the stability constants were calculated from spectrometric data using program SIRKO¹⁵. For fluorescent titration, the stability constant for a complex was obtained from a plot of the quantity $I_o/(I_o-I)$ versus 1/[M]. The ratio of intercept/slope gave the stability constant (the fluorescent of free L; I_o , ligand complexed with metal.¹⁶

3.10 Competition experiments

Hg²⁺ was added to the solution containing ligand and the other metal ions of interest. All test solutions were stirred for 1 min and then allowed to stand at room temperature for 30 min. For fluorescent measurements, excitation was provided at 520 nm, and emission was collected from 530 to 700 nm.

3.11 Preparation of the polymeric thin films:¹⁷

Polymethylmethacrylate PMMA polymer (300 mg) was dissolved in dichloromethane, poured onto a clean glass surface and doped with the ligand **L2** (10 μ M). The solvent was evaporated to dryness, and a homogeneous, non-fluorescent polymer sensor film was obtained. This thin film was used for Hg²⁺ detection. For the erasing process, a solution of sodium hydroxide (NaOH) was sprayed onto film. The non-fluorescent thin film was restored.

3.12 Computational studies

The geometrical structures and the HOMO, LUMO energies of the ligand and the ligand + metals complex were calculated using the density functional theory (DFT) method at the B3LYP/6-31(d) theoretical level under the Gaussian 09 program.



Part I: Highly Selective Detection of Au³⁺ Using Rhodaminebased Modified Polyacrylic acid (PAA)-Coated ITO

Scheme 1 Synthetic part ways of PAA-Rho1-PAA-Rho4

New PAA-based sensors for selective detection of Au³⁺ ions were designed and prepared by sucessfully grafting the rhodamine B into the PAA skelaton having alkylene polyamines as a linker. Rhodamine polyamines were used in this sensor fabrication since the carbonyl O and amine N atoms could capture the metal ions via the formation of ion-ion and cation-dipole interactions.²⁰ Also, the condensation rection was used in order to attach rhodamine B to ethylenediamine, diethylenetriamine, triethylenetetraamine, and tetraethylenepentaamine under N₂ with refluxing for 3 days to afford N-(rhodamine B)lactam-derivatives; rhodamine B В ethylenediamine (Rho1), rhodamine В diethylenetriamine (Rho2), rhodamine triethylenetriamine (Rho3), and rhodamine B tetraethylenetriamine (Rho4), respectively. The coupling reaction was subsequently conducted to graft rhodamine derivatives (Rho1-Rho4) onto the PAA backbone via the formation of amide bonds in the presence of DCC/DMAP as coupling reagents under N2 at reflux for 3 days to yield; PAA-Rho1 (84.2%), PAA-Rho2 (80.3%), PAA-Rho3 (91.9%), and PAA-Rho4 (85.1%) (Scheme 2). All materials were thoroughly characterized and proven by TGA, NMR, SEM, and FTIR.

All characterization data of the synthesized polymeric sensors were demonstrated in Figure 1 and S1-S4. The FTIR spectra of polymeric sensors showed aromatic rhodamine peaks at ~1676 and 1443 cm⁻¹, NH amide groups at ~3300 cm⁻¹, and carboxylic PAA peak at

 \sim 3600-3400 cm⁻¹. The TGA curves indicated the decomposition of PAA and rhodamine moieties at \sim 175-298 °C and 308-470 °C, respectively. In addition, the SEM images (Figure 1c, 1d) illustrated increasing of the crystallinity and crystalline sizes attributing to π - π interactions and hydrogen bonding of the rhodamine moieties on the PAA skelaton which was concerned with XRD parttern, exhibited the sharp peaks after modifired-rhodamine (Figure S5). 1 H NMR spectra (Figure S1-S4) also confirmed the formation of polymeric sensor by showing the characteristic signals of -CH₂ and -CH groups in the region of \sim 1.0–2.9 ppm, amide groups at \sim 7.90 ppm and aromatic protons at \sim 7.71-5.57 ppm, respectively.

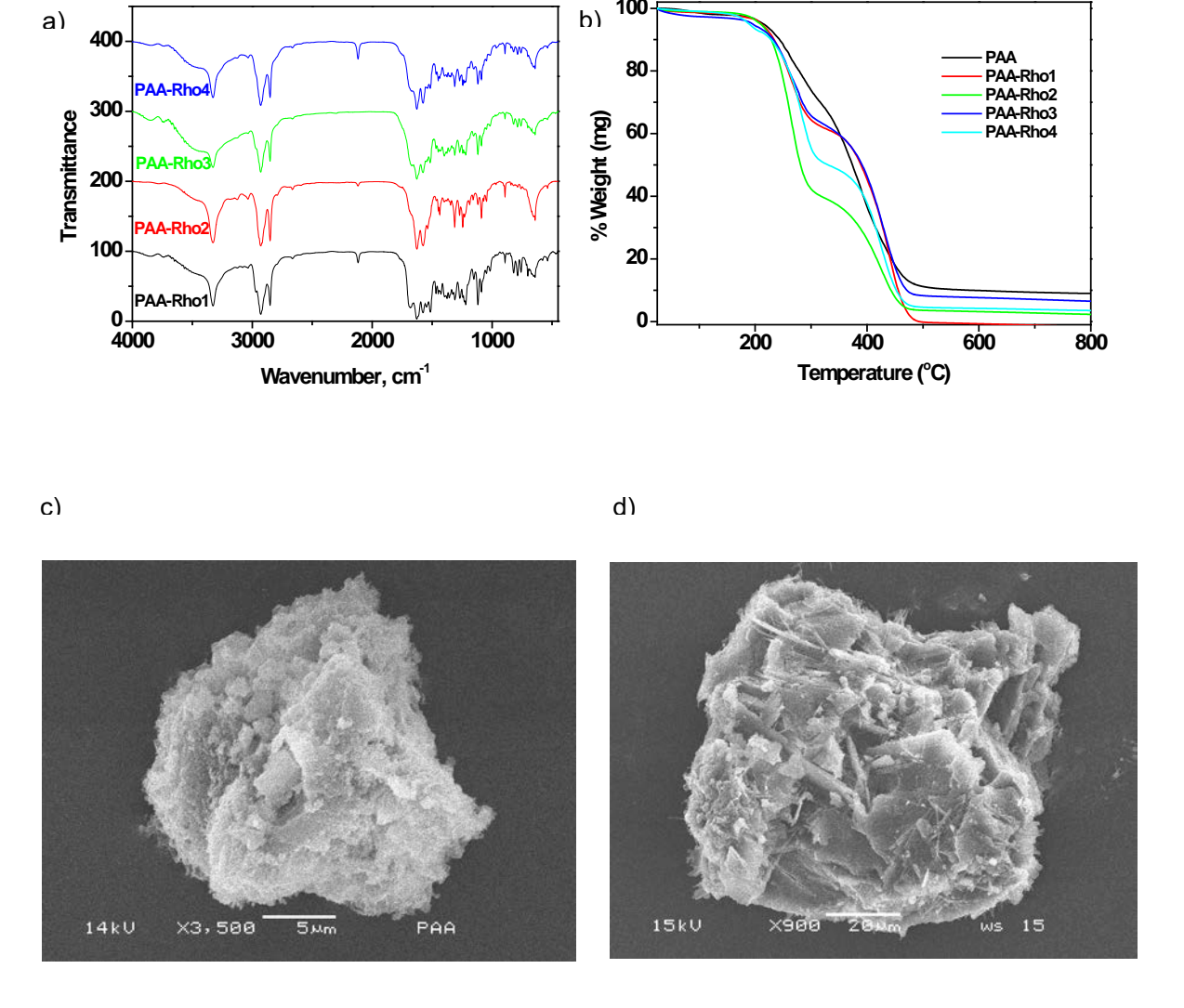
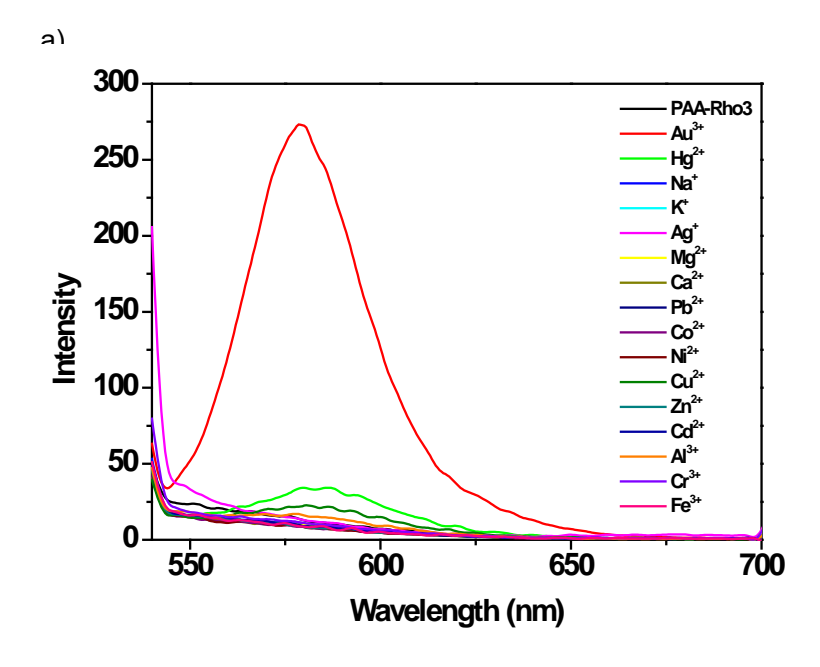


Figure 1. Characterization data of polymeric sensors; (a) FTIR, (b) TGA, (c) SEM (PAA),(d) SEM (PAA-Rho3)

In a similar manner to other rhodamine derivatives, polymeric sensors PAA-Rho1-PAA-Rho4 remained colorless and fluorescence inactive in the DMSO solution. This indicates that the spirolactam form of polymeric sensors predominantly existed in either low or high concentration and was confrimed by the sharp signals in the aromatic protons. Ion-responsive properties of polymeric sensors are firstly investigated by monitoring the fluorescent spectra changes in the mixed organic solutions produced by addition of various metal ions, Au³⁺, Hg²⁺, Na^{+} , K^{+} , Ag^{+} , Mg^{2+} , Ca^{2+} , Pb^{2+} , Co^{2+} , Ni^{2+} , Cu^{2+} , Zn^{2+} , Cd^{2+} , Al^{3+} , Cr^{3+} and Fe^{3+} . Upon addition of 1 μM of cations to a solution of polymeric sensors, only Au^{3+} led to the appearance of a new emission band centered at 590 nm which indicated the opening of the spirolactam ring in polymeric sensors on Au³⁺ coordinationas demonstrated in Figure 2. Remarkable fluorescence enhancements have shown that the highest selectivity and sensitivity for Au³⁺ detection were belong to PAA-Rho3 when compared to other polymerice sensors. This could be explained by the suitable distance, steric hindrance, and the soft property of the receptor structure (PAA-Rho3) to form a complex with Au³⁺. In addition, the excitation of the initial solution of polymeric sensors at 520 nm wavelength did not show any significant emission over the range from 530 to 700 nm (Figure 2). This strongly supports the facts that in absence of metal ions the receptor remains in the spirolactum form, and the non-existence of the highly conjugated xanthene form results in the suppression of emission in the above-mentioned region.



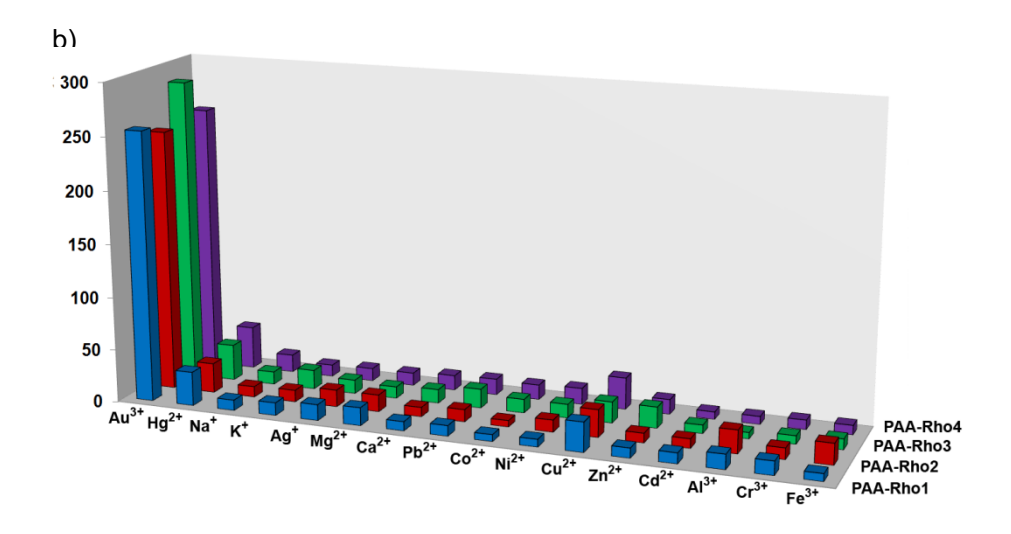
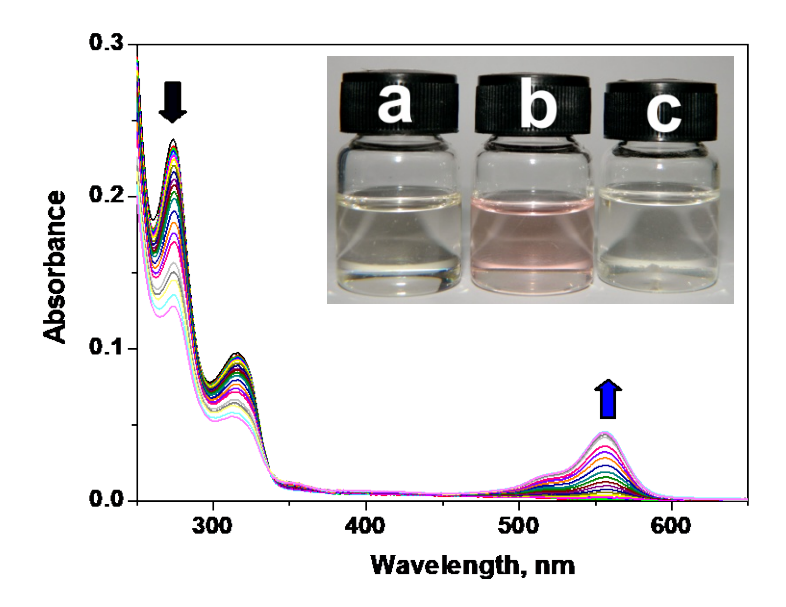


Figure 2. (a) Fluorescence spectral changes of PAA-Rho3 after the addition of 1 μ M of various cations. (b) Fluorescence responses of PAA-Rho1-PAA-Rho4 with 1 μ M of various cations (0.1 g/L of sensors in 0.01 mol/L of TBAPF₆ in DMSO).

To further study an inside into the properties of **PAA-Rho3** as a chemosensor for Au³⁺, the titration of **PAA-Rho3** was performed with increasing the concentration of Au³⁺. A significant enhancement of absorbance intensity in the 500-580 nm wavelength range was obviously observed as a result of the Au³⁺-induced ring opening of the spirolactam form (Figure 3a). The results are also consistent with the selectivity from fluorescent titration. Upon the addition of 10 M Au³⁺, there were changes in the fluorescence spectra of all sensors. Continuous florescence enhancements at 590 nm were monitored (Figure 3b). In addition, the visually color and fluorescence changes were also observed as shown in the inset of Figure 3 and S6. Moreover, the competition experiment was also carried out by adding Au³⁺ to the solution of **PAA-Rho3** in the present of other metal ions in Figure 4. The results indicate that the sensing of Au³⁺ by **PAA-Rho3** is insignificantly affected by these common interfering ions and can be used as a potential Au³⁺-selective chemosensor.



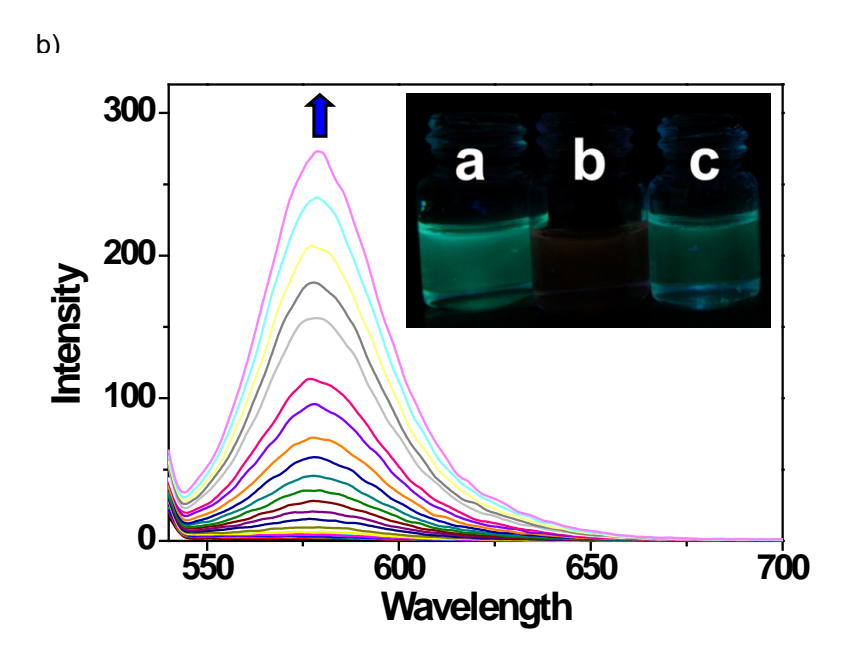


Figure 3. (a) Absorption spectra PAA-Rho3 (0.1 g/L of sensor in 0.01 mol/L of TBAPF₆ in DMSO) in the presence of different amounts of Au³⁺, Inset: the colour changes of (a) PAA-Rho3 and (b) PAA-Rho3 + Au³⁺ (c) PAA-Rho3 + other metal ions. (b) Fluorescence spectra (λ_{ex} =520 nm)of PAA-Rho3 (0.1 g/L) under the same conditions, Inset: the colour changes of (a) PAA-Rho3 and (b) PAA-Rho3 + Au³⁺ (c) PAA-Rho3 + other metal ions.

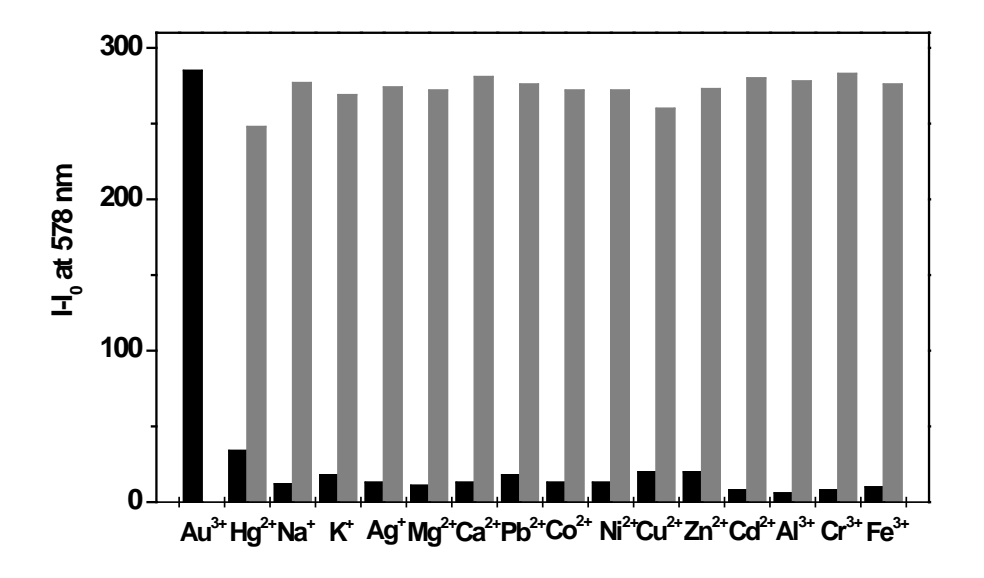


Figure 4.Fluorescence enhancement response of PAA-Rho3 (0.1 g/L) in 0.01 mol/L of TBAPF₆ in DMSO to 1 \square M of different metal ions (the black bar portion) and to the mixture of 1 \square M different metal ions with 10 \square M of Au³⁺ (the gray bar portion).

To prepare the polymeric thin film sensor PAA-Rho3-ITO for using in a real system, PAA-Rho3 was modified on ITO substrat through the amide coupling reaction using DCC and DMAP as coupling reagents. After the solvent was evaporated to dryness, a homogeneous, nonfluorescent polymer sensor film was obtained and subsequently washed with THF and DMF to remove unbound PAA-Rho3. The success of the modification was confirmed by FT-IR and AFM. Figure 5 shows the FT-IR spectra before and after being modified with polymeric sensor. The characteristic peaks at 3528-3290 cm⁻¹ (amide bond) and 2935-2857 cm⁻¹ (rhodamine moities) clearly support that the PAA-Rho3 did bond to the surface.24 The morphology after immobilization on the ITO substrate was characterized by AFM. The result showed that the ultrathin film immobilied on ITO as rougher and patchy films (but complete coverage). The sensing selectivity and sensitivity studies were investigated by open-circuit potentiometry. Changes in potential (ΔE) were simultaneously monitored as a function of time at constant zero-current voltage, which performed using the thin film sensors PAA-Rho3 on ITO against the various concentrations of Au³⁺ in water solution (0.01 M TBACI as supporting electrolyte) as shown in Figure 7. The decreasing of potentials was observed after dipping PAA-Rho3-ITO into the solution of Au3+. The same behaviors were observed in the our previous report. 25 In the lowest concentration of Au $^{3+}$ (10 $^{-7}$ M), the Δ E was suddenly decreased in the first 40 s, followed by a slight decrease until reaching a steadystate, which also observed in the case of other concentrations. The decreasing of potentials implies the increasing of materials conductivity due to metal-induced efficiency of electron transfer on PAA-Rho3-ITO. This result indicates the increasing of the formation of complexation between rhodamine moieties and Au³⁺ through ion-ion and cation-dipole interactions. In addition, changing the colours (pale yellow to pink) and fluorescent are observed on the surface area of PAA-Rho3 on ITO substrate after exposure to the solution of Au³⁺ for 3 min (Figure 8), which results from a ring-opening form of the spirolactam. We also evaluated the reversibility of the above Au³⁺ detection procedure in aqueous solutions treated with aqueous EDTA under basic conditions.²³ As expected, on dipping into the EDTA solution the fuorescence and colour intensity of PAA-Rho3-ITO plus Au³⁺ were quenched. After washing the Au³⁺ and reexposure to Au³⁺, both fuorescence and colour intensity were restored completely. The fuorescence change is reproducible over several cycles of exposure recovery

(Figure S7). According to changes in signaling (Δ E and fluorescence emission) upon adding various Au³⁺ concentration, the limit of detection of **PAA-Rho3-ITO** for Au³⁺ is calculated to be 0.10 μ M,²⁶ which is lower than that observed using uncoated polymeric film **PAA-Rho3** (0.43 μ M) and the detection time is less than 40 seconds. As compared to **PAA-Rho3**, **PAA-Rho3-ITO** sensor gives a lower detection limit and a higher sensitivity toward Au³⁺.

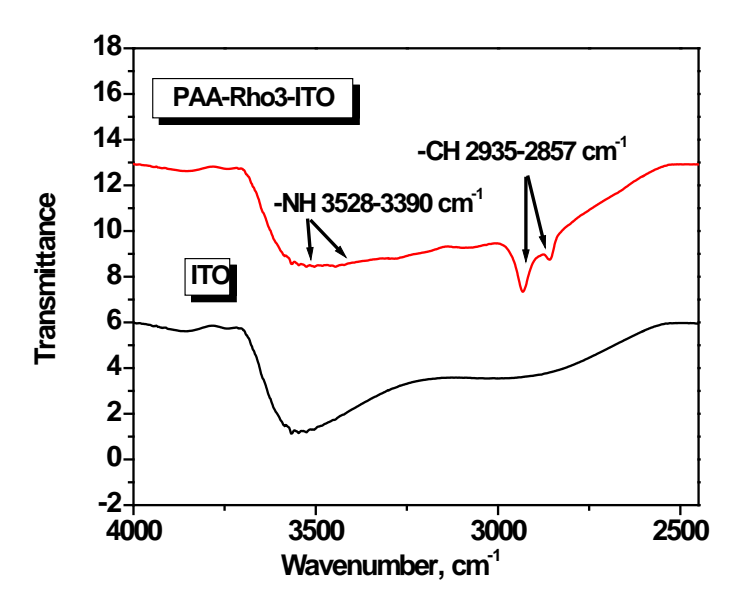


Figure 5. FTIR spectra of the film of PAA-Rho3-ITO on ITO

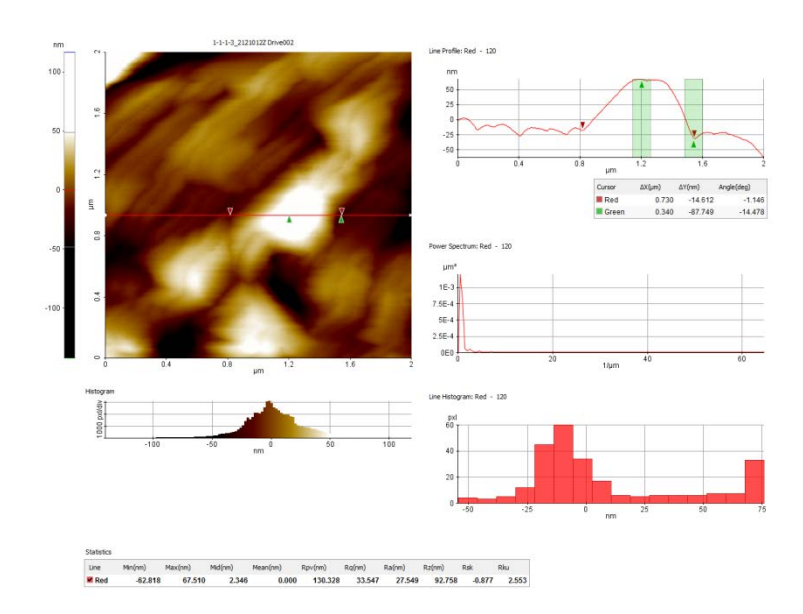


Figure 6. AFM images of the film of PAA-Rho3-ITO

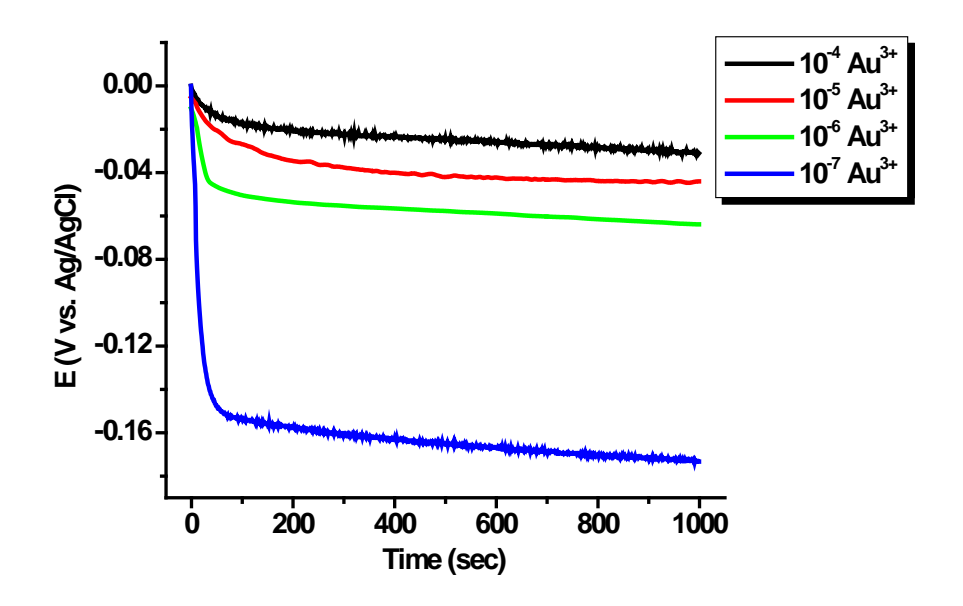


Figure 7. Potentiometric profiles of **PAA-Rho3-ITO** in 0.01 M TBACI aqueous solution which various concentrations of Au³⁺. Plotted data are within 5% deviation from several measurements.

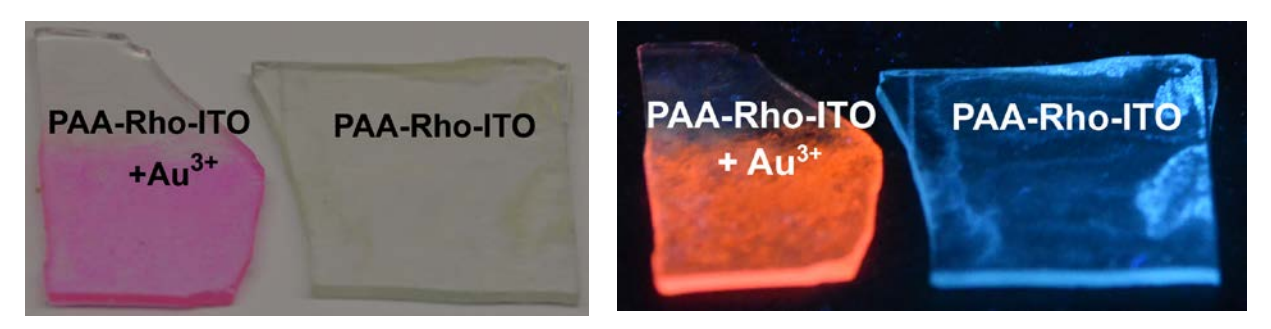
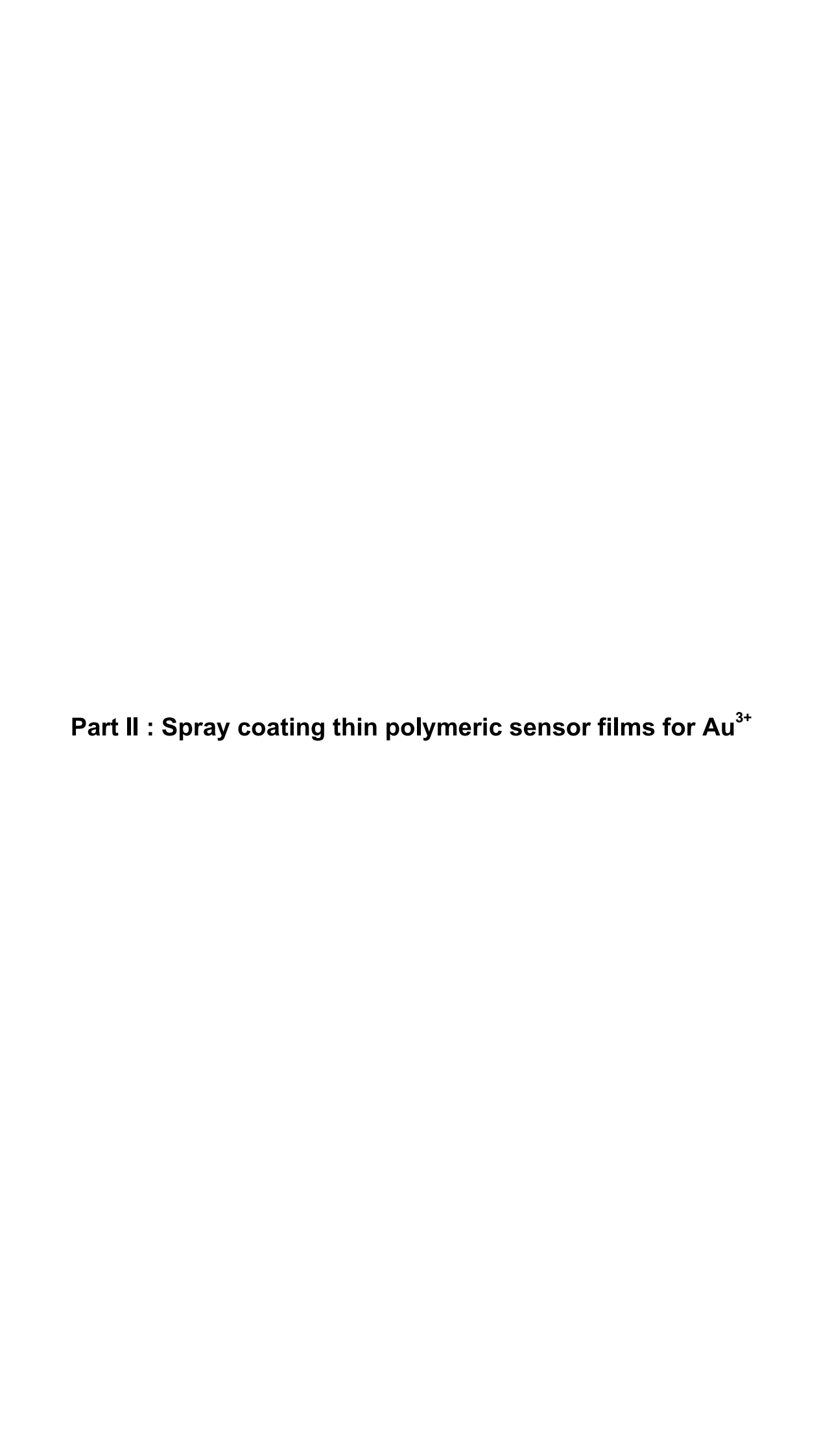


Figure 8. Fluorescence image of **PAA-Rho3-ITO** befor and after added Au³⁺. The polymer film on the ITO was irradiated with a hand-held UV lamp at 360 nm

In addition, our **PAA-Rho3-ITO** sensor provides a better detection limit (DL) toward Au³⁺, easy to recoverand can be used in water as compared to previous reports as listed in Table 1.³³⁻³⁵

Table 1. Selected examples of Au³⁺ sensors.

| Au ³⁺ sensors | Receptor | Working solvent | reversibility | DL (M) |
|---|-----------------|------------------------------|---------------|------------------------|
| Rhodamine-based Modified | rhodamine | H ₂ O | Yes | 0.10 × 10 ⁻ |
| Polyacrylic acid (PAA-Rho3- | | | | 6 |
| ITO) | | | | |
| calix[4]arene Schiff base | Schiff base and | EtOH: H ₂ O (1:1) | No | 0.10 × 10 ⁻ |
| sensor ²⁷ | thiophene | | | 6 |
| Hybrid organic-inorganic | rhodamine | H ₂ O | Yes | 0.83× 10 ⁻⁶ |
| nanomaterial sensors ²³ | | | | |
| Thiocoumarin derivative ²⁸ | Thiocoumarin | ACN: H ₂ O (1:1) | No | 0.11 × 10 ⁻ |
| | | | | 6 |
| Pyridine derivatives dyes ²⁹ | Pyridine | DMSO: H ₂ O | No | 0.3 × 10 ⁻⁶ |
| | | (1:100) | | |



Characterization

PSS-Rho1 – PSS-Rho4 sensors were synthesized by amidation reaction with rhodamine B-ethylenediamine or Rho of various mole ratios in the presence of EDC/DMAP as coupling reagent under N₂ at reflux for 5 days in DMF (Scheme 1). Only PSS-Rho4 can be separated in the precipitation process, but PSS-Rho1 – PSS-Rho3 cannot be precipitated in water which might be due to its good solubility in water. Therefore, only PSS-Rho4 could be developed as a polymeric sensor. The chemical structure was proven by ¹H NMR, ATR-FTIR, and SEM techniques. In addition, it was designed to chelate with metal ions *via* carbonyl-oxygen atom of its structure.

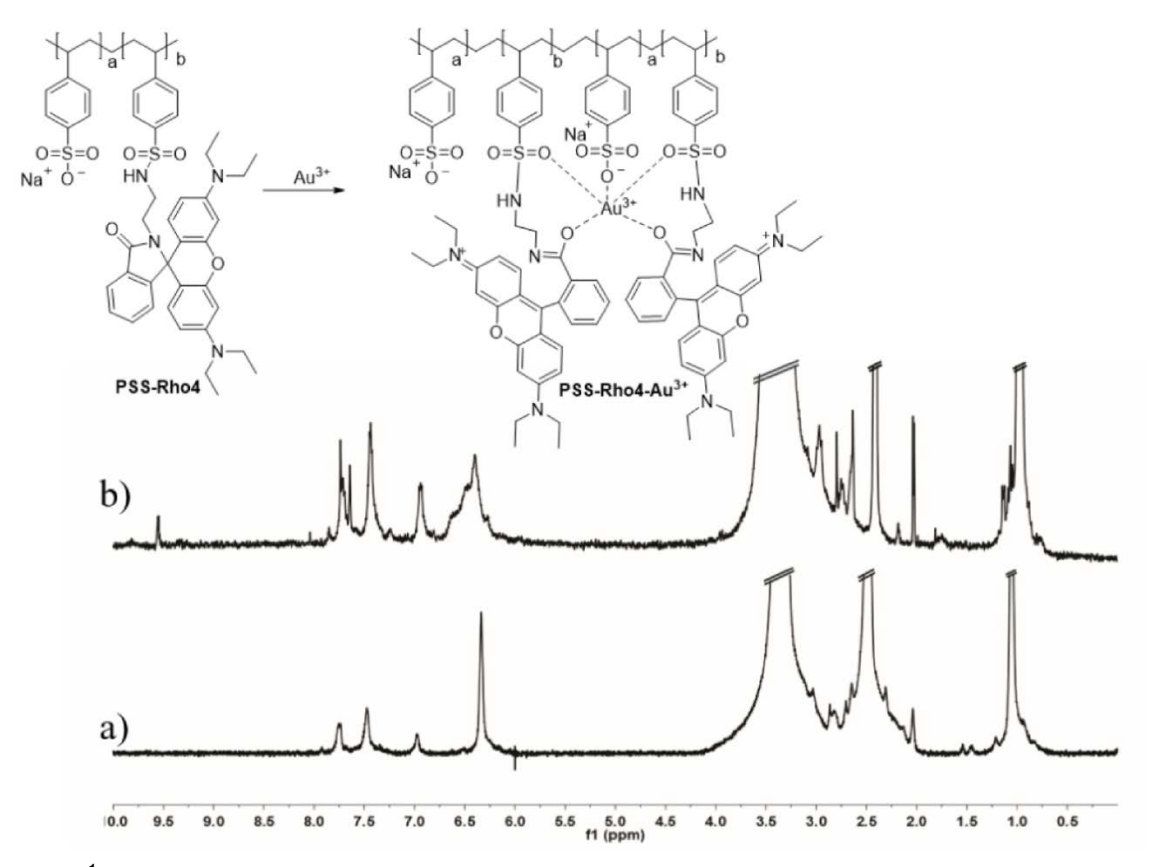


Fig. 1 ¹H NMR spectra of **PSS-Rho4 (**0.1 g/L in MeOH) (a) the absence and (b) the presence of Au³⁺.

The 1 H NMR spectrum of **PSS-Rho4** in DMSO- d_6 is shown in Fig.1, the characteristic signals shown by $-CH_2$ and -CH groups at 1.0-2.1 and 2.2-2.6 ppm aromatic protons at 7.5 ppm of styrene sulfonate ring in the poly (sodium-4-styrenesulfonate). Moreover, the xanthene and benzene rings of rhodamine ethylenediamine were found at 6.3-7.8 ppm. The Fig. 2, ATR-FTIR demonstrated the C=O of rhodamine peaks at 1612 cm⁻¹ and the S=O of sulfonate groups at 1319 and 1109 cm⁻¹. The scanning electron microscopy of **PSS-Rho4** (Fig. 3B) showed the diameter of the particles were in the range 50-100 μ m and dramatically increased of the

crystallinity and crystalline sizes which was attributed to Π – Π interactions and hydrogen bonding of the rhodamine moieties , compared to PSS which showed a sphere, smooth surface (Fig.3A).³¹ These results indicated that we have successful synthesized PSS linked to **Rho**.

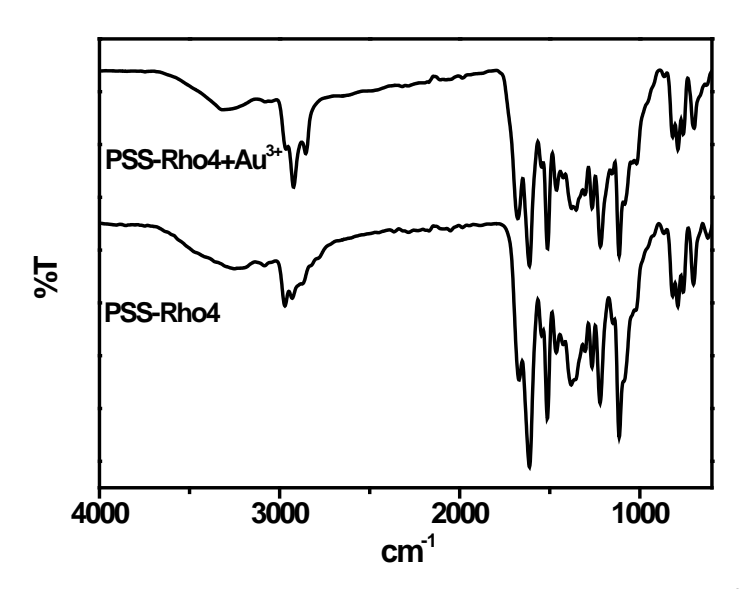


Fig. 2 ATR-FTIR spectra of PSS-Rho4 in the absence and presence of Au³⁺.

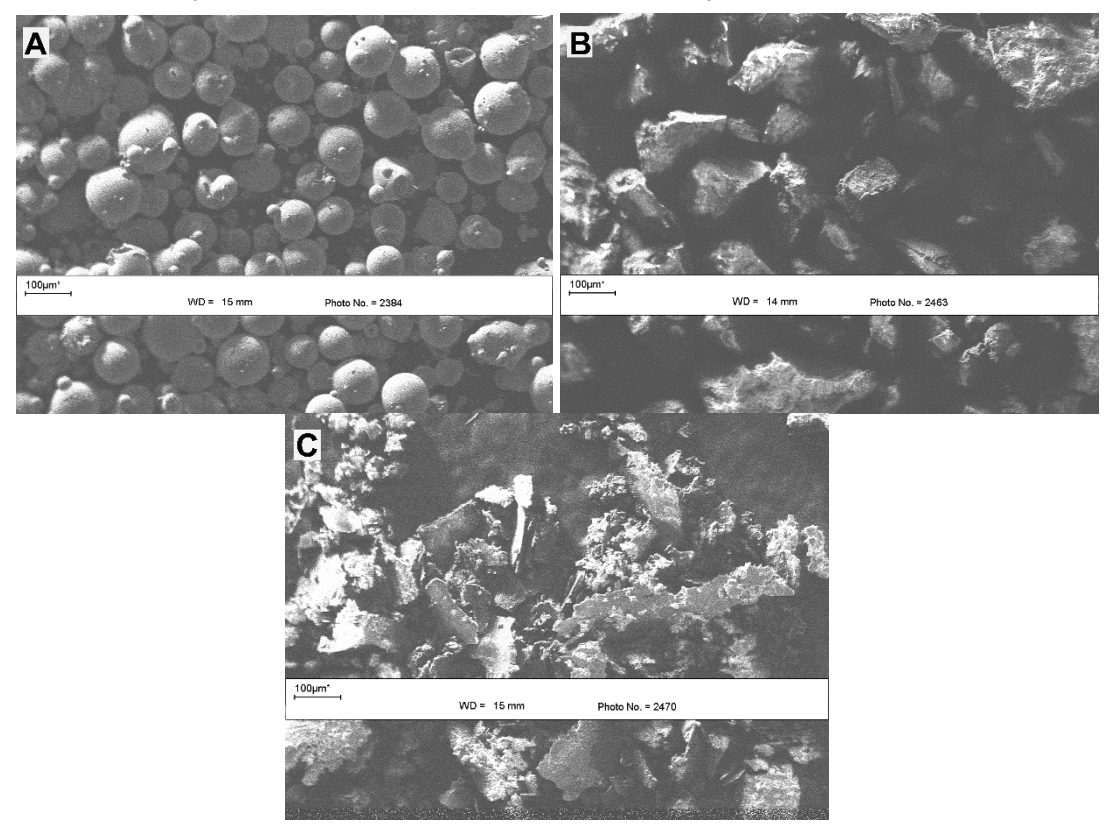


Fig. 3 SEM images of (A) PSS, (B) PSS-Rho4 and (C) PSS-Rho4+Au³⁺.

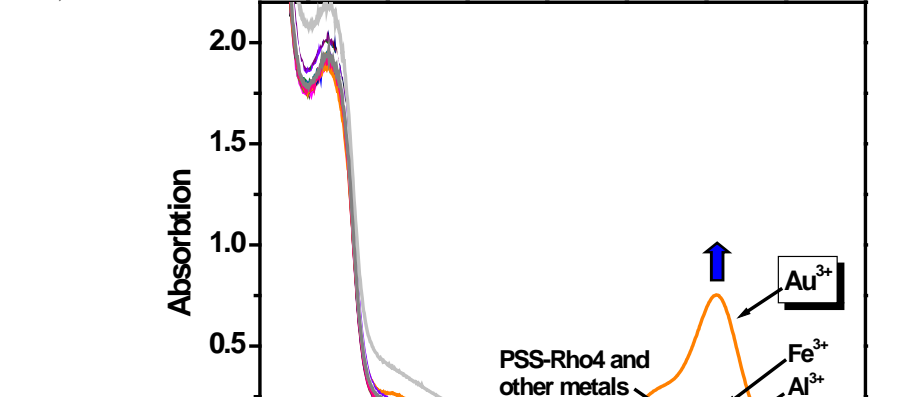
Selectivity and sensitivity studies

a)

0.0

300

The spectroscopic and color changes of the polymeric sensor were investigated to determine the cation binding abilities. Generally, rhodamine derivatives are colorless and non-fluorescent, when a cation or proton induced spirolactam ring opening (an increased fluorescent intensity and pink occurrs). Fig. 4a shows the absorptions of the **PSS-Rho4** at wavelengths of 280 nm and 312 nm corresponding to the π - π * and n- π * transitions and, Fig. 4b displays no the fluorescent emission peaks when sensor was excited at 520 nm which confirmed the ring-closed spirolactam formation of rhodamine moieties. The selectivity studies were performed using **PSS-Rho4** (0.1 g/L) against 0.35 μ M of the various cations in MeOH. The results showed a significant enhancement of the absorbance intensity (at 555 nm) and high-intensity fluorescence (at 580 nm) upon addition of Au³⁺ as compared to other cations. In addition, the color change (colorless to pink) and fluorescence change were observed after exposure to Au³⁺ solution at room temperature (Fig. 5). This strongly supports the fact that in absence of metal ions, the receptor remains in the spirolactam form, and the non-existence of the highly conjugated xanthene form results in the suppression of emission and color changes in the abovementioned region.



400

500

Wavelength, nm

600

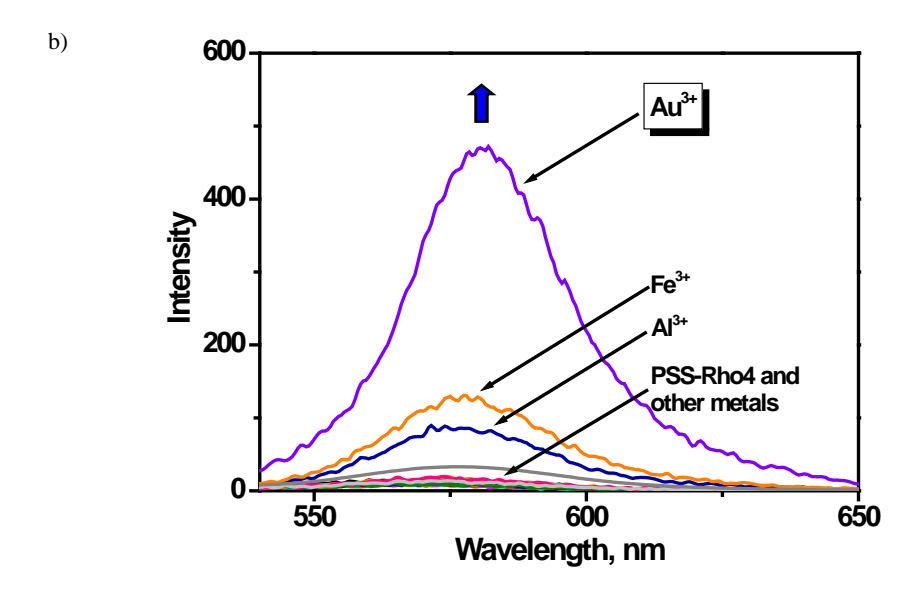


Fig. 4 a) Absorption and b) fluorescence spectrum changes of **PSS-Rho4** (0.1 g/L) before and after the addition of various cations 0.35 μ M in MeOH.

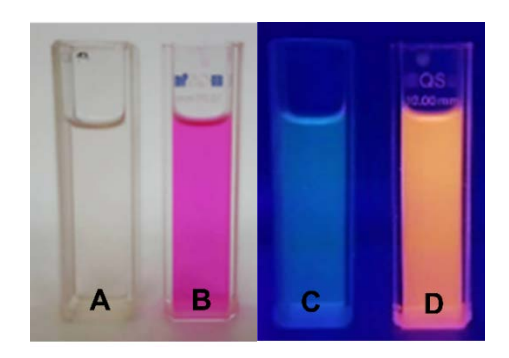


Fig. 5 Color changes (A and B) and fluorescence changes under 254 nm illumination (C and D) of **PSS-Rho4** (0.1 g/L) in the absence and presence of 0.35 μ M Au³⁺: (A and C) **PSS-Rho4** only, (B and D) **PSS-Rho4**+Au³⁺.

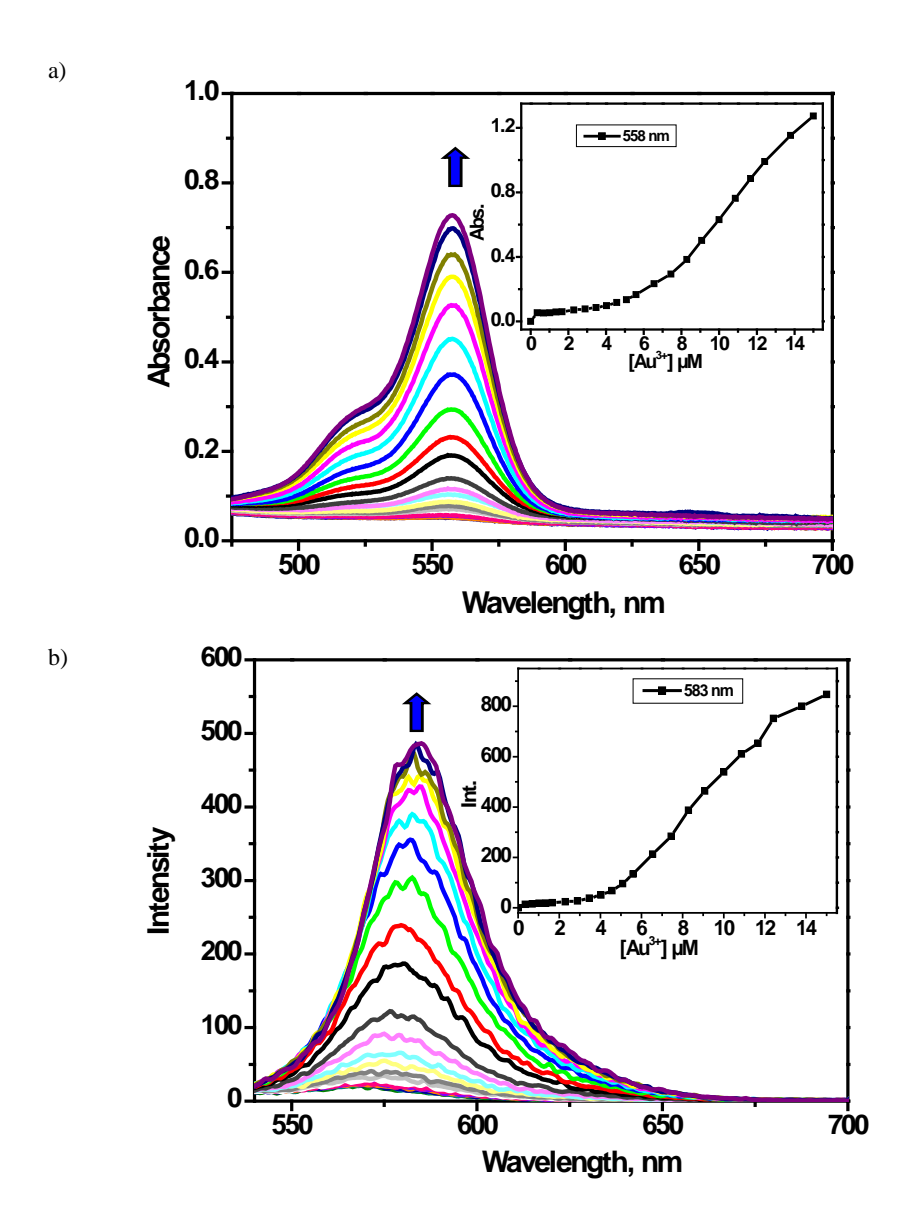


Fig. 6 a) Absorption spectra and b) Fluorescence spectra of **PSS-Rho4** (0.1 g/L in MeOH) with addition increasing the concentration of Au³⁺ in MeOH solution. Inset: Mole ratio plot at a) 558 nm and b) 583 nm.

To further more study the complexation between **PSS-Rho4** and Au^{3+} , ¹H NMR experiments were carried out in DMSO- d_6 and the spectra are demonstrated in Fig. 1. In general, chemical shift of sulfonamide N*H* proton about 6-8 ppm^{32, 33} and protons attached to nitrogen atoms may be exchangeable.³⁴ For free **PSS-Rho4** there was no chemical shift of the sulfonamine N*H* protons which might be attributed to the quick exchange with the residual water in the deuteration solution^{35,36,37} and increased intermolecular hydrogen bonding of polymer, whereas in the presence of Au^{3+} ions, it was appeared and shifted downfield (9.62 ppm). In addition, the chemical shifts of all the protons also showed distinct downfield changes and peak broadening, especially the aromatic protons, which may be due to Au^{3+} complexation and

conformational organization. Infrared spectra (Fig. 2) were also conducted to confirm the binding of carbonyl group of **PSS-Rho4** with Au³⁺ ion. It was clearly observed that upon addition of Au³⁺ ion, the carbonyl stretching band of **PSS-Rho4** at 1612 cm⁻¹ was changed to a lower wavenumber (1604 cm⁻¹). The peak at ~2971 cm⁻¹ (NH) decreased to 2966 cm⁻¹. Particularly, the peak of C-N at ~1376 cm⁻¹ shifted to 1354 cm⁻¹.

The ¹H NMR and ATR-FTIR results firmly supported that the sulfonamide and the carbonyl Au³⁺-induced ring opening of the spirolactam form (Fig. 6a). The results were also consistent with the selectivity measured from fluorescent titration. Fig. 6b shows the emission spectra of **PSS-Rho4** in the presence of different concentrations of Au³⁺. In the absence of Au³⁺, the solution of the sensor provided no emission signals (non-fluorescence), whereas the portioned addition of Au³⁺ resulted in the fluorescence "turn-on", with the intensities of the emitted fluorescence increasing as a function of Au³⁺ concentration. The fluorescence emission was a consequence of rapidly enhanced strong emissions at 583 nm.

The morphologies of **PSS-Rho4** before and after adding Au^{3+} were characterized by SEM (Fig. 3). The SEM micrograph of **PSS-Rho4** showed the increase of the crystallinity and crystalline sizes which were attributed to π - π interactions and hydrogen bonding of the rhodamine moieties. Then, slight decreasing of crystallinity and crystalline sizes was observed after adding Au^{3+} which might be metal-induced breaking hydrogen bond process.³⁹

Competition experiments in the presence of potentially competitive metal ions were conducted, and the results are shown in Fig. 7. The slight turn on effect from some metal ions was observed, but it did not make serious efforts to the recognition ability of the **PSS-Rho4** to Au³⁺. According to changes in signaling (absorption and fluorescence emission) upon adding various Au³⁺ concentrations, the limit of detection (LOD) of **PSS-Rho4** for Au³⁺ was calculated to be 1.2 µM. In addition, the **PSS-Rho4** sensor gave a better LOD toward Au³⁺, be easy to restore and can be used in water as compared to previously reported chemosensors as listed in Table 1. The results suggested that **PSS-Rho4** could potentially be used to detect Au³⁺ ions in real systems.

Table 1. Selected examples of Au³⁺ sensors.

| Sensors | Receptor | Working solvent | Reversible | Detection limit (µm) |
|---|-----------------------------------|------------------|------------|-------------------------|
| Rhodamine-based poly(sodium-4-styernesulfonate) (PSS-Rho4) | Rhodamine | H ₂ O | Yes | 1.2 |
| Fluorol Red GK fluorescent probe ⁴⁰ | Fluorol Red GK | H_2O | NO | 1.23 |
| Graphene oxide (GO)/poly(vinyl alcohol) (PVA) hybrid ⁴¹ | Graphene oxide | H ₂ O | NO | 300 |
| Fluorescein-based fluorescent probe ⁴² | Fluorescein | PBS | NO | 10 |
| Molybdenum disulfide quantum dots sensor ⁴³ | Molybdenum disulfide quantum dots | H ₂ O | NO | 0.064 |

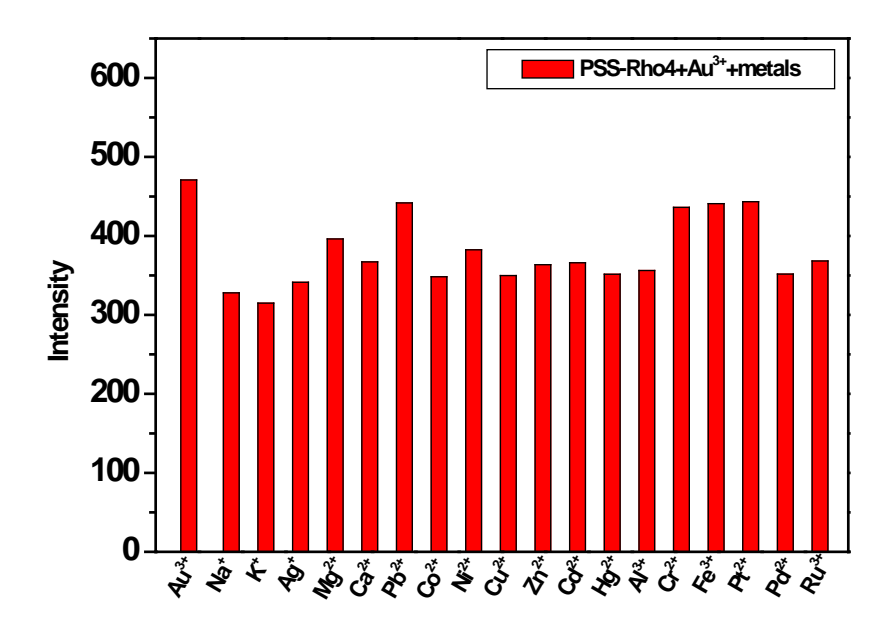


Fig. 7 Fluorescence enhancement response at 583 nm of PSS-Rho4 (0.1 g/L) in MeOH of the mixture of 1 mM different metal ions with 0.35 μ M of Au³⁺.

Studies spraying sensor for cation detection

In order to evaluate the **PSS-Rho4** chemosensor as a molecular device, **PSS-Rho4** was transformed onto the films or coating materials. Spray technique is one of the powerful ways to produce a film or coating materials. Resultant characteristics of this technique are highly beneficial to sensor technology, e.g. the ability to simultaneously provide high throughput, efficient use of material, increase large surface areas, excellent for distribution of chemosensor and comfortably for use.⁴⁵⁻⁴⁸

For the preparation of a fluorescence polymeric chemosensor coated on ITO substrate and filtered paper; **PSS-Rho4** (4 g/L) was dissolved homogeneously in MeOH and coated on a clean ITO substrate and filtered paper (Whatman No. 1) by spraying technique and then dried at room temperature. The various concentrations (1x10⁻³ – 1x10⁻⁶ M) of Au³⁺ ion were prepared in water and sprayed onto the hybrid sensor materials (**PSS-Rho4-**ITO and **PSS-Rho4-**filtered paper). A photograph was taken using a digital camera under normal light and under a UV lamp at 365 nm. Figs. 8 and 9 show the color and fluorescence changes after treatment with Au³⁺ ions at concentrations between 1.0x10⁻³ and 1.0x10⁻⁶ M. The results showed that upon increasing the concentration of Au³⁺ ions on the hybrid sensor materials, the increases of the color and fluorescence intensities were also observed, as expected. After treatment with an aqueous EDTA solution under basic condition, ¹² the color change of **PSS-Rho4** in aqueous solution was found to be reversible as the pink of the complex disappear (Figs.10 and 11). From the SEM image (Fig. 12B) of **PSS-Rho4**-filtered paper, it can be seen

that the integrity of the cellulose fiber was not degraded by the modification. The SEM images showed that the diameter of the fibers in the original and grafted papers were in the range 5–25 µm and showed branched fibers. After treatment with Au³⁺ (Fig. 12C), the fiber structure of grafted paper showed less branching due to the decrease in the hydrogen-bond networks of **PSS-Rho4-**filtered paper by complexation. The different surface morphology of **PSS-Rho4-**ITO after adding Au³⁺ was also observed. The SEM images (Fig. 12F) confirmed the increasing of surface roughness/area and patchiness, which may account for the increase response after sensing. Therefore, these hybrid sensor materials can conveniently and practically detect Au³⁺ ions in real water samples with no requirement of any complicated instruments.

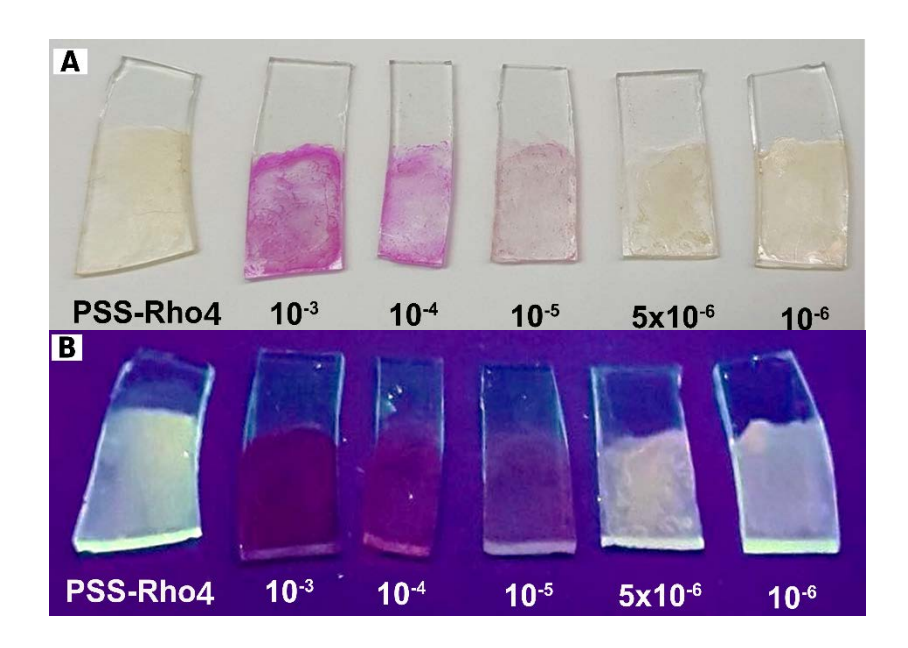


Fig. 8 Visual observation of the **PSS-Rho4**-ITO after treatment with Au^{3+} ions at concentrations between $1.0x10^{-3}$ and $1.0x10^{-6}$ M, (a) under normal light, (b) under fluorescence light.



Fig. 9 Visual observation of the **PSS-Rho4**-filtered paper after treatment with Au^{3+} ions at concentrations between $1.0x10^{-3}$ and $1.0x10^{-6}$ M, (a) under normal light, (b) under fluorescence light.

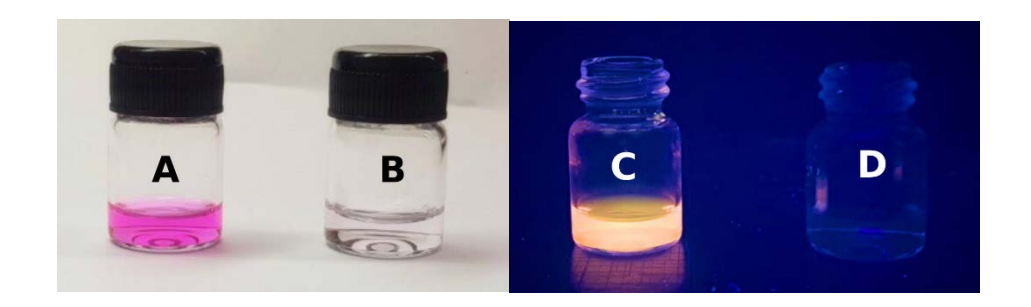


Fig. 10 Color changes (A and B) and fluorescence changes under 254 nm illumination (C and D) of **PSS-Rho4** (0.1 g/L) in the presence of Au³⁺ and EDTA solution: (A and C) **PSS-Rho4**+Au³⁺, (B and D) **PSS-Rho4**+Au³⁺+EDTA.

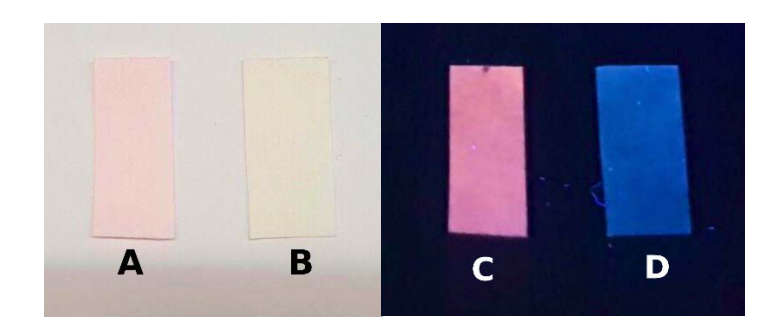


Fig. 11 Visual observation of color changes (A and B) and fluorescence changes under 254 nm illumination (C and D) of **PSS-Rho4**-filtered paper in the presence of Au³⁺ and EDTA solution: (A and C) **PSS-Rho4**+Au³⁺, (B and D) **PSS-Rho4**+Au³⁺+EDTA.

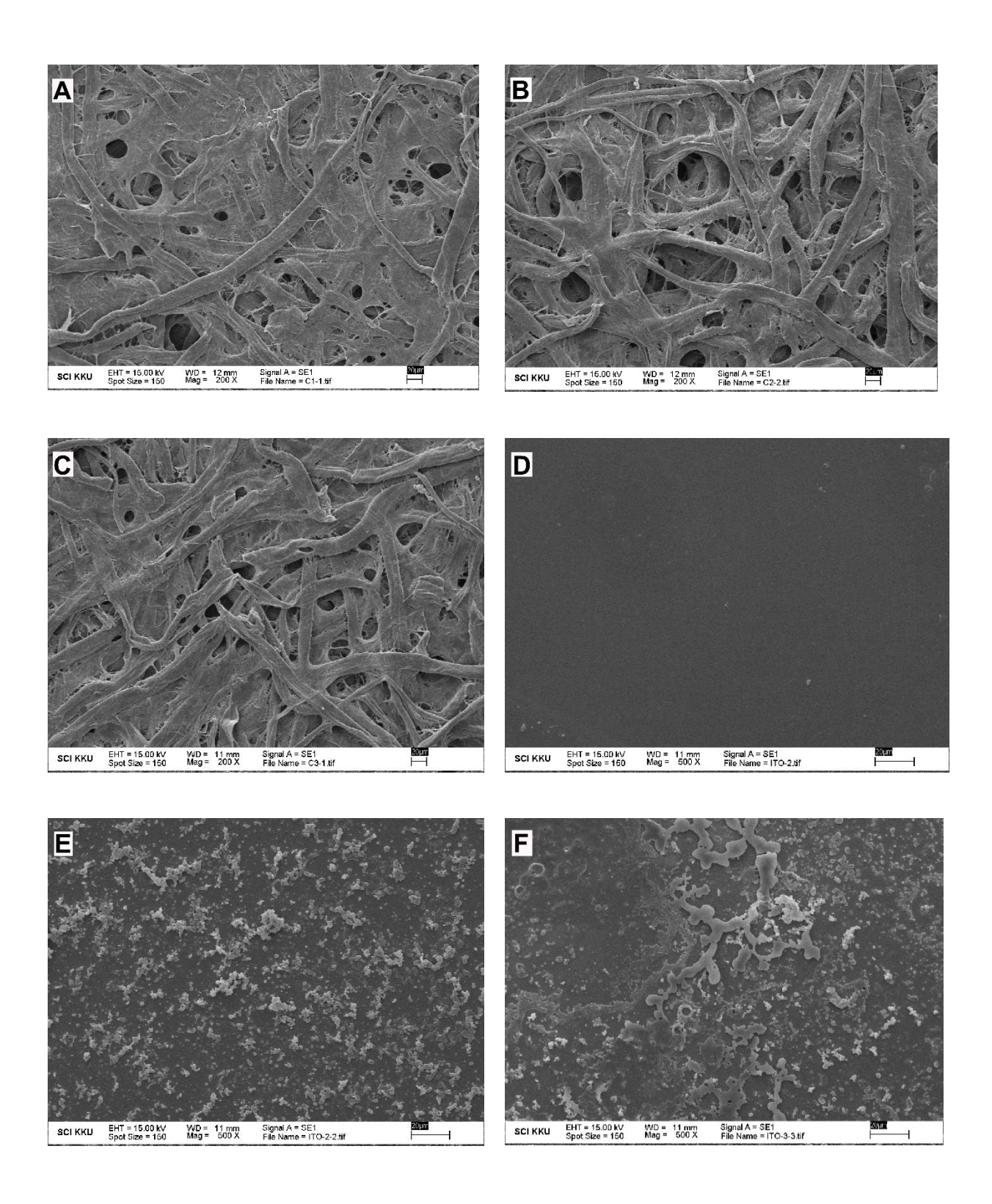


Fig. 12 Characterization of polymeric sensor (A) filtered paper (B) **PSS-Rho4**-filtered paper and (C) **PSS-Rho4**-filtered paper+Au³⁺, (D) ITO (E) **PSS-Rho4**-ITO and (F) **PSS-Rho4**-ITO+Au³⁺.

Computational calculations

The calculation of optimized geometries and the HOMO, LUMO energies of the **PSS-Rho4** and the **PSS-Rho4**+Au³⁺ complex were performed with 2:1 stoichiometry¹² by using the density functional theory (DFT) method at the B3LYP/6-31(d) theoretical level under the Gaussian 09 program.⁴⁹ The calculated results showed that **PSS-Rho4** can form stable complex with Au³⁺ through favorable a cation–dipole interactions from the oxygen atoms of two acyclic lactam groups and the oxygen atoms of two sulfonate group. Moreover, these structural changes were found to affect the HOMO and LUMO energy levels of rhodamine chromophores as shown in Fig. 13. The energy gap between LUMO and HOMO of the **PSS-Rho4** was 0.078 eV, whereas complexes with Au³⁺, its energy gap was changed to the lower level of 0.016 eV resulting in the λ_{max} bands of **PSS-Rho4** was also changed. In which the maximum peak at 312 nm slowly decreased upon Au³⁺ addition, while that peak at 558 nm increased.⁵⁰ These results clearly suggested that complexation between **PSS-Rho4** and Au³⁺ occurred with 2:1 stoichiometry.

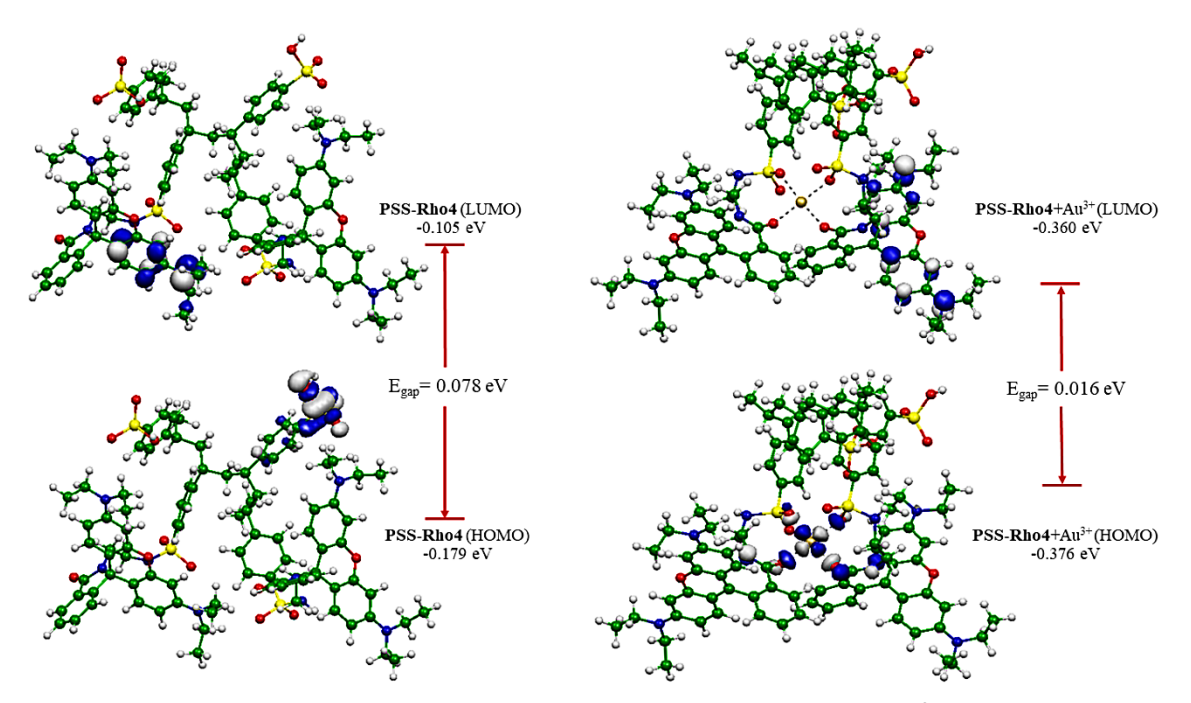
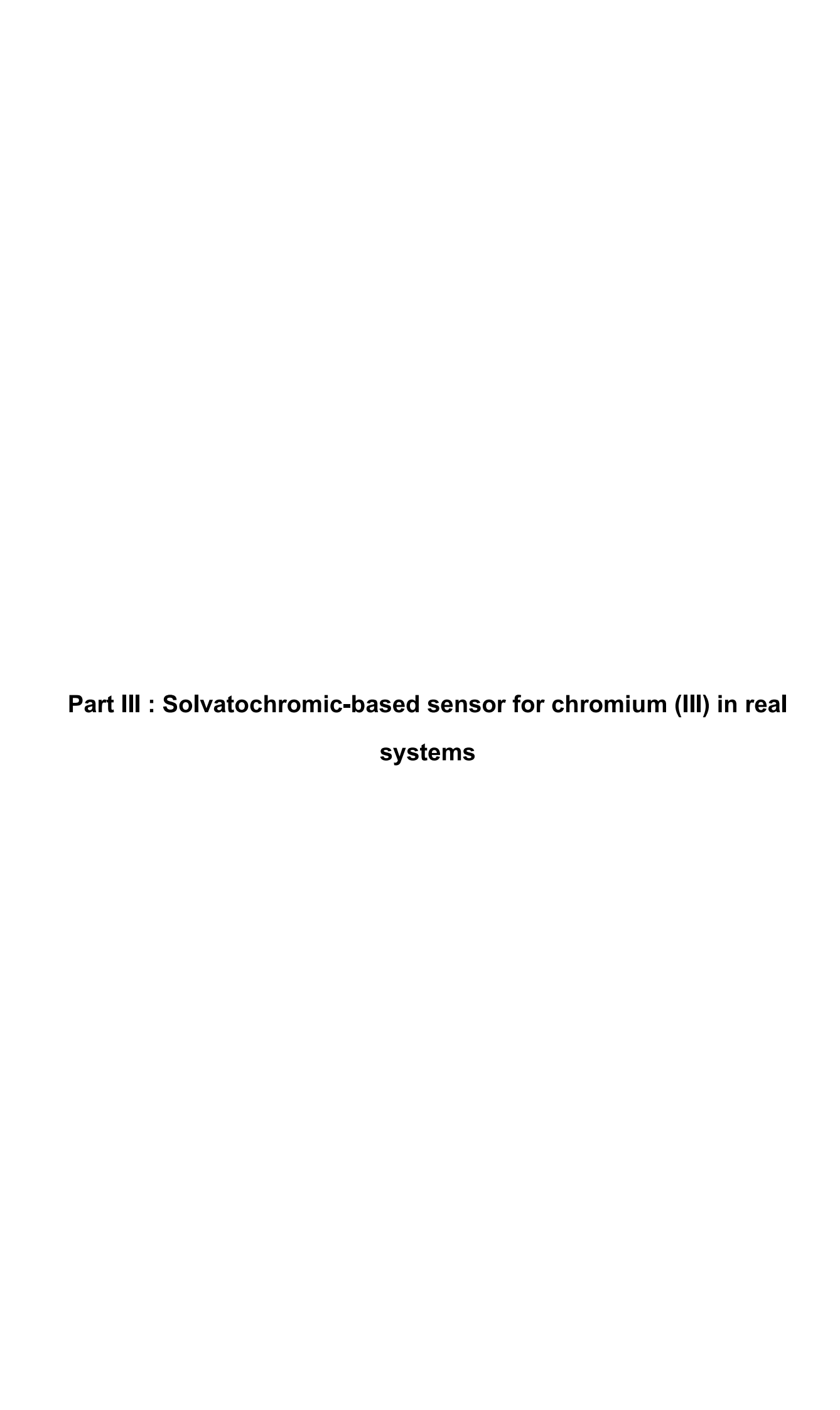


Fig. 13 The optimized structures of **PSS-Rho4** and (2:1) **PSS-Rho4**+Au³⁺ complex, the gap energies ($E_{gap} = E_{LUMO} - E_{HOMO}$)



The development of solvatochromic rhodamine-based sensor followed two separate approaches. First, the effect of solvent on the equilibrium position of the rhodamine lactone—zwitterion equilibrium was investigated. Second, we studied the use of rhodamine lactone (colorless L-form) as a cation selective optical and fluorescent chemosensor by varying type and concentration of cation.

The formation of the rhodamine lactone (colorless L-form).

Normally, the xanthene dye rhodamine B showed two forms in equilibrium mixture which were (1) a colorless lactone (L-form) and (2) a colored zwitterion (Z-form). In order to make the colorless L-form, the commercial rhodamine B was dissolved in a number of solvents (H₂O, MeOH, EtOH, ACN, DMF, DMSO, THF, CHCl₃ and CH₂Cl₂).

Rhodamine B at 10⁻⁵ M, in most solvents showed absorption peaks and fluorescence emission peaks around 550 and 580 nm, respectively (figure 1). These results have been previously observed and are consistent with the lactone–zwitterion equilibrium, indicating that rhodamine B at 10⁻⁵ M in chosen solvents is largely in the zwitterion form.

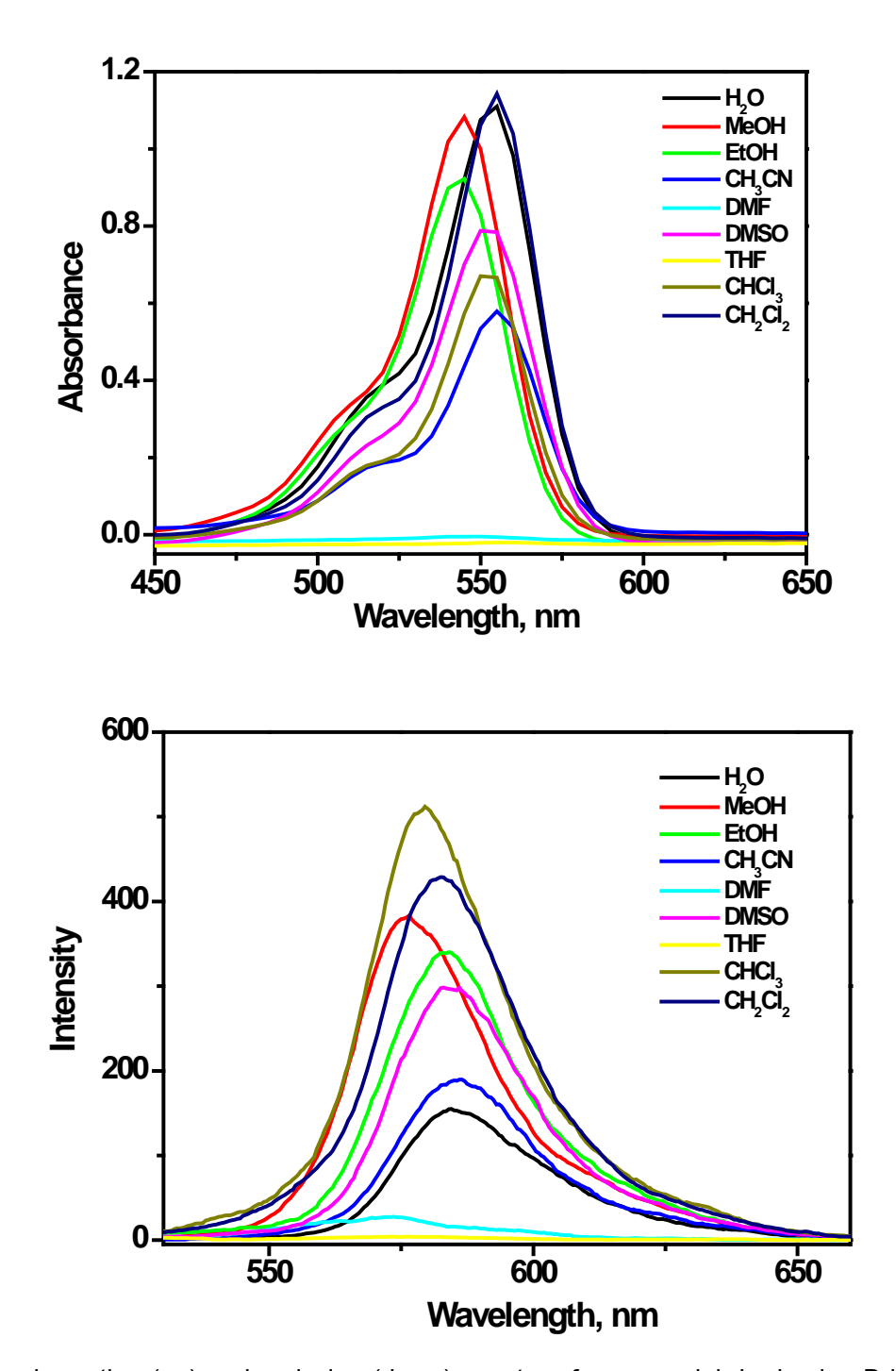


Fig. 1 Visible absorption (up) and emission (down) spectra of commercial rhodamine B in different solvents.

However, with THF as solvent, rhodamine B gave no absorption and emission in the region of 500-650 nm suggesting a complete transformation of the zwitterion into the lactone form. In addition, color and florescence images were employed to monitor the position of the lactone-zwitterion equilibrium of the rhodamine B base isomers. As displayed in Fig. 2 (above), the colorless of rhodamine B dye turned immediately from orange to colorless after exposure to THF solution at room temperature. The emission

color of rhodamine B dye also changed after dissolving in various solvents. Interestingly, in the case of THF, no emission color was demonstrated, because of low polarity and no hydrogen bond donor to stabilize Z-form of its. In the case of CHCl₃ and CH₂Cl₂ (lower polarity than THF), the dimer Z-form species were predominated instant of L-form. The results were consistent with previous which strongly indicated that the equilibrium shifted toward the lactone form.¹⁰

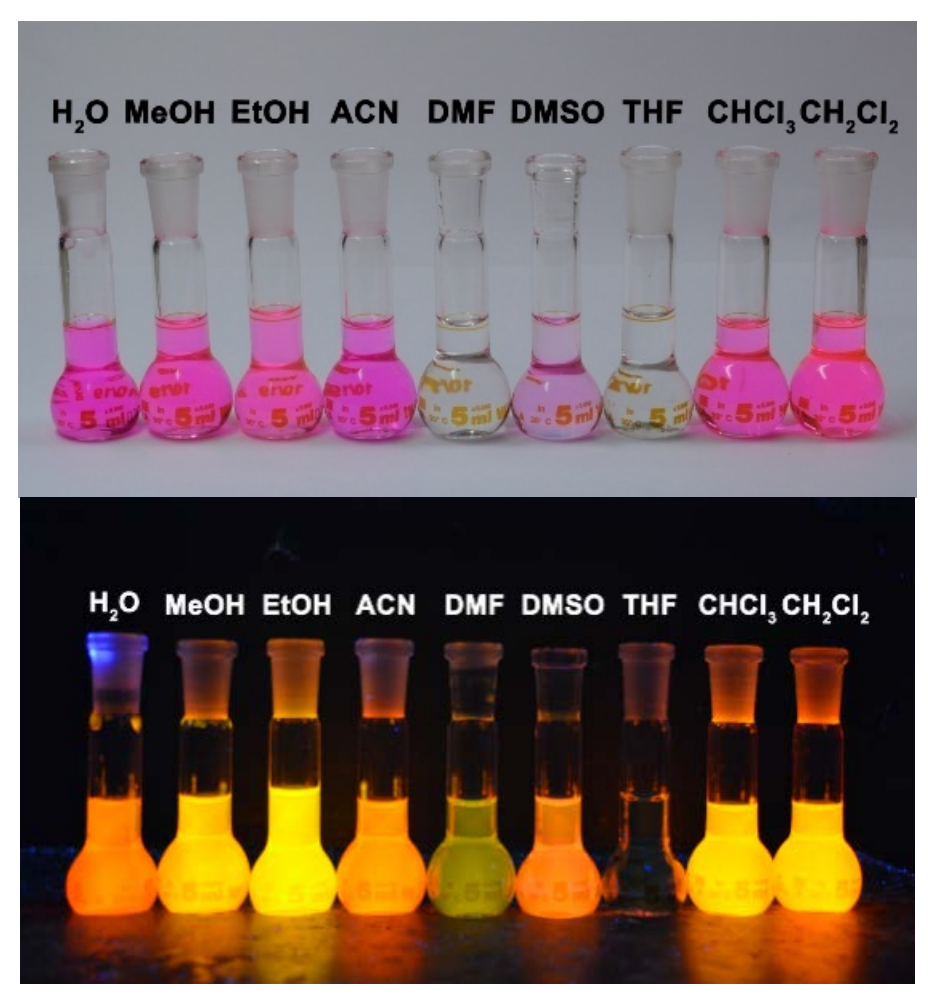


Fig. **2.** Digital images of rhodamine B in different solvents at 10 μ M taken under normal illumination (above) and demonstrating skeletal fluorescence under 365nm illumination (below).

As we already knew from above results that the lactone-zwitterion equilibrium can be disturbed by water, we examined how water content influenced the sensing properties and also studied the sensing properties in aqueous solution. For this reason, the content of water in sensing experiments was studied by varying the ratio of water (0.1 - 0.3 mL) to THF in the solution in which the rhodamine B was dissolved (Fig 3). It was found that the fluorescent intensity of chemosensor slightly increases with increasing ratio of water. At 0.3 mL of water, we found that the fluorescent intensity was

about 140 a.u. and was constant for 3 days. Therefore, the proposed optical sensor can be used for metal ion monitoring in water:THF ratio of 0.3 : 2.2.

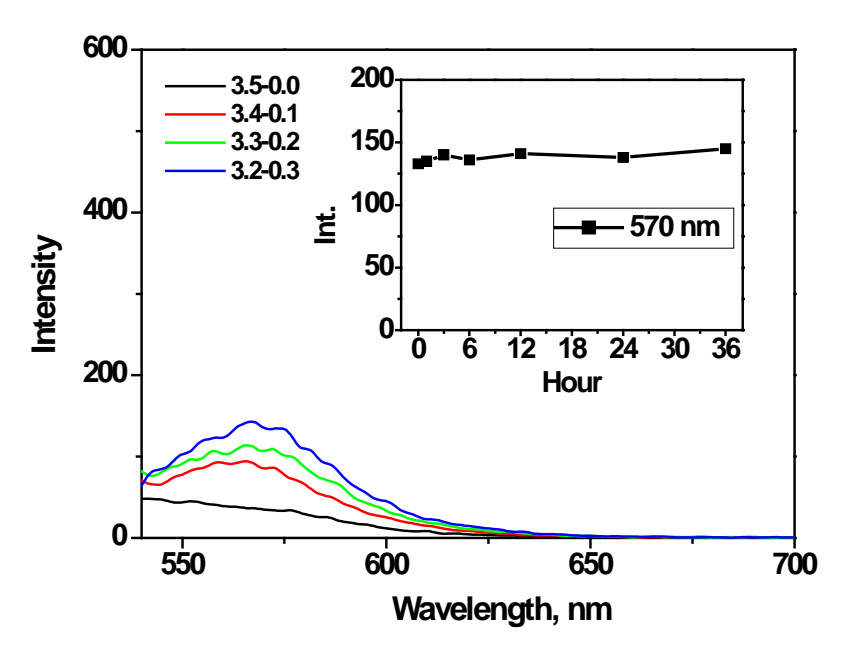


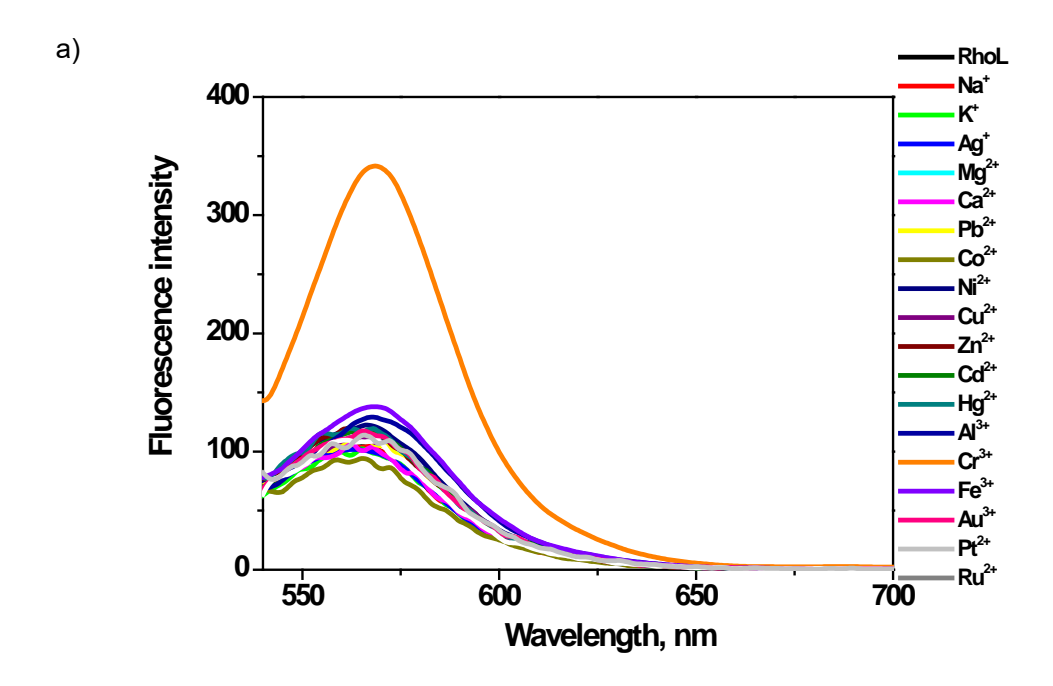
Fig 3. Emission spectra of rhodamine B lactone by varying the ratio of water (0.1 - 0.3 mL) in THF solution, Inset: fluorescent intensity was about 140 a.u. and was constant for 3 days.

Ion binding ability of solvatochromic-based sensor

The fluorescence intensity changes of a solvatocromic-based sensor were investigated to determine its cation binding abilities. Fig. 4 shows the fluorescence spectra of the sensor in the presence and absence of 10 μ M of various cations in H₂O:THF solution. The results revealed an obvious high intensity fluorescence band at 573 nm upon addition of Cr^{3+} into solutions of the sensor. The band was characteristic of the emission peak of the ring-opened rhodamine. However, other metal ions did not induce any distinct emission spectra changes in this wavelength, indicating that the sensor has no specific binding ability for those metal ions. In addition, the ratio of fluorescent enhancements revealed high selectivity of sensor for Cr^{3+} as demonstrated in figure 4b. However, for some other metal ions like Au^{3+} and Fe^{3+} , it has minimal effect (Fig. 4b) i.e. 8% of fluorescence enhancing. Therefore, rhodamine B lactone can used as a fluorescent sensor to detect Cr^{3+} ions in aqueous medium.

To gain further insights into the properties of RhoL as a chemosensor for Cr³⁺, fluorescence titration of RhoL was performed with increasing the concentrations of Cr³⁺. A significant enhancement of florescence intensity at 573 nm wavelengths was observed as a result of the Cr³⁺-induced ring opening of the spirolactam form (Fig. 5). This binding mode was determined

by the data of mole ratio plots evaluated from the emission spectra of RhoL and Cr^{3+} (insert Fig. 5) in which a 1 : 1 stoichiometry for the RhoL- Cr^{3+} complex with log β = 5.42 (calculation from a Benesi-Hildebrand plot analysis 15).



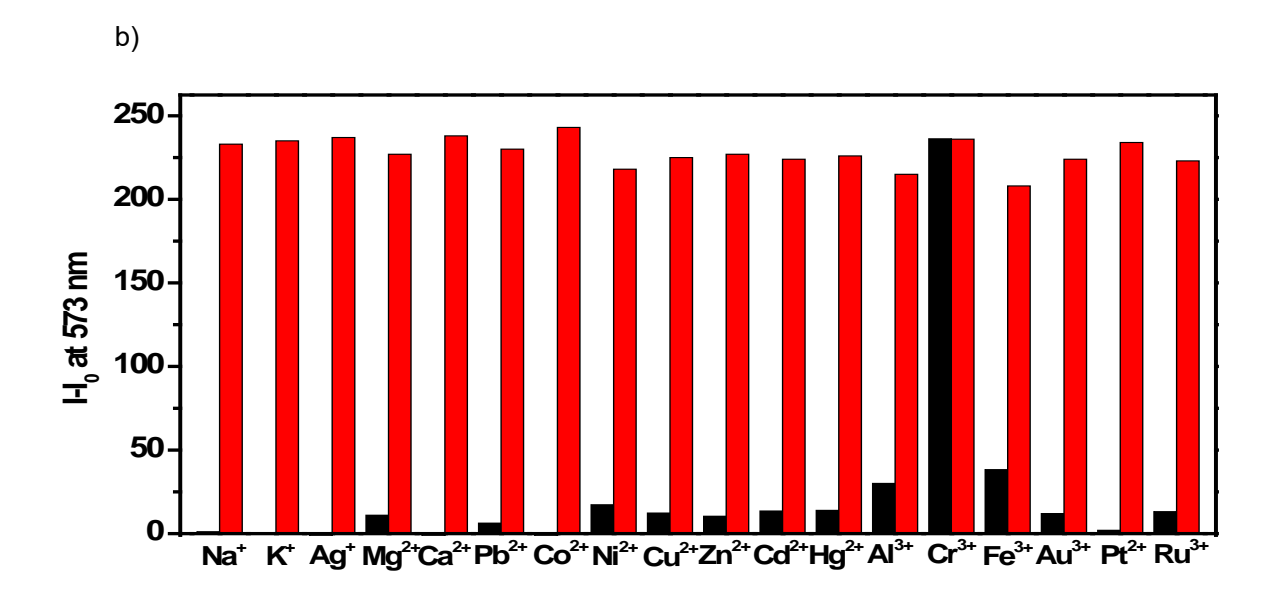


Fig 4. (a) Fluorescence spectral changes of RhoL after the addition of 10 μ M of various cations. (b) Fig. 5. Fluorescence responses at 573 nm of RhoL (10 μ M) upon addition of various metal ions (10 μ M) (black bars: RhoL with other metal ions; red bars: RhoL with other metal ions and Cr3+) in THF:H2O (λ ex = 520 nm).

Moreover, the competition experiment was also carried out by adding Cr^{3+} to the solution of RhoL in the presence of other metal ions in Fig. 4b. The results showed that all background metal ions did not significantly interfere with the sensing of Cr^{3+} , and the dye can be used as a potential Cr^{3+} -selective chemosensor. Similar to most rhodamine-based spirolactam chemosensors, the selective binding of Cr^{3+} must be due to the ring-opening mechanism. Chromium can chelate with carboxylate speices and the other coordination sites can be occupied by nitrate and water ligands which also could stabilize the ring-opening from of rhodamine.

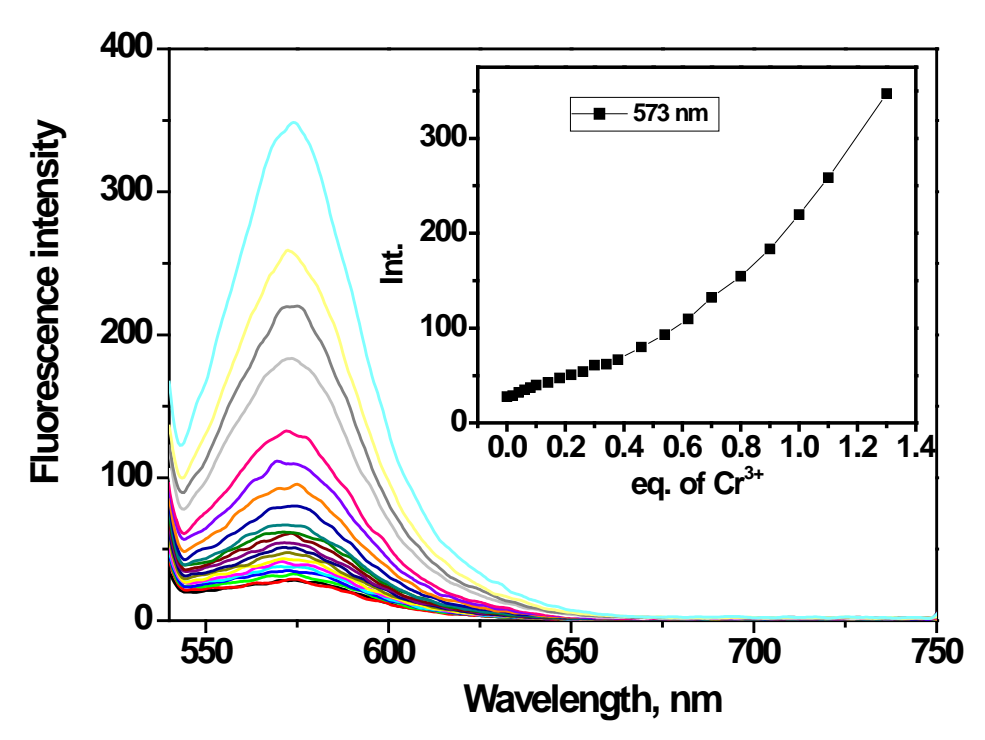


Fig 5. The fluorescence emission spectrum of RhoL (10 μ M) upon addition of Cr³⁺ (0-1.3 equiv.) in THF:H2O (λ ex = 520 nm). Inset: Mole ratio plot at 573 nm.

Fabrication of RhoL coated paper

In order to fabricate RhoL coated paper for determination of the response of a paper sensor for detecting Cr^{3+} in aqueous solutions with different concentrations, seven different solutions with various concentration of the Cr^{3+} (10^{-3} , $5x10^{-4}$, 10^{-4} , $5x10^{-5}$, 10^{-5} , $5x10^{-6}$, 10^{-6} M) were prepared. 4 μ L RhoL (5 mM) in THF solution was dropped on a piece of filter paper (Whattman No.1). The paper was allowed to dry in air at room temperature. Solutions of various concentrations of C^{r3+} were placed on the paper and after 40 s a photograph was taken using a digital camera under normal light and under a UV lamp at 365 nm. Figure 6 shows how the color and fluorescence changed with Cr^{3+} ion concentration. The

results showed that when increasing the concentration of Cr^{3+} ions on the paper-based sensor, increases of the color and fluorescent intensities were also observed, as expected. Therefore, a test paper based on RhoL can conveniently and practically detect Cr^{3+} ions in real water samples with no requirement of any complicated instruments. In addition, the detection limit of this sensor was found to be about 1 μ M which is lower than the critical standard level of Cr^{3+} allowed in wastewater (19.23 μ M).

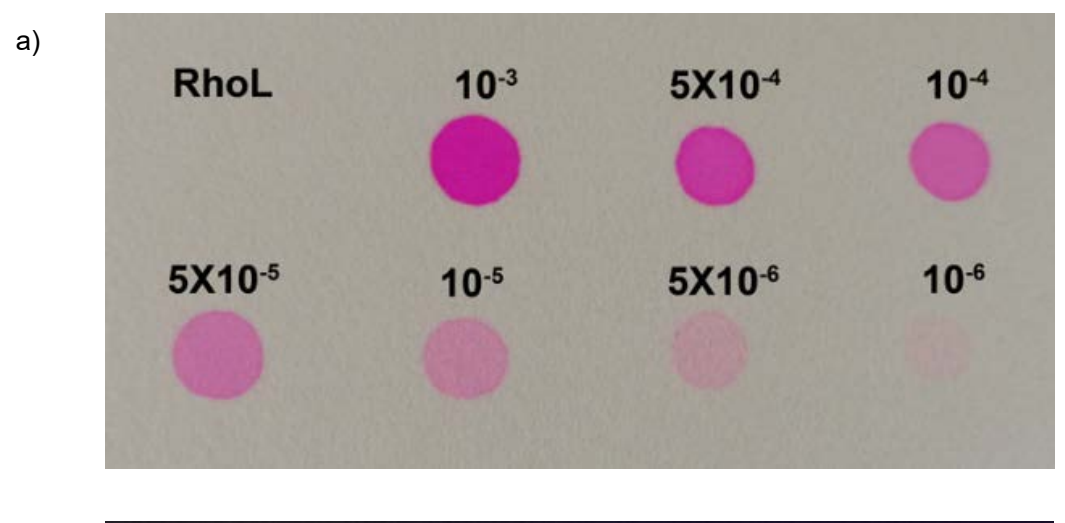




Fig 6. Photographs of the **RhoL** coated paper by varying the concentration of Cr³⁺ under (a) normal light and (b) fluorescence images under 365 nm UV light.

Part IV : Gold sensing with rhodamine immobilized hydrogelbased colorimetric sensor

The formation of the RhoL

The **RhoL** was synthesized by slight modification to the methods described previously [11]. In this work, we also added NaOH to help a complete transformation of the zwitterion into the lactone form in $H_2O:THF$ (1:1.39) solution. No emission and absorption spectra (at around 550 to 580 nm) were demonstrated in this conditions, which strongly indicated that the equilibrium was shifted toward the rhodamine lactone form (Fig. 1).

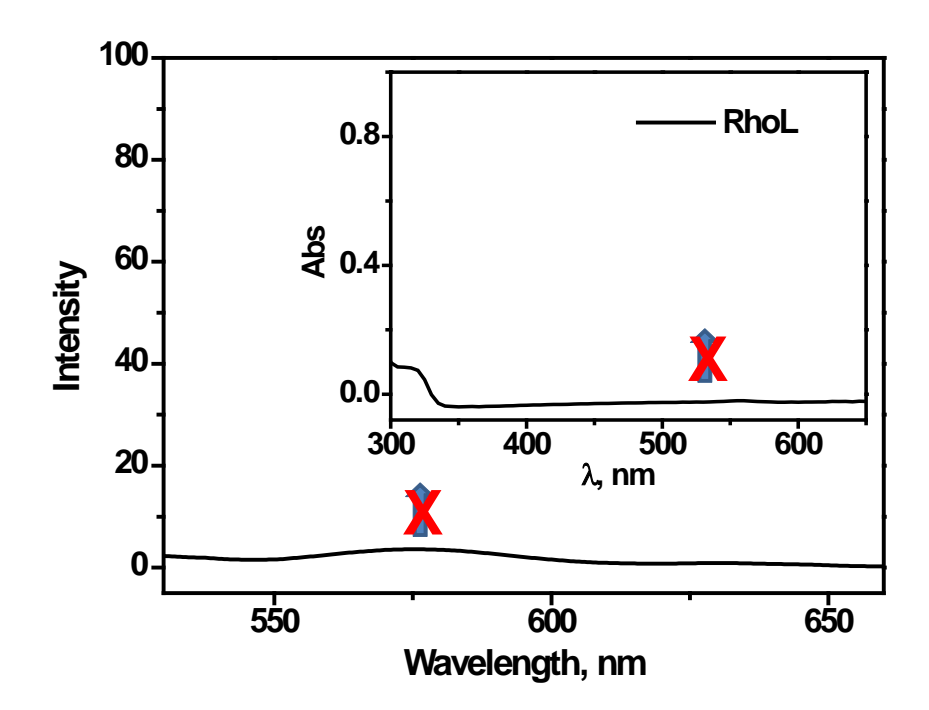


Fig 1. Visible absorption and emission spectra of commercial rhodamine B in H₂O:THF solution.

3.2 Characterization of Arg-RhoL

After immobilization of **RhoL** on agarose membranes to form **Arg-RhoL**, ATR-FTIR, SEM, TGA and UV-vis were employed to characterize the sensing material. First, ATR-FTIR is useful to investigate the functional groups present on the adsorbent and is also useful in checking on the loading of dye onto the hydrogel. The FTIR spectra of **Arg-RhoL** showed a weak intensity band at 1150 cm⁻¹ (plane bending), 888 cm⁻¹ (out of plane bending) and at 690 cm⁻¹ (wagging vibrations) attributed to aromatic C–H vibrations and the band at 1638 cm⁻¹ is characteristic of the C=O stretching vibration of Rhodamine constituents [12, 13], while the band at 3343 cm⁻¹ is associated with O–H bond stretching of agarose constituent [14] (Fig. 2).

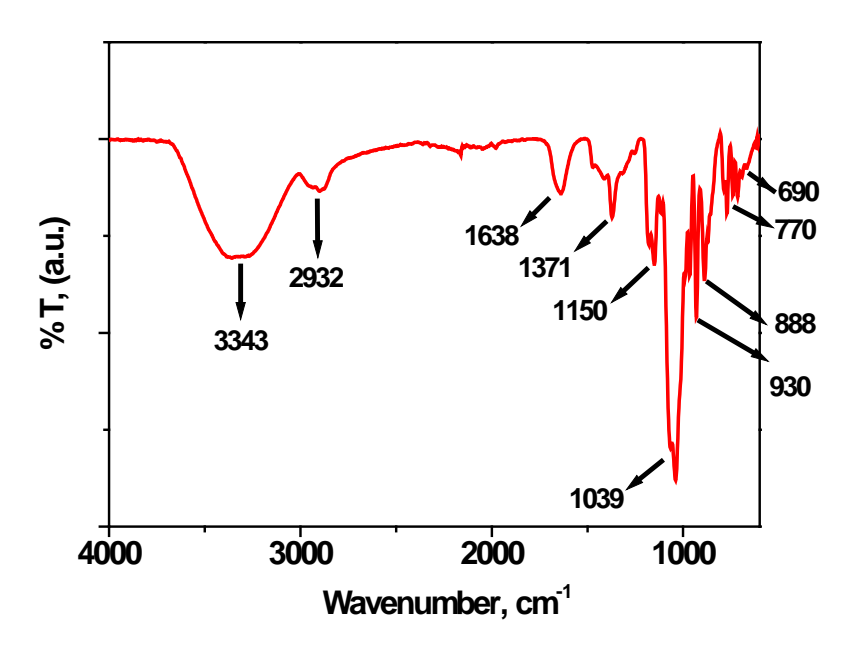
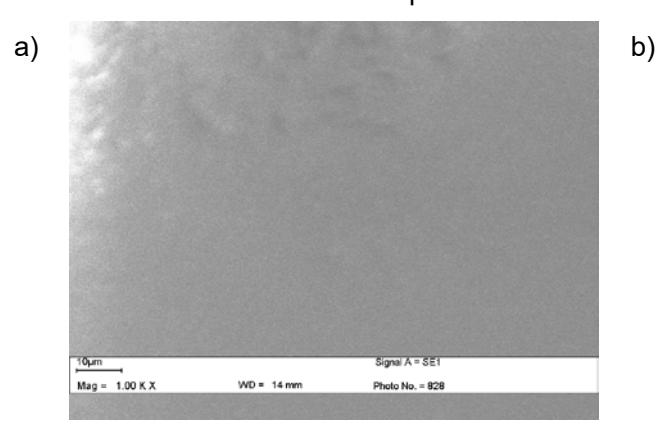
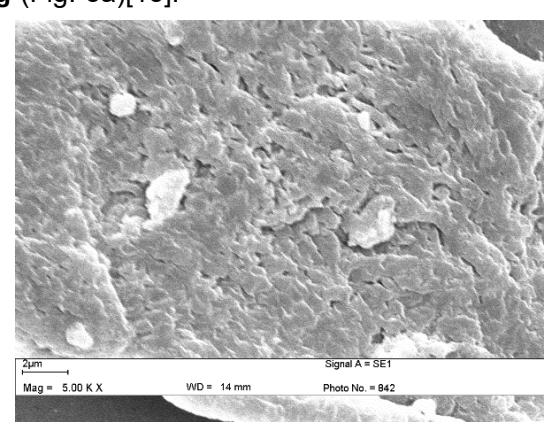


Fig 2. ATR-FTIR spectrum of Arg-RhoL.

The loading of dye within agarose hydrogel was also monitored by SEM techniques. From Figure 2, the distribution of **RhoL** on the agarose hydrogel film was revealed from the SEM images of **Arg-RhoL** (Fig. 3b), which demonstrated a significant increase in surface roughness. However, such distribution was absent in hydrogel film and in fact the film surface was found to be smooth in comparison to that of **Arg** (Fig. 3a)[15].





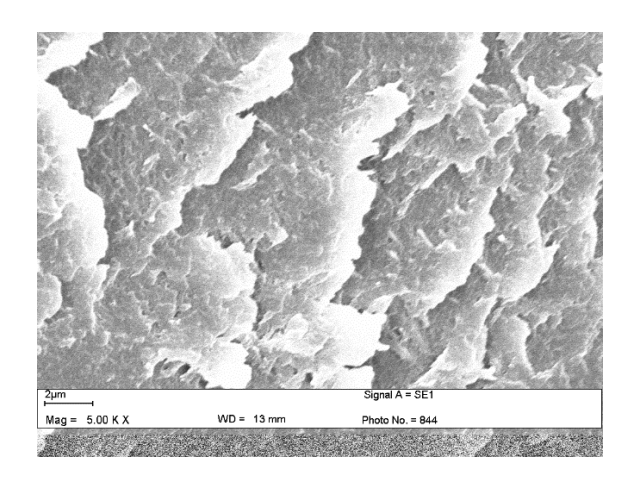


Fig 3. Scanning electron microscope (SEM) images of (a) **Arg** (b) **Arg-RhoL** and (c) **Arg-RhoL+Au**³⁺.

The electrostatic interactions between the hydrogel and rhodamine B are also effected the thermal behavior of hydrogel films investigated by thermogravimetric analysis (TGA) under nitrogen flow. The TGA profiles (Fig. 4) showed that the decomposition of **Arg** and **Arg-RhoL** composite materials took place in two stages in which the first transition occurred below 100°C due to weight loss of samples by moisture vaporization; in the second stage degradation occurred from 180 to 320°C, which was attributed to thermal degradation temperature of native and composite materials. In addition, **Arg-RhoL** was more stable than **Arg** at high temperature due to the interaction of hydrogel with Rhodamine B.

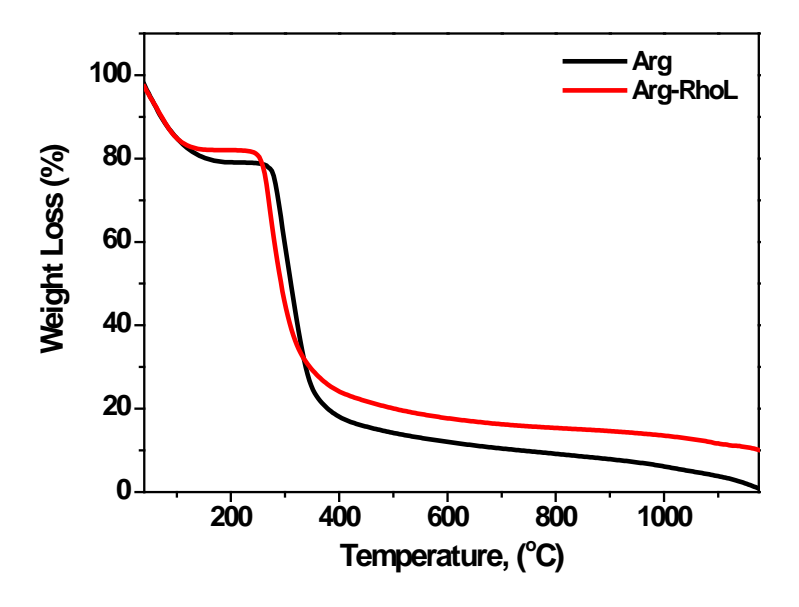


Fig 4. Thermogravimetric analysis of Arg and Arg-RhoL

The UV-vis analysis was done in reflectance mode from 750 to 220 nm to study the behavioral change in **Arg** and **Arg-RhoL**. The **Arg-RhoL** UV-vis spectrum exhibited an absorbance peak at around 300 nm, namely Π - Π^* , n - Π^* which was a characteristic of Rhodamine B [17, 18]. In the case of agarose hydrogel, no absorption peak was observed around 300 nm (Fig. 5).

All the techniques mentioned above (ATR-FTIR, SEM), TGA and UV-vis) showed evidences that **RhoL** can be immobilized into an agarose hydrogel.

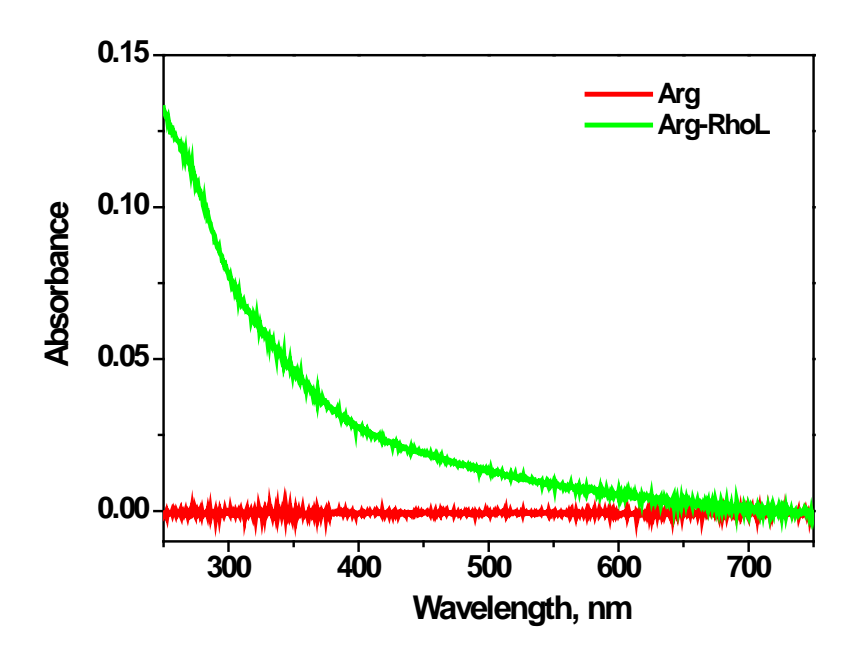


Fig 5. UV-vis spectra of Arg and Arg-RhoL

Selectivity of Arg-RhoL

The UV-vis spectra changes of **Arg-RhoL** were investigated to determine its cation binding abilities in aqueous solution. Fig. 6 shows UV-vis spectra of **Arg-RhoL** in the presence and absence of 10 mM of various cations. Normally, the absorption spectra of **Arg-RhoL** exhibited absorbance peaks from 450 to 650 nm. Upon the addition of metal solutions such as transition metals (Ni²⁺, Co²⁺, Cd²⁺, Hg²⁺, Pb²⁺, Zn²⁺, Ag⁺, Cu²⁺, Pt²⁺, Fe³⁺, Au³⁺, Ru³⁺), alkali metals (Li⁺, Na⁺, K⁺) and alkaline earth metals (Ca²⁺, Mg²⁺). It can be observed that only Au³⁺ produced an obvious absorbance enhancement at about 540 nm as a result of Au³⁺-induced ring opening of the spirolactam form. This can be explained by the suitable distance and the soft properties of the receptor structure (**Arg-RhoL**) to form a complex with Au³⁺ ion.

Moreover, according to change in signaling upon adding various Au^{3+} concentration, the limit of detection of Arg-RhoL for Au^{3+} was calculated to be 5 μ M. In addition, no significant absorbance spectra changes of solution occurred in the presence of other metal ions under identical conditions.

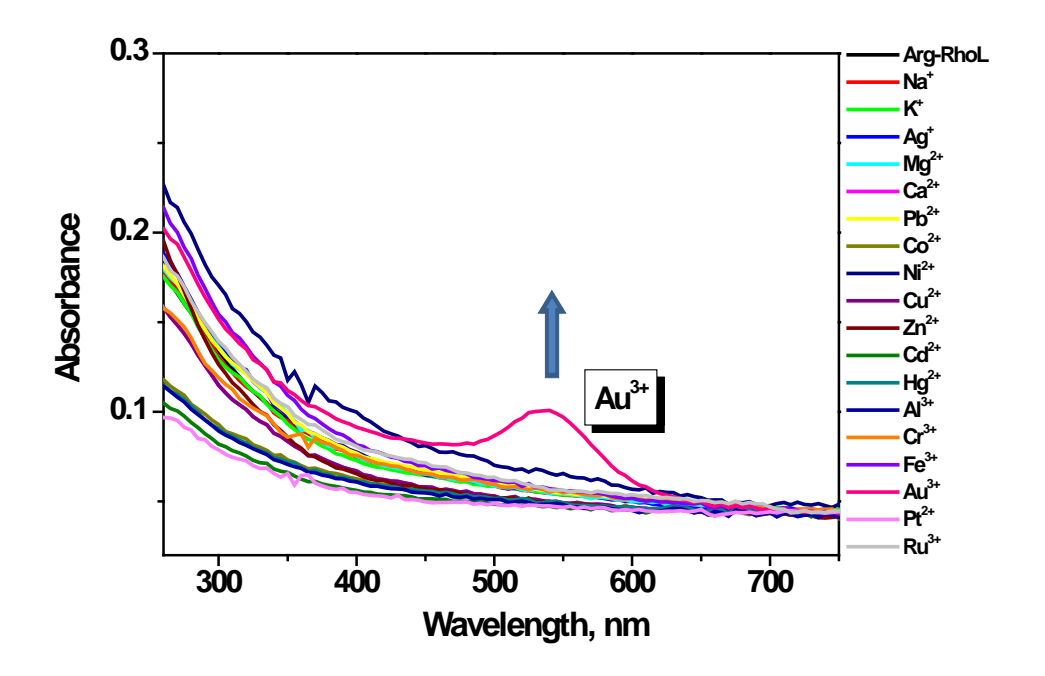


Fig 6. UV-vis spectra changes of Arg-RhoL after the addition of 10 μM of various cations.

Color changes observable with the naked eye upon immersing **Arg-RhoL** into various cations are shown in Fig. 7. The **Arg-RhoL** showed a distinct color change from colorless to pink only upon addition of Au³⁺. These results suggested that the immobilization of rhodamine lactone to agarose hydrogel could be a good colorimetric chemosensor for Au³⁺.



Fig 7. Color changes of the Arg-RhoL with various cations.

In order to further explore the formation of $Arg-RhoL+Au^{3+}$ complexes, Arg-RhoL in the presence and absence of Au^{3+} was investigated by X-Ray Diffraction Analysis (Fig. 8). The presence of $Arg-RhoL+Au^{3+}$ film produced distinct spectra showing the characteristic diffraction peaks of Au^{3+} ion which were lacking in Arg-RhoL without Au^{3+} . For Arg-RhoL treated with Au^{3+} , the gold experimental diffraction peak was found to be at 2θ value of 38.1° which was the Au^{3+} peak according to the JCPDS card (NO.1-1172). In addition, such porous surface from SEM image (Fig. 3c) was absent in hydrogel film due to complexation between Arg-RhoL with Au^{3+} and in fact the film surface was found to be smooth in comparison to that of Arg-RhoL.

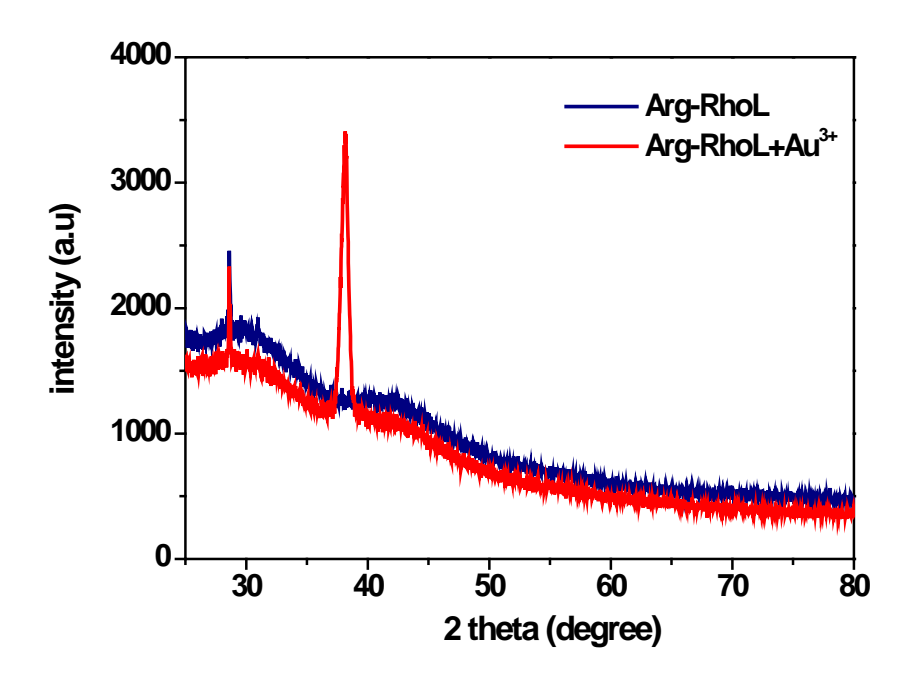


Fig 8. The XRD analysis of the Arg-RhoL and Arg-RhoL+Au³⁺ films.

Computational methods

The structural and electronic properties of the **Arg-RhoL** and **Arg-RhoL**+Au³⁺, and the highest selectivity metal complexes were calculated using the density functional theory (DFT) method via the Gaussian 09 program.

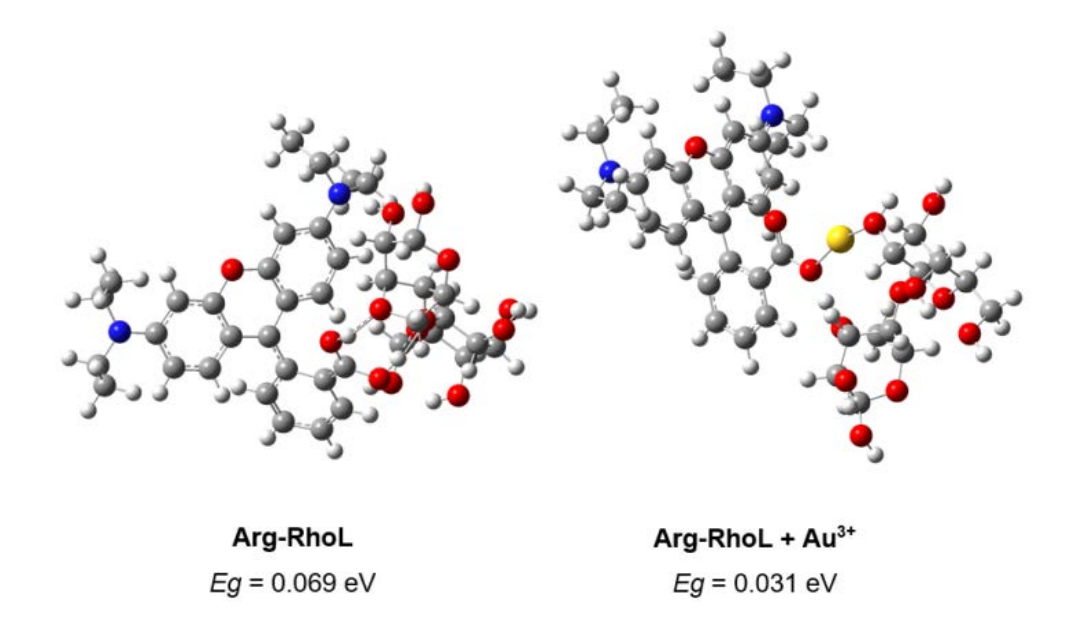


Fig 9. The optimized structures of **Arg-RhoL** and **Arg-RhoL**+Au³⁺ complexes, the gap energies ($Eg=E_{LUMO}-E_{HOMO}$).

The optimized geometries and the HOMO and LUMO energies of the **Arg-RhoL** and **Arg-RhoL** + Au³⁺ complex were calculated by the density functional theory (DFT) calculations at the B3LYP/LanL2DZ level using the Gaussian 09 program (Fig. 9). The structural changes were found to affect the HOMO-LUMO energy levels of rhodamine chromophores. Moreover, the energy gaps of thecomplex also decreased from 0.069 eV to 0.031 eV. The results suggested that the **Arg-RhoL** formed stable complexes with Au³⁺ via a carboxylic group of rhodamine and an alcohol group of agarose hydrogel.

Part V: A pH optical and fluorescent sensor based on rhodamine modified on activated cellulose paper

Synthesis and characterization of RhA

RhA was readily synthesized in two steps. First, rhodamine B was converted to rhodamine ethylenediamine (Rhen) using a condensation reaction of rhodamine B and ethylenediamine under N₂ refluxed for 3 days in small amount of MeOH. Then, amidation reactions between Rhen and succinic anhydride was prepared in dry DCM at room temperature for 2 hr to give RhA in 80% yield (scheme 1). Chemical structure and purity of chemosensors were proven by UV-vis, fluorescence, ATR-FTIR and SEM.

Scheme 2. The synthetic route for the RhA and CP-RhA

From figure 1, the $^1\text{H-NMR}$ spectra showed characteristic signals of $-\text{CH}_2$ and -CH groups in the region of 1.0–2.1 and 2.2–2.6 ppm, aromatic protons at 7.8–5.5 ppm and a carboxylic proton in 11-12 ppm, respectively. UV-vis absorption spectra of **RhA** appeared at 270 and 315 nm due to ligand localized n– Π^* and Π – Π^* transitions. Moreover, the UV-vis

absorption and fluorescence emission spectrum of **RhA** in the 400-600 nm disappeared (figure 2) and the solution was colorless which confirmed that the rhodamine ring-closed spirolactam form was present in these compounds.^[35]

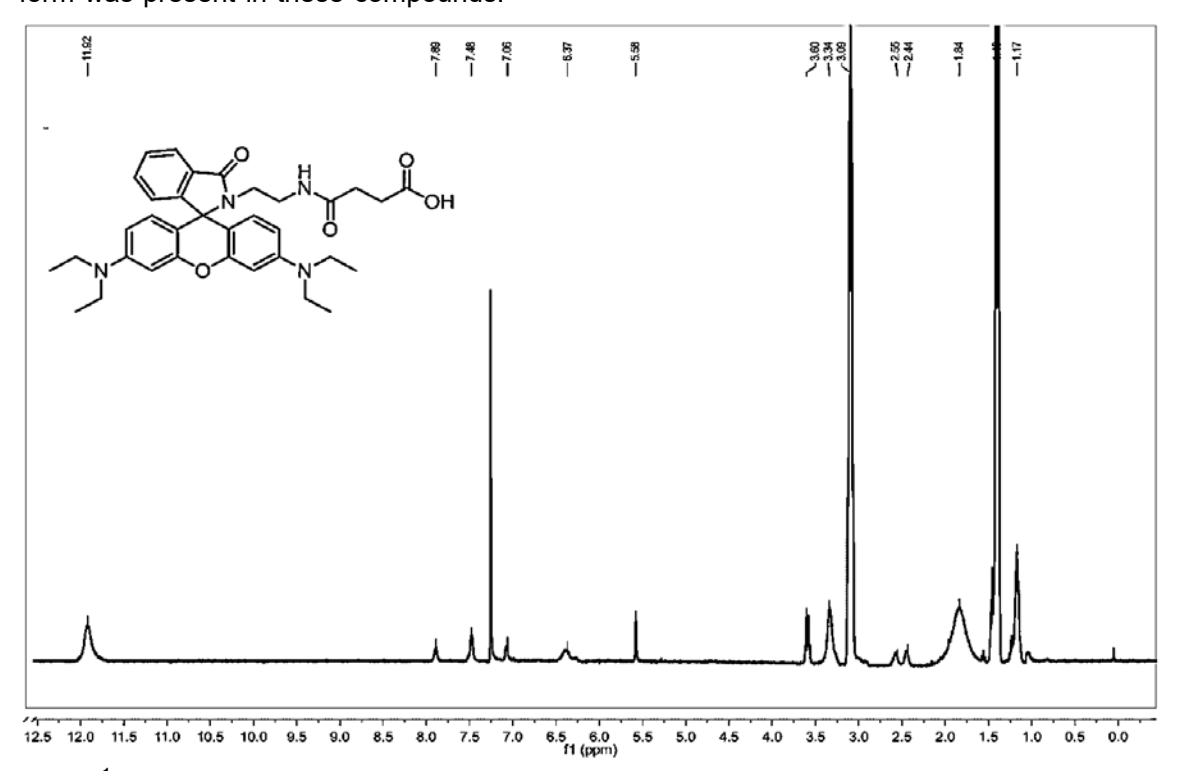


Fig 1. ¹H-NMR spectrum of RhA in CDCl₃

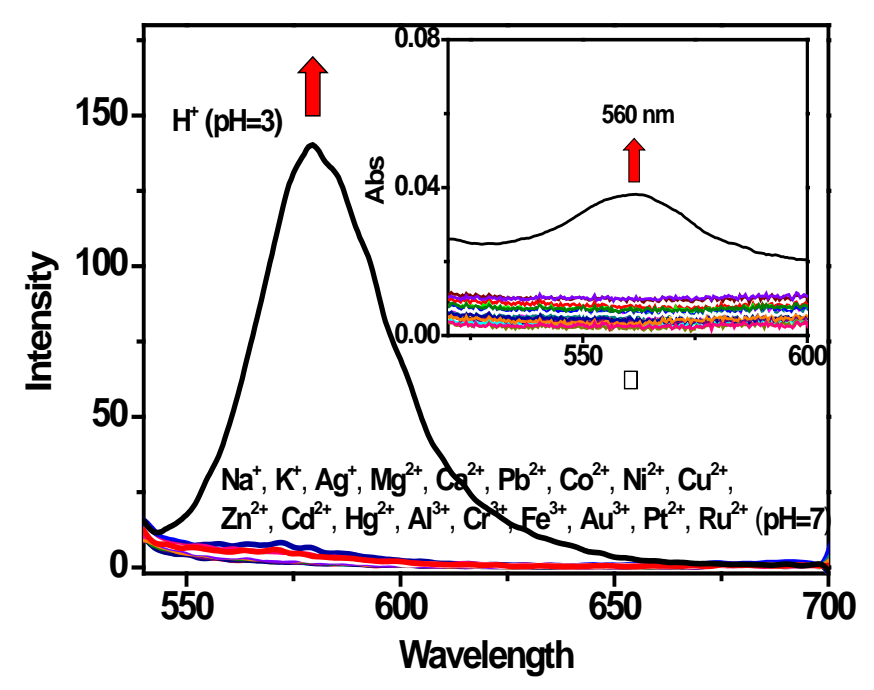


Fig 2. Fluorescence spectrum of RhA in the present various metal ions (10 μ M) and proton. in MeOH : H₂O (Ratio 1:1)

Selectivity of RhA

Considering that oxygen and nitrogen atoms can bind with various metal ions in solution, it is very important to determine whether other ions have potential to interfere. Upon addition of Na⁺, K⁺, Ag⁺, Mg²⁺, Ca²⁺, Pb²⁺, Co²⁺, Ni²⁺, Cu²⁺, Zn²⁺, Cd²⁺, Hg²⁺, Al³⁺, Cr³⁺, Fe³⁺, Au³⁺, Pt²⁺, Ru²⁺ at 10 µM to **RhA** solutions at neutral pH, no significant changes were observed in the fluorescence spectrum as shown in figure 2. It might be that there are not sufficient coordination sites between various metal ions and **RhA**, which cannot induce the spirolactam ring-opening and fluorescence emission from rhodamine b. However, lower pH (higher concentrations of H⁺) can induce spirolactam ring-opening and fluorescence emission. The results demonstrate that **RhA** can selectively detect pH changes in the presence of various metal ions. Characterization of **CP-RhA** and application as portable pH sensor

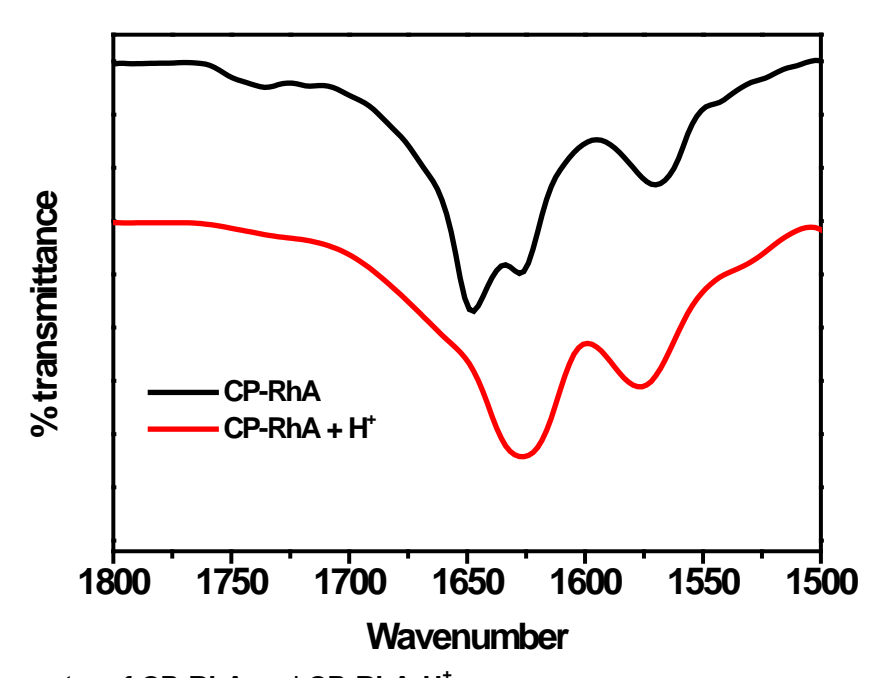
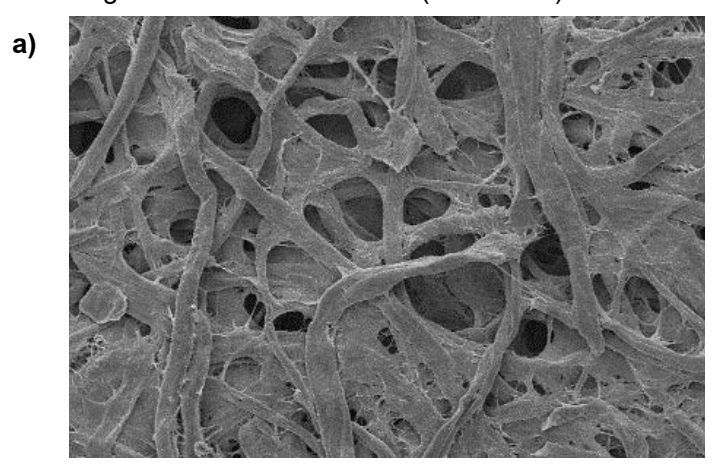


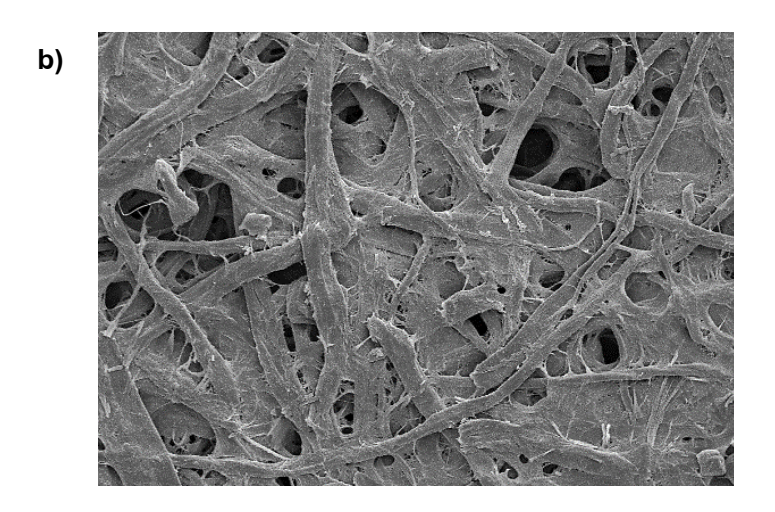
Fig 3. FT-IR spectra of CP-RhA and CP-RhA•H⁺

Characterization of CP-RhA and application

To further apply the **RhA** as a portable pH sensor, the Rhodamine ethylenediamine anhydride (**RhA**) was grafted into activated cellulose paper. In this strategy, the rhodamine moiety supplied the pH sensitive component via acid induced ring-opening reaction. The successive chemical modification of **RhA** on cellulose paper (**CP-RhA**) was proven using ATR-FTIR, SEM and solid stated fluorescent. The FTIR spectrum of **CP-RhA** exhibited characteristic absorption bands of cellulose material in the region of 3500 (O-H), 2900 (C-H) and 1100 (C-O) cm⁻¹ and showed absorption bands of rhodamine at 1648 and 1626 (C=O) cm⁻¹. Moreover, the NH amide linked peak at 3450 cm⁻¹ was confirmed the chemical

modification of **RhA** on cellulose paper. In addition, ATR-FTIR was also used to confirm the binding of the carbonyl group on rhodamine moieties of **CP-RhA** with H⁺. This is clearly observed that upon addition of H⁺ as shown in Figure 3, the carbonyl stretching band of **CP-RhA** at 1647 cm⁻¹ was changed to the lower number (1626 cm⁻¹).





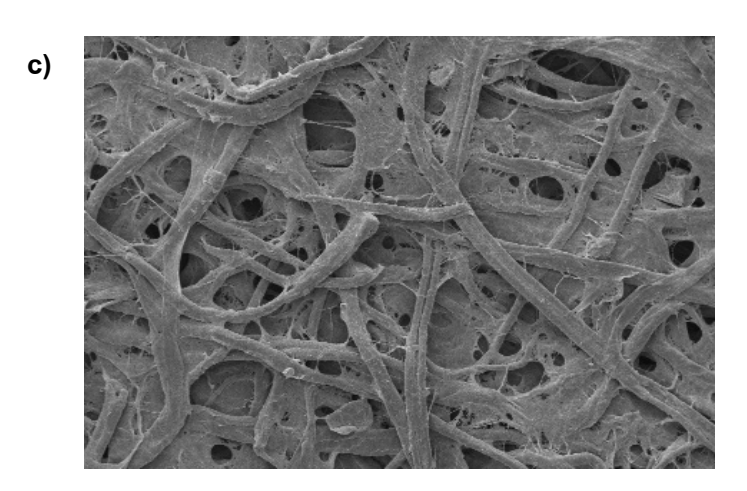
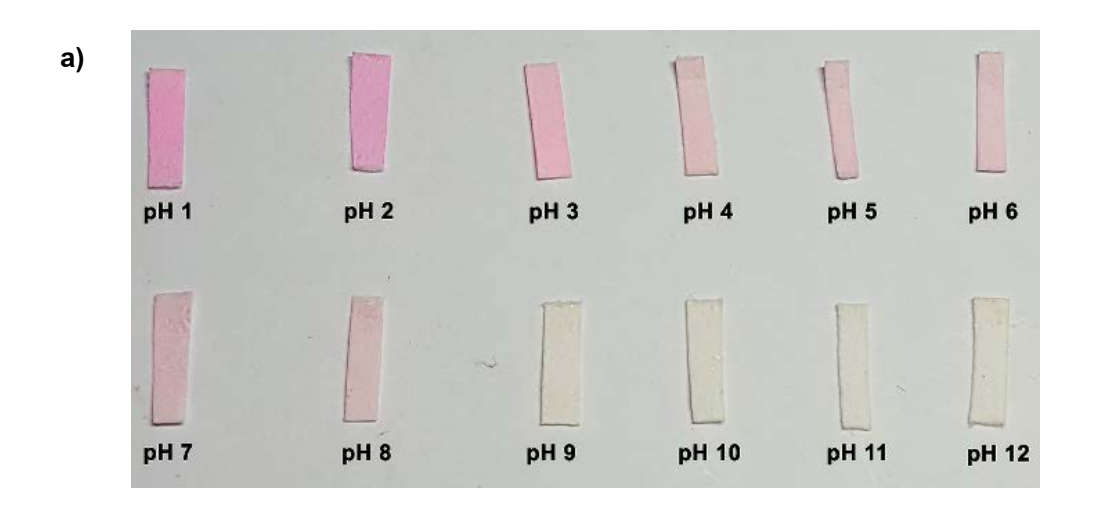


Fig 4. SEM images of (a) original cellulose paper, (b) paper-grafted **RhA** and (c) paper-grafted **RhA** treated with H⁺

From the SEM image (figure 4) of **CP-RhA**, the integrity of the cellulose fiber was not degraded by modification. SEM images showed that the diameter of fibers in original and grafted-papers were in the range of 6–20 μ M. The fiber structure of grafted-paper after treatment with H $^+$ showed the smooth and dark areas due to the increased hydrogen bond networks of **CP-RhA** by proton protonation.



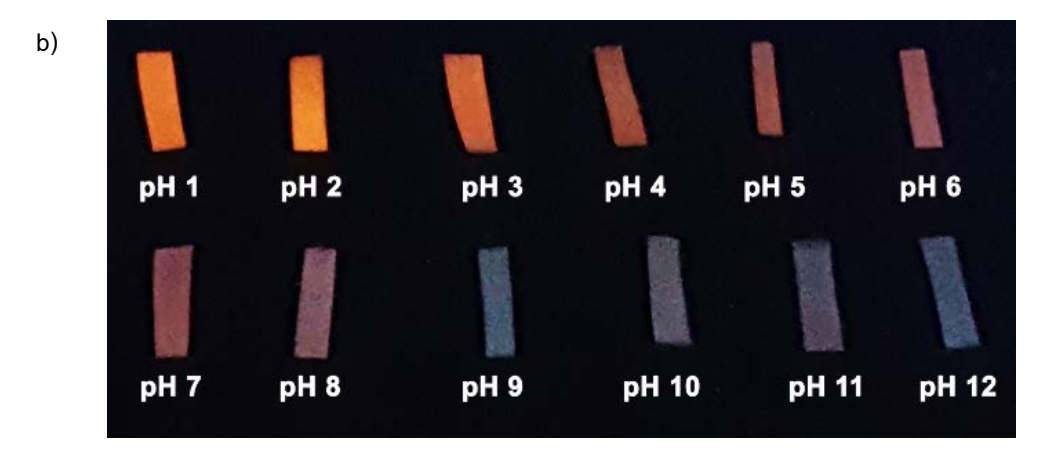


Fig 5. Colorimetric (a) and fluorescence (b) photographs of CP-RhA with different pH.

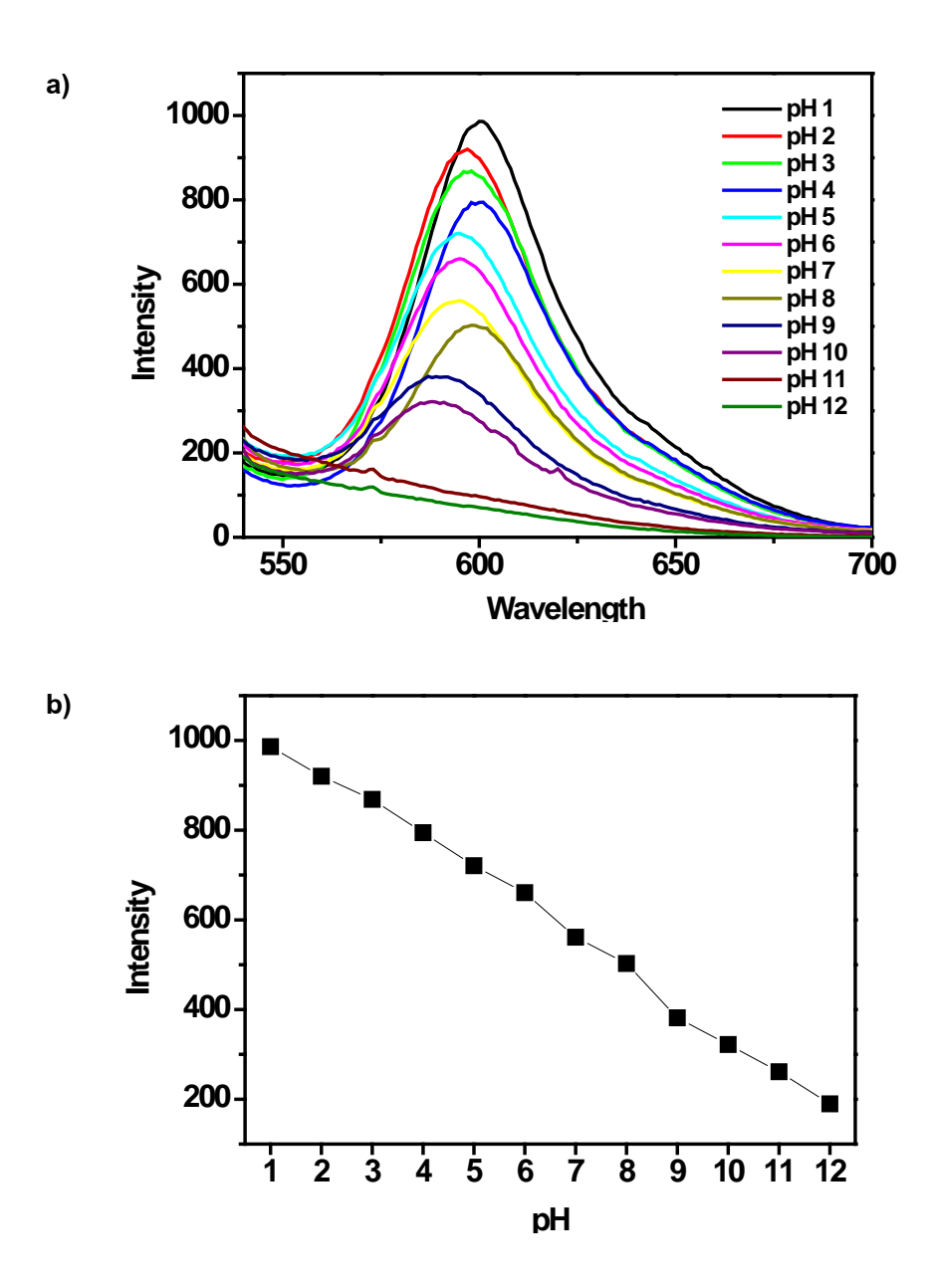


Fig 6. The solid-state fluorescence spectra of CP-RhA (a) upon soak in vary pH (1-12) from 540-700 nm, (b) The plot of maximum fluorescence intensities versus pH 1-12; $\lambda_{\rm ex}$ = 520 nm

In order to evaluate the **CP-RhA** for pH detection, a series of visible color change experiments were carried out with different pH in the range of 1.0–12.0 by adjusting various amount of HCl or NaOH aqueous solution. The fluorescence images of **CP-RhA** proceeded under UV light at 365 nm are shown in figure 5. It was observed that the **CP-RhA** displayed an enhanced orange fluorescence at low pH (1-5) due to H⁺- induced spirolactam ring-opening and decreased fluorescence when pH increases. Meanwhile, the fluorescence spectra also showed a significant decrease at 580-600 nm with increasing pH as demonstrated in figure 6 Similar results were observed under visible-light irradiation, the **CP-RhA** showed pink–red

colors for low pH values and turning to colorless at high pH.

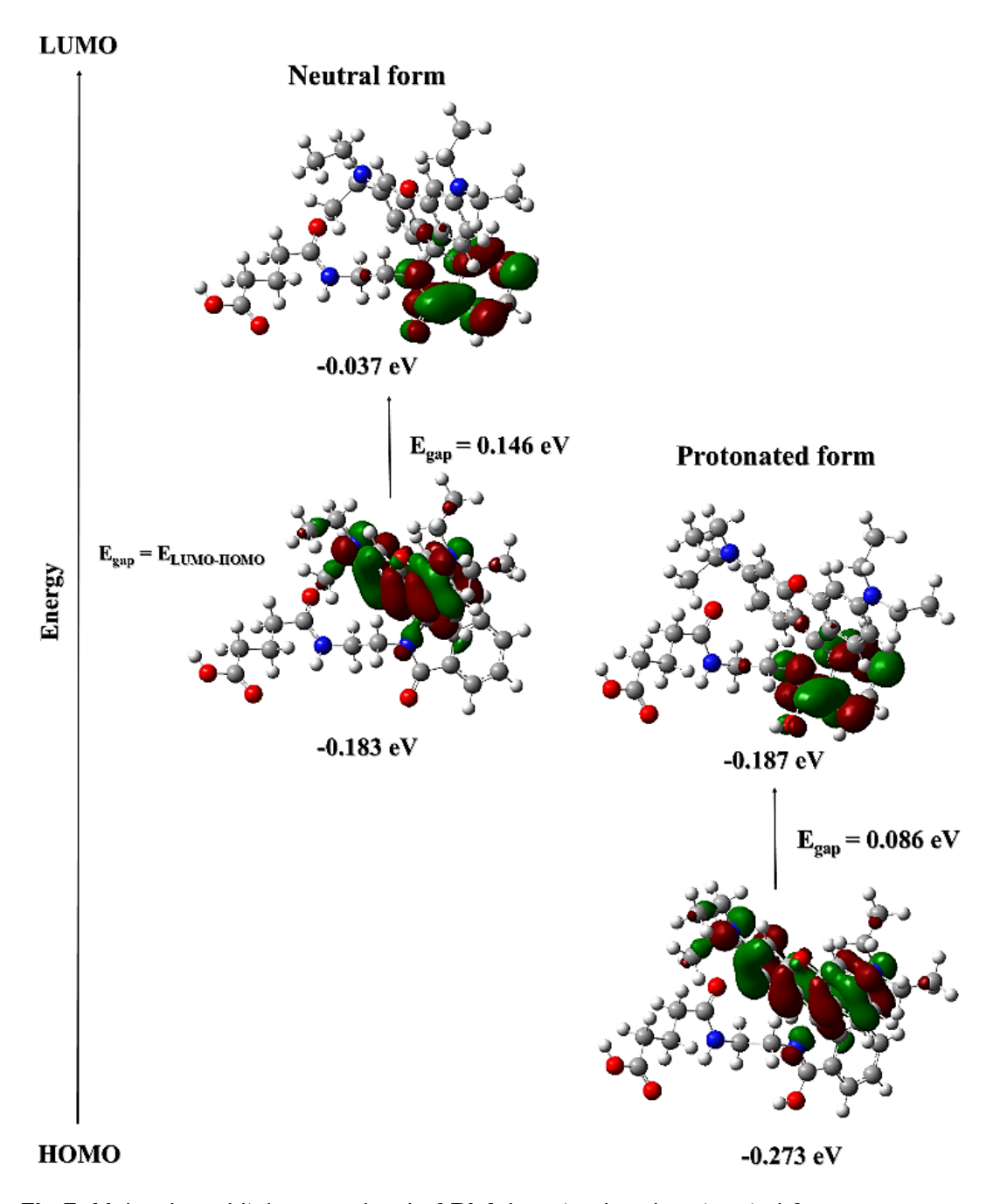


Fig 7. Molecular orbital energy level of RhA in natural and protonated form.

Computational calculations of RhA

Theoretical calculations were performed with density functional theory using the Gaussian 05 software package. The chemical structures, electronic distributions and transitions of **RhA** are optimized at the B3LYP/ LanL2DZ level. The electron distributions and orbital energies of the highest occupied molecular orbital (HOMO) and the lowest unoccupied molecular orbital (LUMO) of **RhA** in neutral form and protonated form are shown in figure 7.

The HOMO of neutral **RhA** was localized on the xanthenes moiety, while LUMO was mainly contributed by the spirolactam units. However, both HOMO and LUMO of protonated **RhA** were changed from neutral one. In addition, a decreased energy band-gap from 0.146 eV to 0.086 eV after protonation was discovered which was in well accordance with the blue-shift spectra.



PART I

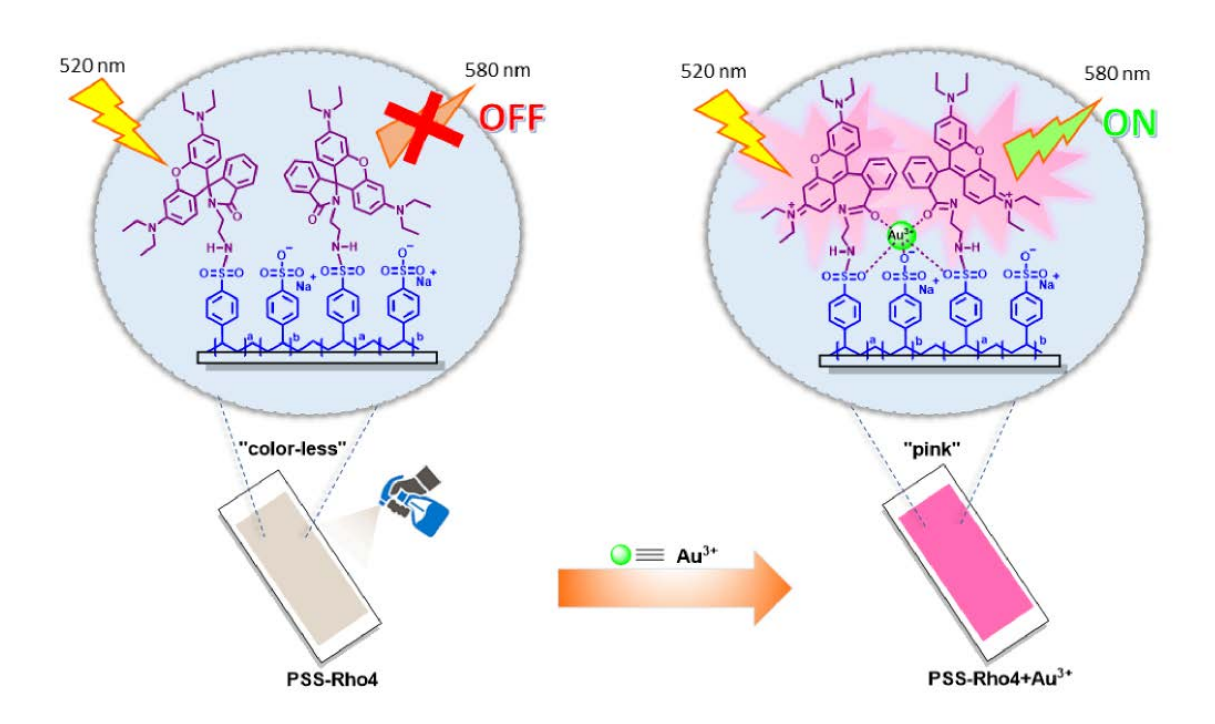
We have designed and synthesized the polymeric sensors by grafting rhodamine derivatives as colorimetric, fluorescent probes into polyacrylic acid skeleton for selective detection of Au³⁺ ions. New polymeric sensors were simply prepared by amidation reactions between PAA and rhodamine derivatives, which contain various chain lengths and a number of polyamine units with the rhodamine building blocks. Complexation studies showed that PAA-Rho3 exhibited the highest selectivity and sensitivity towards Au³⁺ when compared to the other polymeric sensors. The polymeric sensors were non-fluorescence in the spirolactam form and were selectively converted to the fluorescence-active ring-opened amide form in the presence of Au³⁺ ions leading to the fluorescence enhancement and colorimetric change. Common coexisting metal ions displayed insignificant interference to the detection of Au³⁺. In addition, the polymeric thin film sensors PAA-Rho3-ITO was successfully prepared and used as Au³⁺ probe in water solution. The limit of detection of PAA-Rho3-ITO for Au³⁺ was 0.1 µM, lower than that of PAA-Rho3, 0.43 µM, and the detection time was less than 40 seconds. After sensing Au³⁺, the **PAA-Rho3-ITO** was found to be recovered by dipping in the aqueous EDTA solution under basic conditions. Therefore, this approach can be used to fabricate a reversible polymeric thin film sensor for selective detection of Au³⁺.

Scheme 1. Proposed selective detection mechanism of Au³⁺ by using rhodamine-based modified poly acrylic acid (PAA-Rho)-coated ITO

PART II

Polymeric sensor based on rhodamine-based modified poly(sodium-4-styrenesulfonate) (PSS) has been developed as highly sensitive chemosensors for Au³⁺ ion. The polymeric sensor was characterized by ¹H NMR, SEM, and ATR-FTIR. It was found that **PSS-Rho4** was an efficient "off–on" switcher toward Au³⁺. The **PSS-Rho4** was spirolactam form (fluorescence "off") and was selectively transformed to the ring-opened amide form (fluorescence "on") upon

addition of Au^{3+} ion that induced fluorescence enhancement and colorimetric change with a detection limit down to micromolar values (1.2 μ M). Moreover, the DFT calculation results suggested that the polymeric sensor PSS-Rho4 formed stable complexes with Au^{3+} through a large number of cation–dipole interactions. Furthermore, a spray coating thin polymeric sensor film was produced on ITO and filtered paper (**PSS-Rho4-**ITO and **PSS-Rho4-**filtered paper) producing a fast, portable and easy-to-use molecular device for detection Au^{3+} with a naked-eye colorimetric sensor on ITO in the real system. The polymeric sensor was found to be restored by rinsing EDTA solution. We believe that, this approach may provide an easily handled and inherently sensitive method for Au^{3+} detection in environmental and biological applications.

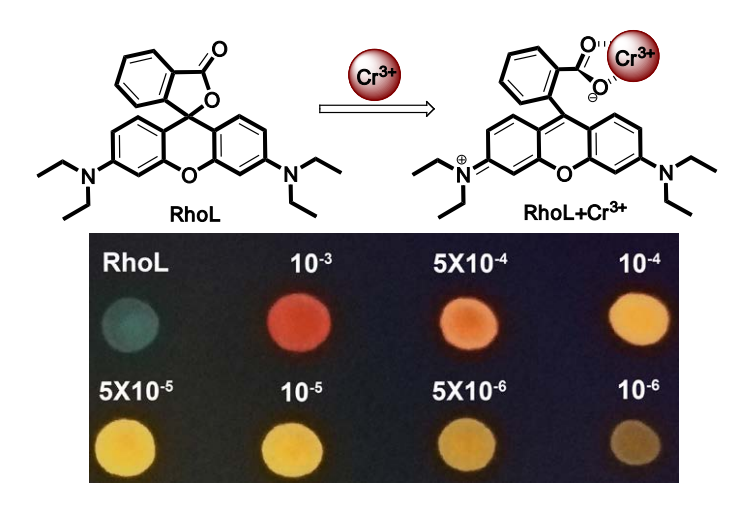


Scheme 2. Proposed selective detection mechanism of Au³⁺ by using rhodamine-based modified poly(sodium-4-styrenesulfonate)

PART III

We have designed and synthesized a solvatochromic-based sensor for detection of Cr³⁺using a commercially available and inexpensive dye (rhodamine) via rhodamine lactone—zwitterion equilibrium. An on-off type fluorescent enhancement was observed by the formation of the ring-opened rhodamine lactone form, which was induced by the interactions between Cr³⁺ and the chemosensor. Common co-existing metal ions displayed insignificant interference to the detection of Cr³⁺. More interestingly, **RhoL** could directly and rapidly detect Cr³⁺ when

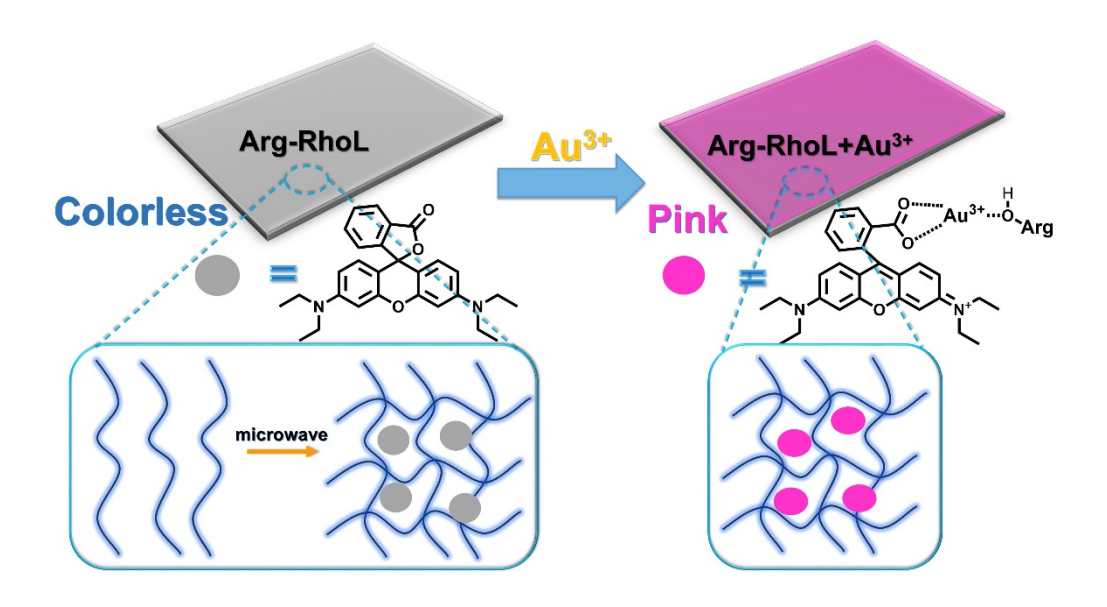
coated onto a paper surface using drop-casting technique which showed a low detection limit (1 μ M) without resorting to additional instrumental analysis. We believe that this approach may provide an easily measurable and inherently sensitive method for Cr^{3+} detection in environmental and biological applications.



Scheme 3. Proposed selective detection mechanism of Cr³⁺ by using solvatochromic-based sensor

PART IV

We have synthesized and immobilized of rhodamine lactone form into agarose hydrogel for use as in colorimetric-optical hydrogel film detection of Au³⁺ ions in real systems. The ATR-FTIR, SEM, TGA and UV-vis provided evidence that **RhoL** can be immobilized into an agarose hydrogel and showed suitable properties to produce a simple portable sensor. The color change (from colorless to pink) was observed in **Arg-RhoL** hydrogel film and was produced by the formation of **Arg-RhoL**-Au³⁺ chelates leading to Au³⁺-induced ring-opening of the rhodamine spirolactam. Theoretical calculations showed that **Arg-RhoL** formed stable complexes with Au³⁺ via a carboxylic group of rhodamine and an alcohol group of agarose hydrogel. We believe that, this approach may provide an easily measurable and inherently sensitive method for Au³⁺ detection in environmental and biological applications.



Scheme 4. Proposed selective detection mechanism of Au³⁺ by using immobilization of rhodamine derivative on agarose hydrogel (Arg-RhoL)

PART V

In summary, we have successfully synthesized a rhodamine ethylenediamine anhydride (**RhA**) and functionalized it on activated cellulose paper (**CP-RhA**) for use as a pH sensor. In aqueous solution, **RhA** showed fluorescence enhancement at 580 nm upon addition of H⁺. No interference with the pH sensor was observed from various metal ions (Na⁺, K⁺, Ag⁺, Mg²⁺, Ca²⁺, Pb²⁺, Co²⁺, Ni²⁺, Cu²⁺, Zn²⁺, Cd²⁺, Hg²⁺, Al³⁺, Cr³⁺, Fe³⁺, Au³⁺, Pt²⁺ and Ru²⁺). To further study its potential as a portable pH sensor, **RhA** was immobilized on activated cellulose paper to obtain the composites pH sensor (**CP-RhA**). In modified paper (**CP-RhA**), the fluorescence image showed high orange fluorescence and a deep pink color visible at low pH. The DFT calculations showed greater stability in the protonated form compared with the natural form. These results indicated the rhodamine modified on activated cellulose paper could be used as an optical and "off-on" fluorescent pH indicator.

Scheme 5. Proposed selective detection mechanism of pH optical and fluorescent sensor based on rhodamine modified on activated cellulose paper (**CP-RhA**).



- [1] M. Navarro, Gold complexes as potential anti-parasitic agents, Coord. Chem. Rev. 2009, 253, 1619–1626.
- [2] P. Claus, Heterogeneously catalysed hydrogenation using gold catalysts, Appl. Catal. A: Gen. 2005, 291, 222–229.
- [3] P. Goodman, Current and future uses of gold in electronics, Gold Bull. 2002, 35, 21–26.
- [4] M. Suwalsky, R. González, F. Villena, L.F. Aguilar, C.P. Sotomayor, S. Bolognin, P. Zatta, Human erythrocytes and neuroblastoma cells are affected in vitro by Au(III) ions, Biochem. Biophys. Res. Commun. 2010, 397(2), 226-231.
- [5] D. Parajuli, C. R. Adhikari, H. Kawakita, S. Yamada, K. Ohto, K. Inoue, Chestnut pellicle for the recovery of gold, Bioresour. Technol. 2009, 100, 1000–1002.
- [6] J. R. Cui, L. F. Zhang, Metallurgical recovery of metals from electronic waste: a review, J. Hazard. Mater. 2008, 158, 228–256.
- [7] P. F. Sorensen, Gold recovery from carbon-in-pulp eluates by precipitation with a mineral acid I. Precipitation of gold in eluates contaminated with base metals, Hydrometallurgy, 1988, 21, 235–241.
- [8] C. P. Gomes, M. F. Almeida, J. M. Loureiro, Gold recovery with ion exchange used resins, Sep. Purif. Technol. 2001, 24, 35–57.
- [9] F. J. Alguacil, P. Adeva, M. Alonso, Processing of residual gold (III) solutions via ion exchange, Gold Bull. 38 (2005) 9–13.
- [10] C. Mack, B. Wilhelmi, J. R. Duncan, J. E. Burgess, Biosorption of precious metals, Biotechnol. Adv. 2007, 25, 264–271.
- [11] H. Kim, M. Lee, H. Kim, J. Kim, J. Yoon, A new trend in rhodamine-based chemosensors: application of spirolactam ring-opening to sensing ions, Chem. Soc. Rev. 2008, 37, 1465–1472.
- [12] V. Dujols, F. Ford and A. W. Czarnik, A long-wavelength fluorescent chemodosimeter selective for Cu(II) ion in water, J. Am. Chem. Soc., 1997, 119, 7386-7387.
- [13] J. Y. Kwon, Y. J. Jang, Y. L. Lee, K. M. Kim, M. S. Seo, W. Nam, and J. Yoon, A highly selective fluorescent chemosensor for Pb²⁺, J. Am. Chem. Soc. 2005, 127, 10107-10111.
- [14] Y. Xiang, A. Tong, P. Jin, Y. Ju, New fluorescent rhodamine hydrazone chemosensor for Cu(II) with high selectivity and sensitivity, Org. Lett. 2006, 8, 2863-2866.
- [15] P. Mahato, S. Saha, E. Suresh, R. D. Liddo, P. P. Parnigotto, M. T. Conconi, M. K. Kesharwani, B. Ganguly and A. Das, Ratiometric detection of Cr³⁺ and Hg²⁺ by a naphthalimide-rhodamine based fluorescent probe, Inorg. Chem., 2012, 51, 1769–1777.
- [16] X. Puhui, G. Fengqi, X. Ruirui, W. Yao, Y. Denghui, Y. Guoyu, X. Lixia, A rhodamine–dansyl conjugate as a FRET based sensor for Fe³⁺ in the red spectral region,

- J. Lumines., 2014, 145, 849-854.
- [17] C. Kaewtong, J. Noiseephum, Y. Uppa, N. Morakot, N. Morakot, B. Wanno, T. Tuntulani,
- B. Pulpoka, A reversible Em-FRET rhodamine-based chemosensor for carboxylate anions using a ditopic receptor strategy. New J. Chem., 2010, 34; 1104-1108.
- [18] C. Kaewtong, B. Pulpoka, T. Tuntulani, Reversible Fluorescent and Colorimetric Rhodamine Based-Chemosensor of Cu²⁺ Contact Ion-pairs using a Ditopic Receptors. Dyes. Pigm., 2015, doi:10.1016/j.dyepig.2015.08.001.
- [19] C. Kaewtong , Y. Uppa, N. Morakot, B. Wanno, T. Tuntulani, B. Pulpoka, Facile Synthesis of Rhodamine-Based Highly Sensitive and Fast Responsive Colorimetric and Off-On Fluorescent Reversible Chemosensors for Hg²⁺: Preparation of a Fluorescent Thin Film Sensor. Dalton Trans., 2011, 46, 12578-12583.
- [20] N. R. Chereddy, S. Thennarasu, A. B. Mandal, Incorporation of triazole into a quinoline-rhodamine conjugate imparts iron(III) selective complexation permitting detection at nanomolar levels. Dalton Trans., 2012, 41, 11753–11759
- [21] X. Guan, W. Lin, W. Huang, Development of a new rhodamine-based FRET platform and its application as a Cu²⁺ probe. Org. Biomol. Chem., 2014, 12, 3944–3949.
- [22] S. Ji, X. Meng, W. Ye, Y. Feng, H. Sheng, Y. Cai, J. Liu, X. Zhu, Q. Guo, Dalton Trans., 2014, 43, 1583–1588
- [23] G. Chen, A. S. Hoffman, Graft copolymers that exhibit temperature-induced phase transitions over a wide range of pH, Nature, 1995, 373, 49⁻⁵².
- [24] N. Niamsa, C. Kaewtong, V. Srinonmuang, B. Wanno, B. Pulpoka, T. Tuntulani, Hybrid organic–inorganic nanomaterial sensors for selective detection of Au³⁺ using rhodamine-based modified polyacrylic acid (PAA)-coated FeNPs. Polym. Chem., 2013, 4, 3039–3046.
- [25] C. Kaewtong, N. Niamsa, B. Wanno, N. Morakot, B. Pulpoka, T. Tuntulani, Optical chemosensors for Hg²⁺ from terthiophene appended rhodamine derivatives: FRET based molecular and in situ hybrid gold nanoparticle sensors. New J. Chem., 2014, 38, 3831-3839.
- [26] C. Kaewtong, G. Jiang, Y. Park, A. Baba, T. Fulghum, B. Pulpoka, R. Advincula, Azacalix[3]arene-Carbazole Conjugated Polymer Network Ultrathin Films for Specific Cation Sensing. Chem. Materials. 2008, 20, 4915-4924.
- [27] C. Kaewtong, N. Niamsa, B. Pulpoka, T. Tuntulani, Reversible sensing of aqueous mercury using a rhodamine-appended polyterthiophene network on indium tin oxide substrates. RSC Advances, 2014, 4, 52235-52240.



Output จากโครงการวิจัยที่ได้รับทุนจาก สกว.

- 1. ผลงานตีพิมพ์ในวารสารวิชาการนานาชาติ (ระบุชื่อผู้แต่ง ชื่อเรื่อง ชื่อวารสาร ปี เล่มที่ เลขที่ และหน้า)
 - 1.1 Chatthai Kaewtong, Sastiya Kampaengsri, Burapol Singhana, Buncha Pulpoka. Highly selective detection of Au³⁺ using rhodamine-based modified polyacrylic acid (PAA)-coated ITO. Dyes and Pigments, 2017, 141:277-285
 - 1.2 Chatthai Kaewtong, Sastiya Kampaengsri, Buncha Pulpoka and Thawatchai Tuntulani. Solvatochromic-based sensor for chromium (III) in real systems. New Journal of Chemistry, 2018, 42;9930-9934
 - 1.3 Thianthan Taweetanavanich, Banchob Wanno, Thawatchai Tuntulani, Buncha Pulpoka, Chatthai Kaewtong. A pH optical and fluorescent sensor based on rhodamine modified on activated cellulose paper. Journal of the Chinese Chemical Society, 2018, 1-7.
 - 1.4 Sastiya Kampaengsri, Banchob Wanno, Thawatchai Tuntulani, Buncha Pulpoka & Chatthai Kaewtong. Gold sensing with rhodamine immobilized hydrogelbased colorimetric sensor, Environmental Technology, 2019, DOI: 10.1080/09593330.2019.1595163.
 - 1.5 Prangtip Chansri, Banchob Wanno, Somchai Keawwangchai, Thawatchai Tuntulani, Buncha Pulpoka and Chatthai Kaewtong. Spray coating thin polymeric sensor films for Au³⁺, Journal of Applied Polymer Science, Manuscript revision.
- 2. การนำผลงานวิจัยไปใช้ประโยชน์
 - เชิงพาณิชย์ (มีการนำไปผลิต/ขาย/ก่อให้เกิดรายได้ หรือมีการนำไปประยุกต์ใช้โดย ภาคธุรกิจ/บุคคลทั่วไป)
 - เชิงนโยบาย (มีการกำหนดนโยบายอิงงานวิจัย/เกิดมาตรการใหม่/เปลี่ยนแปลง ระเบียบข้อบังคับหรือวิธีทำงาน)
 - เชิงสาธารณะ (มีเครือข่ายความร่วมมือ/สร้างกระแสความสนใจในวงกว้าง)
 - เชิงวิชาการ (มีการพัฒนาการเรียนการสอน/สร้างนักวิจัยใหม่)
 - 1) ใช้ในการเรียนการสอนวิชา 0202314 เคมีซุปราโมเลกุล และ 0202619 เคมีซูปราโมเลกุล
 - 2) ใช้ในการเขียนหนังสือเรื่อง "ตรวจวัดทางเคมี (Chemosensors)"
 - มีการสร้างนักวิจัยใหม่
 ป เอก 1 คน (นางสาวสุชนา วานิช)

- ป โท 3 คน (นางสาว ปรางทิพย์ จันทร์ศรี, นาย ศาสตริยา คำแพงศรี, นายเธียรธัญ ทวีธน วาณิชย์)
- ป ตรี 4 คน (นางสาว กานต์ธีรา จุลยะโชค, นางสาว ณัฐมล เอกตาแสง, นายเกียรติศักดิ์ ชุม ศรี, นายพิพัฒพงศ์ จันหาญ)
- 3. อื่นๆ (เช่น ผลงานตีพิมพ์ในวารสารวิชาการในประเทศ การเสนอผลงานในที่ประชุม วิชาการ หนังสือ การจดสิทธิบัตร)
 - 1) นักวิจัยรุ่นใหม่ พบ เมธีวิจัยอาวุโส ครั้งที่ 17 ณ โรงแรมเดอะรีเจนท์ ชะอำ บีช รีสอร์ท จังหวัดเพชรบุรี
 - 2) นักวิจัยรุ่นใหม่ พบ เมธีวิจัยอาวุโส ครั้งที่ 18 ณ โรงแรมเดอะรีเจนท์ ชะอำ บีช รีสอร์ท จังหวัดเพชรบุรี
 - การประชุมวิชาการศูนย์ความเป็นเลิศด้านนวัตกรรมทางเคมี ครั้งที่ 10
 ณ โรงแรมจอมเทียน ปาล์ม บีช รีสอร์ท เมืองพัทยา จังหวัดชลบุรี
 (Invited speaker)
 - 4) การประชุมวิชาการระดับชาติของนักศึกษาระดับปริญญาตรี คณะ วิทยาศาสตร์และเทคโนโลยี ครั้งที่ 4 ประจำปีการศึกษา 2560 (USTC-4) (Invited speaker)
 - 5) วิทยากรโครงการสัมมนาเพื่อพัฒนาศักยภาพนักวิจัย คณะวิทยาศาสตร์ มหาวิทยาลัยนครพนม (Invited speaker)



รูปแบบรายการเงิน

| | รายงานสรุปการเงิน | | | | |
|---|---------------------------------------|---------------------------|---------------------|--|--|
| ชื่อหัวหน้าโครงก | ารวิจัยผู้รับทุน | | | | |
| รายงานในช่วงตั้ | ึ่งแต่วันที่ | | ถึงวันที่ | | |
| | | <u>รายจ่าย</u> | | | |
| หมวด (ตามสัญญา) | รายจ่ายสะสม จากรายงาน ครั้งก่อน | ค่าใช้จ่าย งวดปัจจุบัน | | งบประมาณ คงเห รวมทั้งโครงการ (หรือเกิ | |
| 1. ค่าตอบแทน 2. ค่าจ้าง 3. ค่าวัสดุ 4. ค่าใชัสอย 5. ค่าครุภัณฑ์ | | | | | |
| 6 | | | | | |
| รวม | | | | | |
| | | <u>จำนวนเงินที่ได้</u> | ์ รับและจำนวนเงิ | นคงเหลื <u>อ</u> | |
| | ู้นที่ได้รับ | | | | |
| งวดที่ 1 | | | | บาท เมื่อ | |
| | | | | | |
| งวดที่ 2 | ครุงท 1 | | | บาท เมื่อ | |
| ดอกเบี้ย | | | | | |
| | | รวม | | บาท ๋๋ ๋๋ | |
| ดอกเบี้ย | | | าใช้จ่าย | บาท ๋ | |
| ดอกเบี้ย ฯลฯ | | | | 91090 | |
| ดอกเบี้ย ฯลฯ งวดที่ 1 | 1 | | าใช้จ่าย | | |
| ดอกเบี้ย ฯลฯ งวดที่ 1 | เป็นเงิน เป็นเงิน | | าใช้จ่าย | บาท | |
| ดอกเบี้ย ฯลฯ งวดที่ 1 งวดที่ 2 | เป็นเงิน เป็นเงิน | | าใช้จ่าย | บาท | |